Johannes Gutenberg-University Mainz

Faculty of Biology

MECHANISMS BEHIND T CELL-MEDIATED NEUROINFLAMMATION

A doctoral dissertation
submitted in partial fulfillment
of the requirements for the degree of
doctor rerum naturalium

by

René Gollan, Dipl.-Biol. B.Sc.

Mainz, 2015

The author attests that permission has been obtained for the use of any copyrighted material appearing in this thesis (other than brief excerpts requiring only proper acknowledgement in scholarly writing) and that all such use is clearly acknowledged. Furthermore the author assures that he has independently produced this work and has not used any sources and aids other than stated, with quotations duly marked as such.

_____

Signature of Author

Permission is herewith granted to the Faculty of Biology of the Johannes Gutenberg-University Mainz to circulate and to have copied for non-commercial purposes, at its discretion, the above title upon the request of individuals or institutions.

The author reserves other publication rights, and neither the thesis nor extensive extracts from it may be printed or otherwise reproduced without the author's written permission.

Contents

MECHANISMS BEHIND T CELL-MEDIATED NEUROINFLAMMATION

René Gollan, Dipl. bio. B.sc.

Thesis Advisors: Volker Siffrin, PD MD and Frauke Zipp, Prof. MD

ABSTRACT

Multiple sclerosis (MS) is a chronic demyelinating inflammatory and neurodegenerative autoimmune disease of the central nervous system (CNS) causing long-term neurological disability. According to our current understanding, MS is mainly driven by autoreactive lymphocytes, which are thought to orchestrate repetitive CNS invasions by immune cells, resulting in the destruction of the myelin sheath and the neuronal compartment. This thesis focuses on the mechanisms behind T cell-mediated neuroinflammation in the context of the murine MS model experimental autoimmune encephalomyelitis (EAE). At first the impact and fate of distinct T cell subsets in the course of EAE, especially during the second wave of CNS infiltration was addressed. While Th1 and Th2 cells infiltrated the CNS less efficiently than Th17 cells a strong influence of the second wave of autoreactive T cells on the EAE-inducing population was observed. Th1 and Th2 reduced EAE severity, presumably by competing with Th17 cells, by promoting plasticity of the EAE-inducing population, and by expressing more anti-inflammatory cytokines in response to contact with the neuronal compartment. Secondly the ambivalent role of the neuronal adhesion molecule ICAM-5 was investigated in the context of EAE. It was demonstrated that membrane bound ICAM-5 is not essential as an adhesion molecule for T cell-mediated neuroinflammation. However, the shedded soluble form, sICAM-5, shows regulatory features in immune responses, probably by inhibiting T cell (re)stimulation via antigen presenting cells. Thus, sICAM5 might serve locally as an endogenous neuronal defense mechanism during ongoing neuroinflammation. Thirdly the potential of axonal and neuronal ion-channel blocking in preventing neurodegeneration in EAE was tested. We investigated the effect of the antiepileptic drug Lamotrigine (LTG) by using intravital live imaging. Intriguingly, a reduction of intraneuronal free calcium concentrations, as an early sign for neuronal damage, was observed by the application of low-dose LTG but not in axons or if given in high-dose. Clinical EAE studies confirmed that ion-channel blocking by low-dose LTG improves neurological deficits. Taken together this thesis gives new insights beginning with the contribution of distinct T cell in the perpetuation of CNS inflammation, across a potential neuronal defense mechanism as an endogenous response to T cells, up to the prevention of neurodegeneration as the consequence of the detrimental cascade of T cell-mediated neuroinflammation.

MECHANISMEN T ZELL-INDUZIERTER NEUROINFLAMMATION

René Gollan, Dipl. bio. B.sc.

Thesis Betreuer: Volker Siffrin, PD MD and Frauke Zipp, Prof. MD

ZUSAMMENFASSUNG

Multiple Sklerose ist eine Autoimmunerkrankung des Zentralen Nerven Systems (ZNS), charakterisiert durch inflammatorische, demyelinisierende und neurodegenerative Prozesse, die in chronischen neuronalen Schädigungen resultieren. Nach aktuellem Erkenntnisstand fördern autoreaktive Lymphozyten repetitive Infiltrationen von Immunzellen in das ZNS, was letztendlich zur Degenerierung von Myelinscheiden und Nervenzellen führt. Diese Arbeit behandelt die einer solchen T Zell-induzierten Neuroinflammation zugrundeliegenden Mechanismen im murinen MS-Modell der Experimentellen autoimmunen Enzephalomyelitis (EAE). Im ersten Teil wurde der Einfluss verschiedener T Zell Subpopulationen auf den Verlauf der EAE, insbesondere während des zweiten Schubes von ZNS-infiltrierenden T Zellen, untersucht. Es zeigte sich, dass Th1 und Th2 Zellen das ZNS ineffizienter infiltrieren als Th17 Zellen und einen starken Einfluss auf die EAE-induzierende Population haben. Th1 und Th2 Zellen begünstigen den Krankheitsverlauf, indem sie mit Th17 Zellen konkurrieren, die EAE-induzierenden T Zellen verändern und lokal anti-inflammatorische Zytokine sekretieren. Im zweiten Teil wurde die ambivalente Rolle des neuronalen Adhesionsproteins ICAM-5 im Kontext der EAE näher untersucht. Es konnte bewiesen werden, dass membran-gebundenes ICAM-5 für T Zell-induzierte Neuroinflammation nicht essentiell ist. Jedoch zeigte die lösliche Form des Proteins, sICAM-5, immunregulatorische Eigenschaften, indem es die Stimulation von T Zellen durch antigenpräsentierenden Zellen blockiert. sICAM könnte demnach Teil eines endogenen neuronalen Schutzmechanismus vor neuroinflammatorischen Prozessen darstellen. Im dritten Teil wurde das neuroprotektive Potential der Inhibierung von Ionenkanälen an Axonen und Neuronen während der EAE untersucht. Die Anwendung des Antiepileptikums Lamotrigin führte zu einer Reduktion intraneuronaler Calcium-konzentrationen, welche als frühe Anzeichen neuronaler Schädigung zu verstehen sind. Interessanterweise wurde dieser Effekt ausschließlich an Neuronen und bei niedrigen Dosierungen beobachtet und zeigt, dass Blockierung von Ionenkanälen therapeutisch eingesetzt werden kann. Zusammenfassend beschreibt diese Arbeit neue Erkenntnisse über die Mechanismen T Zell-induzierter Neuroinflammation, beginnend mit dem Einfluss verschiedener T Zell Populationen, über neuroprotektive neuronale Schutzantworten, bis hin zu Behandlungsmöglichleiten von sekundären neurodegenerativen Prozessen.

Publication List

The doctoral thesis is based on following own publications structured by relevance:

(1) *"Local interaction of T helper subsets improves neuroinflammation by modulating disease inducing Th17 cells."*

Gollan R, Larochelle C, Wolf C, Bühler U, Zipp F, Siffrin V
in preparation

---

(2) *"Preventing clinical disability in experimental autoimmune encephalomyelitis by reducing neuronal somatic free [Ca^{2+}] by low-dose Lamotrigine."*

Gollan R, Luchtman D, Bühler U, Belikan P, Wolf C, Liefländer C, Zipp F, Siffrin V
in preparation

(3) ---

"The Role of ICAM-5 in experimental autoimmune encephalomyelitis."

Gollan R, Rohne P, Larochelle C, Prochnow H, Mandal S, Baiersdörfer M, Gahmberg C, Siffrin V, Zipp F.
in preparation

(4) ---

"Cross-Recognition of a Myelin Peptide by $CD8^+$ T Cells in the CNS Is Not Sufficient to Promote Neuronal Damage."

Reuter E*, **Gollan R***, Grohmann N*, Paterka M, Salmon H, Birkenstock J, Richers S, Leuenberger T, Brandt AU, Kuhlmann T, Zipp F, Siffrin V.
The Journal of Neuroscience, 2015; *equally contributing

(5) ---

"Gatekeeper role of central nervous system $CD11c^+$ cells in neuroinflammation."

Siffrin V, Paterka M, Hoppmann N, Werr J, Voss JO, **Gollan R**, Belikan P, Birkenstock J, Bopp T, Esplugues E, Flavell RA, Zipp F.
The EMBO Journal, 2015

(6) ---

"FRET based ratiometric Ca^{2+} imaging to investigate immune-mediated neuronal and axonal damage processes in experimental autoimmune encephalomyelitis."

Siffrin V, Birkenstock J, Luchtman DW, **Gollan R**, Baumgart J, Niesner RA, Griesbeck O, Zipp F.
Journal of Neuroscience Methods, 2015

---

(7) *"Role of IL-17-producing lymphocytes in severity of multiple sclerosis upon natalizumab treatment."*

Bühler U, Fleischer V, Lüssi F, Rezk A, Graetz C, **Gollan R**, Wolf C, Lutz J, Bar-Or A, Siffrin V, Zipp F
Neurology, submitted

---

(8) *"In vivo and in vitro effects of multiple sclerosis immunomodulatory therapeutics on glutamatergic excitotoxicity."*

Luchtman D, **Gollan R**, Ellwardt E, Birkenstock J, Robohm K, Siffrin V, Zipp F
Journal of Neurochemistry, in revision

---

(9) "Perivascular microglia promote blood vessel disintegration in the ischemic penumbra."

Jolivel V, Bicker F, Binamé F, Ploen R, Keller S, **Gollan R**, Jurek B, Birkenstock J, Poisa-Beiro L, Bruttger J, Opitz V, Thal SC, Waisman A, Bäuerle T, Schäfer MK, Zipp F, Schmidt MH.
Acta Neuropathologica, 2015

---

(10) "Both Tumor Necrosis Factor Receptor Signaling Pathways Contribute to Mortality but not to Splenomegaly in Generalized Lymphoproliferative Disorder."

Wiede F, Roomberg A, Darby J, **Gollan R**, Körner H.
Antibodies, 2015

(11 "Non-Secreted Clusterin Isoforms Are Translated in Rare Amounts from Distinct Human mRNA Variants and Do Not Affect Bax-Mediated Apoptosis or the NF-κB Signaling Pathway."

Prochnow H, **Gollan R**, Rohne P, Hassemer M, Koch-Brandt C, Baiersdörfer M.
PLoS One, 2013

---

(12) "Redundancy of interleukin-6 in the differentiation of T cell and monocyte subsets during cutaneous leishmaniasis."

Kling J, **Gollan R**, Fromm P, Körner H.
Experimental Parasitology, 2011

1. Introduction

Multiple Sclerosis

Multiple sclerosis (MS) is a chronic demyelinating inflammatory and neurodegenerative autoimmune disease of the central nervous system (CNS) which commonly manifests in young adults, causing long-term neurological disability (Compston and Coles, 2008). MS most often begins with a relapsing-remitting course, characterized by inflammatory attacks, myelin destruction, reversible neurologic dysfunction, or residual deficit with variable periods of remission and merges into a secondary progressive form with a steady increase of disability accompanied by CNS atrophy and neurodegeneration (Figure 1).

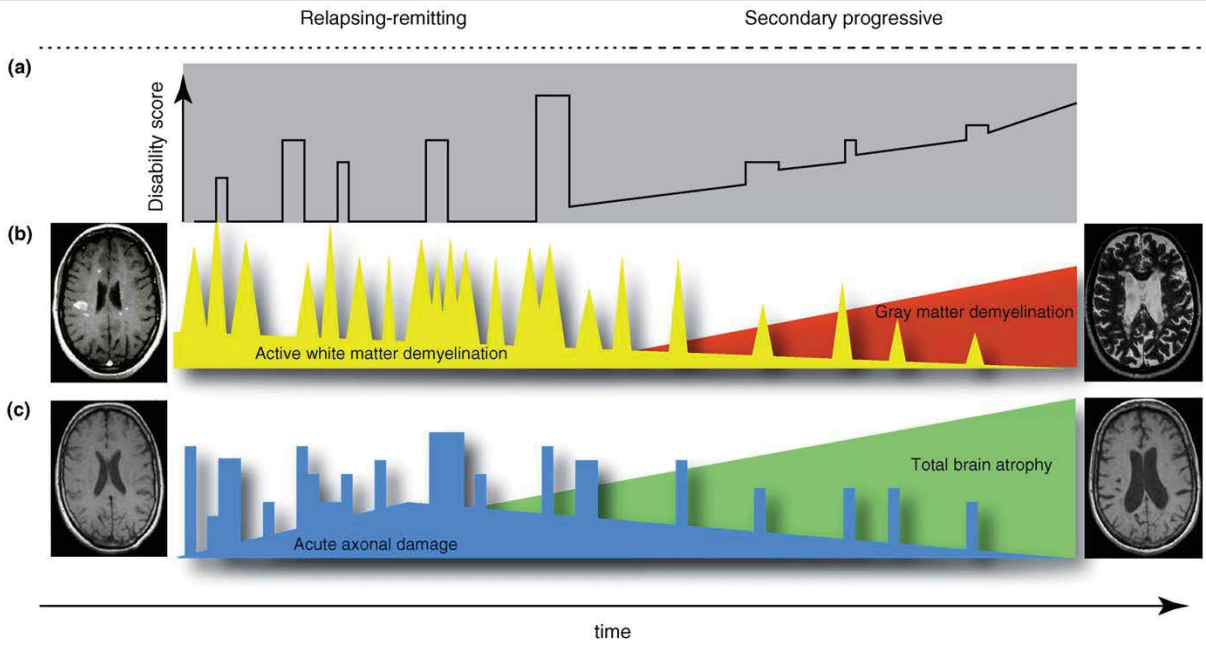

Figure 1: Schematic disease progression in multiple sclerosis (figure from Siffrin et al., 2010b)
(a) Progression of relapsing remitting MS passes into the secondary progressive form. Upper left MRI T1 picture shows correlation white matter plaques. (b) White matter demyelination occurs in severe recurrent attacks and declines over time replaced by steadily increasing gray matter impairment. (c) Acute axonal damage shares a similar pattern at the beginning of the disease and merges into a phase of massive tissue destruction accompanied with clinically creeping deterioration. Lower left and right MRI T1 pictures show brain atrophy at the beginning and in later stages, respectively. Upper right MRI T2 picture is another example for late stage atrophy.

According to our current understanding, MS is mainly driven by autoreactive inflammatory lymphocytes, in particular T cells, which are thought to orchestrate repetitive CNS invasion by immune cells, resulting in the destruction of the myelin sheath and the neuronal compartment (Merrill et al., 1992; Sawcer et al., 2011). This thesis focuses on the mechanisms behind T cell-mediated neuroinflammation.

Mechanisms behind T cell-mediated neuroinflammation

MS is based on a misguided immune response leading to both inflammatory demyelination and neuronal and axonal damage (Siffrin et al., 2007). In this context, neurodegeneration is linked to inflammation and demyelination in light of a variety of cellular interactions shaping distinct clinical manifestations in such a complex way, that an arrangement of these factors in a sequence from initiator to epiphenomenon has not been established yet. However, the identification of genetic risk factors for MS showed an evident overrepresentation of immune cell-associated, and in particular T cell-associated, genes (Sawcer et al., 2011). These findings underline the primary role of cells of the adaptive immune system in the pathophysiology of MS. A particular focus is put on CNS-reactive T cells considering their potential to invade the CNS and to contribute to the disease progression. Autoreactive T cells, which are also present in the healthy and balanced immune system, are supposed to cross the blood brain barrier (BBB) while being attracted by a chemokine gradient (Larochelle et al., 2011). In the perivascular compartment, T cells can be reactivated by local antigen presenting cells (APCs), possibly dendritic cells, and proceed to the CNS parenchyma (Siffrin et al., 2015a). Here they may initiate neuroinflammation accompanied with the recruitment of other immune cells via the release of cytokines and stressors, such as reactive oxygen species, as well as via cell contact-dependent mechanisms (Goverman, 2009). In parallel to their effector properties also regulatory functions of T cells are described (Kohm et al., 2002). Thus, bearing in mind that neuroinflammation in MS might comprise entirely distinct mechanisms in different progression states of the disease, the task to distinguish initiating crucial processes from protective, alongside or parallel occurring ones remains to be the core challenge of MS research.

Here, I summarized my work of the last four years on the mechanisms behind T cell-mediated neuroinflammation. Based on observations from our laboratory that $CD4^+$ T cells induce neurodegeneration in neuroinflammation (Siffrin et al., 2010b), we tested complementary the ability of CNS-antigen specific $CD8^+$ T cells to promote neuronal damage (Reuter, Gollan and Grohmann et al., 2015). This led to the general question of the impact and fate of distinct T cell subsets in the course of autoimmune neuroinflammation, especially during the second wave of CNS infiltration, which is addressed in the first part of this thesis (Figure 2, (1)).

Secondly a gatekeeper role of central nervous system CD11c$^+$ cells in neuroinflammation described recently by our group (Siffrin et al., 2015a) gave rise to the question whether sICAM-5 might act as a neuronal regulator of neuroinflammation by inhibiting locally the restimulation of T cells by APCs. This project is described in the second part (Figure 2, (2)).

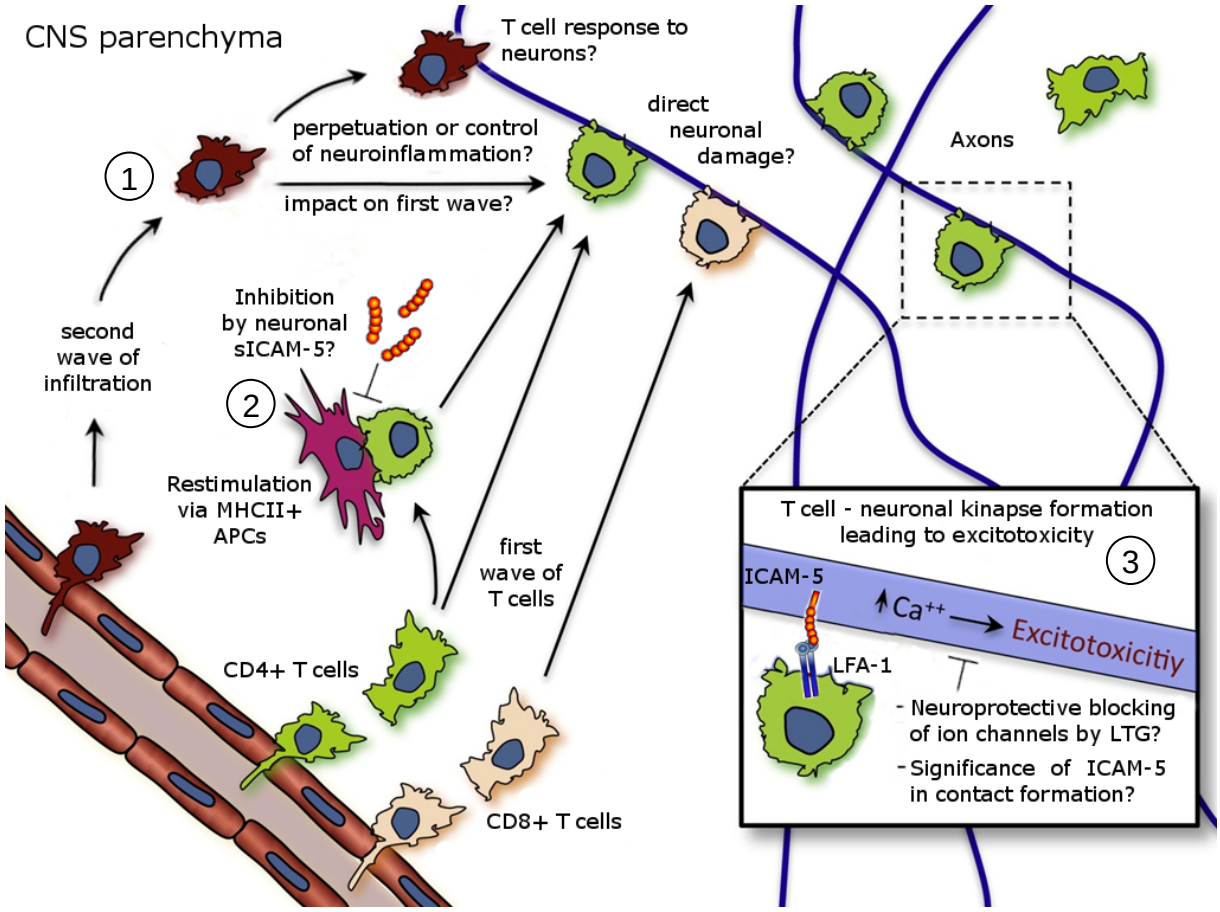

Figure 2: Mechanisms behind T cell-mediated neuroinflammation I (adapted from Egen and Ouyang, 2010)
T cell-mediated neuroinflammation begins with the infiltration of autoreactive CD4$^+$ and CD8$^+$ effector T cells into the CNS parenchyma. Here they may orchestrate repetitive immune invasions by the release of cytokines and stressors as well as via cell contact-dependent mechanisms. While the potential of different T cell subsets to invade the CNS and initiate neuroinflammatory processes is established, their capacity to modulate ongoing CNS inflammation, response to the neuronal compartment and to impact encephalitogenic T cell populations in the active and chronic phase of the disease is largely unexplored (1). CNS hosted APCs trigger the migration of T cells into and their survival within the CNS via antigen presentation and reactivation. A soluble form of the adhesion molecule ICAM5, shedded from the membrane of neurons, has the potential to block APC-T cell interaction *in vitro*, while its relevance *in vivo* is unclear (2). Neuronal and axonal Ca^{2+}-fluctuation occur as an early sign for T cell-contact induced damage and provides novel approaches for neuroprotective treatment by selective blocking of ion-channels during neuroinflammation. The role for membrane bound ICAM-5 during T cell-neuronal contact formation has not been investigated *in vivo* (3).

Finally, we addressed the question if blocking of axonal and neuronal ion channels may limit or even prevent neurodegeneration following neuroinflammation. To monitor the activity of calcium channels in neuroinflammation we developed a FRET based ratiometric calcium imaging technique in experimental autoimmune encephalomyelitis (Siffrin et al., 2015b). This subject is matter of the third and last part of this thesis (Figure 2, (3)).

1.1 Impact and fate of distinct T cell subsets in the course of autoimmune neuroinflammation

Autoreactive T cells are considered to be the initial driving force of autoimmune neuroinflammation in the context of MS and EAE. To gain insight into the impact of the distinct T cell subsets not only in the initial phase of the disease but also during ongoing inflammation could help to understand the instable chronic phase characterized by remissions and relapses. The fate of T cells might give hints on changing effector functions during disease progression and mutual influence between T cells.

T cells can be classified into two major groups depending on their expression of the surface receptors cluster of differentiation (CD) 8 and CD4, both subtype are specifically involved in antigen recognition via the major histocompatibility complex MHCI and II. Since the MHC-class II-related HLA-DR allele constitutes the main predisposing genetic risk factor for MS, $CD4^+$ T helper (Th) cells and their effector functions are in the focus of MS research (Liblau et al., 2013; Sawcer et al., 2011). In experimental autoimmune encephalomyelitis (EAE), an animal model mimicking aspects of MS pathology, the capacity of distinct $CD4^+$ T cell subsets to induce neuroinflammation (encephalitogenicity) has been well characterized. CNS antigen-specific Th1 and Th17 but not Th2 cells are capable of initiating severe debilitating neuroinflammatory processes (Jäger et al., 2009). Th1 cells have the ability to transfer EAE and secrete high amounts of pro-inflammatory cytokines, such as IFN-γ and TNF-α. Therefore, Th1 cells had been considered to be the main pathogenic subset in MS, although early experiments in IFN-γ KO animals showed unexpected exacerbation of the disease (Ferber et al., 1996). Differential deletion of IL-12 (Th1 promoting cytokine) vs. IL-23 (Th17 promoting cytokine) and more recently T-bet (Th1 promoting transcription factor) knockout experiments suggested a crucial role for IL-23 and the Th17 cell subset in this model (Cua et al., 2003; Grifka-Walk et al., 2013; Langrish et al., 2005; O'Connor et al., 2013). Th17 cells induce EAE efficiently as they can destabilize the blood-brain barrier, recruit immune cells to the CNS, and cause direct neuronal injury in mice and humans (Kebir et al., 2007; Siffrin et al., 2010b).

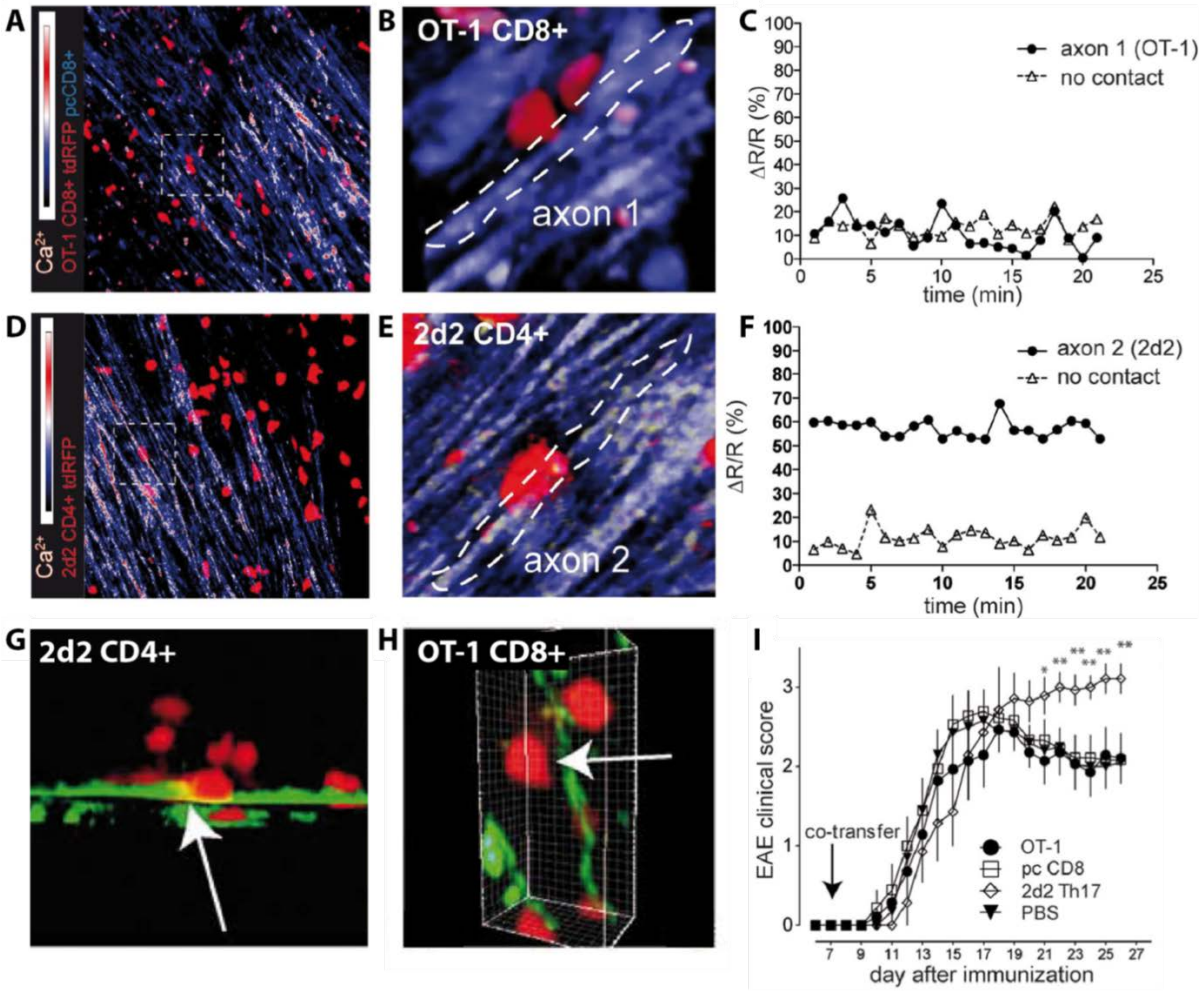

Figure 3: Among T cell CNS infiltration CD4$^+$ cells promote neuronal damage (adapted from Reuter, Gollan and Grohmann et al., 2015)

(A+D) Intravital TPLSM microscopy of the brain stem of anaesthetized mice reveals that, in EAE, CNS-antigen specific CD8$^+$ and CD4$^+$ T cells (red) infiltrate the CNS and interact with axons (blue). Strong contact formations of CD4$^+$ T cells and axons are formed shown by tightly enwrapped axons (green) by T lymphocytes (red) (G, arrow). In contrast CD8$^+$ T cell display a distance between axons and lymphocyte cell body suggesting a lack of direct interactivity with axons (H, arrow). The close contact formation of CD4$^+$ T cells and axons led to axonal thinning and an increase of axonal Ca^{2+} concentration as an early sign for axonal damage and imminent dissection (E, color-coded: blue = low [Ca^{2+}]; white = high [Ca^{2+}], (F) Time-laps measurement of [Ca^{2+}] in comparison to an axon without T cell contact). Axonal interaction with CD8$^+$ T cells was weakly associated with axonal Ca^{2+} increase (B+C). Consistently the transfer of CD8+ T cells in passive EAE mice did not accelerate disease progression, while the co-transfer of CD4$^+$ T cells induced disease exacerbation (I).

Both Th1 and Th17 cells have been associated with MS exacerbations and are found in MS lesions, and differential infiltration capacities of spinal cord or brain and even collaboration through Th1-facilitated CNS entry of Th17 cells has been proposed, indicating a pro-inflammatory contribution of the two subsets to EAE and MS (O'Connor et al., 2008; Rothhammer et al., 2011). In contrast, it has been suggested that regulatory T cells (T_{reg}) and

IL-4 producing Th2 cells do not transfer EAE but can be induced by disease-modifying therapies in MS and likely ameliorate T cell-mediated CNS-autoimmunity (Bettelli et al., 2007; Kohm et al., 2002; Walsh et al., 2015).

The detrimental consequence of $CD4^+$ T cell participation in neuroinflammation has been demonstrated by our laboratory in 2010 (Siffrin et al., 2010b). By using intravital time-resolved two-photon laser-scanning microscopy (TPLSM) of EAE lesions in the brainstem of living anaesthetized mice sustained interaction between autoreactive 2d2 (T cell receptor [TCR] specific for myelin oligodendrocyte glycoprotein specific [$MOG_{35–55}$]) $CD4^+$ T cells and neurons has been detected leading to neuronal damage. Those synapse- or kinapse-like, MHC-II independent contact formations occurred on the cell body as well as on processes of neurons leading to reversible and irreversible neuronal dysfunction visualized by Ca^{2+} fluctuations and axonal fragmentation (Fig 3 D, E, F, G). This process, which potentially induces excitotoxicity, has been shown particularly in the disease progression peak and was positively correlated to neuronal pathology and clinical disease severity suggesting $CD4^+$ T cells as inducers of neurodegeneration during neuroinflammation (Egen and Ouyang, 2010).

In line with their prevailing numbers in MS lesions $CD8^+$ T cells have also been reported as a capable disease inducing T cell subset (Huseby et al., 2001; Sun et al., 2001). However, several studies contradict this observation by displaying $CD8^+$ T cells as epiphenomena of $CD4^+$ T cell-mediated neuroinflammation (Leuenberger et al., 2013) or even infiltrates with regulatory properties (Najafian et al., 2003; Ortega et al., 2013). In our study, we determined that murine ovalbumin-transgenic (OT-1) $CD8^+$ T cells are targeted also against a CNS-antigen by recognizing $MOG_{40–54}$ both *in vitro* and in *vivo*. Such cross-recognizing $CD8^+$ T cells display recognition motility within the CNS leading to a selective enrichment in inflammatory lesions and interaction with the neuronal compartment (Figure 3 A, B, H). However, this did not result in clinically or subclinically significant damage, which is different from myelin-specific $CD4^+$ T cell autoimmune pathology (Figure 3 B, C, H, I). Therefore, intravital imaging demonstrates that local myelin recognition by autoreactive $CD8^+$ T cells in inflammatory CNS lesions alone is not sufficient to induce disability or increase axonal injury (Reuter, Gollan and Grohman et al., 2015). Although this does not exclude other pro-inflammatory and neurodegeneration-promoting mechanisms by $CD8^+$, we focused in the follow up projects on $CD4^+$ T cells.

Since MS is a multiphasic disease with receptive CNS-infiltration we continued our research by investigating the collaboration between distinct $CD4^+$ T cell subsets entering the CNS in different waves and their role in the perpetuation of ongoing neuroinflammation. While the potential of the different T cell subsets to invade the CNS and initiate neuroinflammatory processes is established, their capacity to modulate ongoing CNS inflammation and to impact encephalitogenic T cell populations in the active and chronic phase of the disease is largely unexplored. Moreover, differentiated $CD4^+$ Th cells have the potential to change their cytokine or even genetic signature depending on their microenvironment, known as plasticity and transdifferentiation, respectively, which might lead to distinct effector functions at different stages of the disease (Gagliani et al., 2015; Martinez-Sanchez et al., 2015). With the advance of human trials using blockers of T cell differentiation or transfers of differentiated T cells for therapeutic purposes, our aim in the first project to understand the capacity of the distinct $CD4^+$ subsets to modulate the course of EAE and MS is of clinical importance (Roncarolo and Battaglia, 2007).

We report that myelin-specific (2d2) Th1 and Th2 cells co-transferred 7 days after disease-induction by adoptive transfer EAE in lymphopenic hosts significantly attenuated the clinical course of EAE, as compared to co-transfer of Th17 cells. The co-transferred 2d2 Th1 and Th2 cells infiltrated the CNS less efficiently than 2d2 Th17. The co-transferred Th1 and Th2 cell populations modified the expression of cytokines of the disease-inducing CNS-infiltrating Th17 population. To analyze a potential modulation of CNS invading T cells by CNS endogenous cells, T cell co-cultures were performed with primary cortical neurons. Here, the pro-inflammatory $CD4^+$ T cell subsets showed differential results after contact with neurons. Th17 cells displayed higher IL-17 expression in response to contact with primary neurons in vitro, while the Th1 subset showed an enhanced IL-10 expression. Th2 did not change their cytokine profile. We conclude that Th1 and Th2 cells can improve the course of Th17-induced neuroinflammation, presumably by competing with Th17 cells, by promoting plasticity of the disease-inducing population, and by expressing a more protective cytokine profile in response to contact with CNS endogenous cells. This suggests that even after disease initiation, the influx of further Th17, Th1 and Th2 subsets will affect the CNS microenvironment differently, and contribute to either the perpetuation or control of ongoing neuroinflammatory processes.

1.2 sICAM-5 as a neuronal regulator of neuroinflammation

After elucidating the role of different T cell subsets in the induction and perpetuation of EAE, a following step in the cascade of T cell-mediated neuroinflammation is the reactivation of encephalitogenic T cells and their contact formation with neurons via adhesion proteins.

Adhesion proteins play a central role in the mechanisms of T cell-mediated neuroinflammation. Throughout the pathogenesis of MS or EAE adhesion proteins are crucial beginning with the entry of T cells into the CNS through the BBB, the reactivation of T cells via APCs and finally during the contact-dependent attack of neurons (Larochelle et al., 2011; Siffrin et al., 2010b, 2015a). Intercellular adhesion molecule-5 (ICAM-5 or telencephalin), is an adhesion protein belonging to the immunoglobulin (Ig) superfamily subset of five distinct ICAMs binding to β2 integrins (Ning et al., 2012). Its structure comprises a NH_2-terminal signal peptide, a characteristic extracellular region with nine Ig-like domains, a single transmembrane region, and a COOH-terminal cytoplasmic tail and is highly conserved between mice and humans (Yang, 2012). In the adult mammalian brain ICAM-5 is exclusively expressed in the somatodendritic membranes of telencephalic neurons, while, in rodents, it can be detected in the hippocampus, amygdala, caudate nucleus, striatum, olfactory cortex, and neocortex (Oka et al., 1990). The protein has been suggested to function in the synaptogenesis in the developing brain since its expression correlates with postnatal CNS maturation including dendritic elongation and branching (Yang, 2012). But also its participation in immune system interactions through its leukocyte β2 integrin binding site has been proposed.

The Gahmberg laboratory has demonstrated that ICAM-5 binds to the integrin receptor CD11a/CD18 (LFA-1), which is expressed by lymphocytes and serves as a ligand for T cells to adhere on neurons (Tian et al., 1997, 2000). Furthermore, a LFA-1-dependend neuronal interaction with microglia leading to rapid cell spreading was reported (Mizuno et al., 1999). We showed that direct interaction of T cells and neuronal cells in demyelinating lesions was associated with extensive axonal damage (Figure 3). By combining confocal, electron, and intravital microscopy, we demonstrated that these contacts remarkably resembled immune synapses or kinapses, albeit with the absence of potential T cell receptor engagement. Quantification of dead ($TUNEL^+$) neurons in co-cultures with T cells showed similar impact of T cell with MHCII-deficiency compared to WT T cells and reduced cell death induction in

the absence of LFA-1 (Itgal$^{-/-}$) on Th17 cells (Siffrin et al., 2010b). Moreover, IL-25 prevents T cell mediated neurotoxicity by decreasing LFA-1 expression (Turner et al., 2013). Additionally, translation to the human system revealed that vulnerability of neurons to T cell-mediated cytotoxicity is LFA-1 dependent (Giuliani et al., 2003). This led to the hypothesis that LFA-1 dependent adhesion of T cells to neurons with ICAM-5 as the potential neuronal counterpart is driving contact-induced neurodegeneration in chronic neuroinflammation.

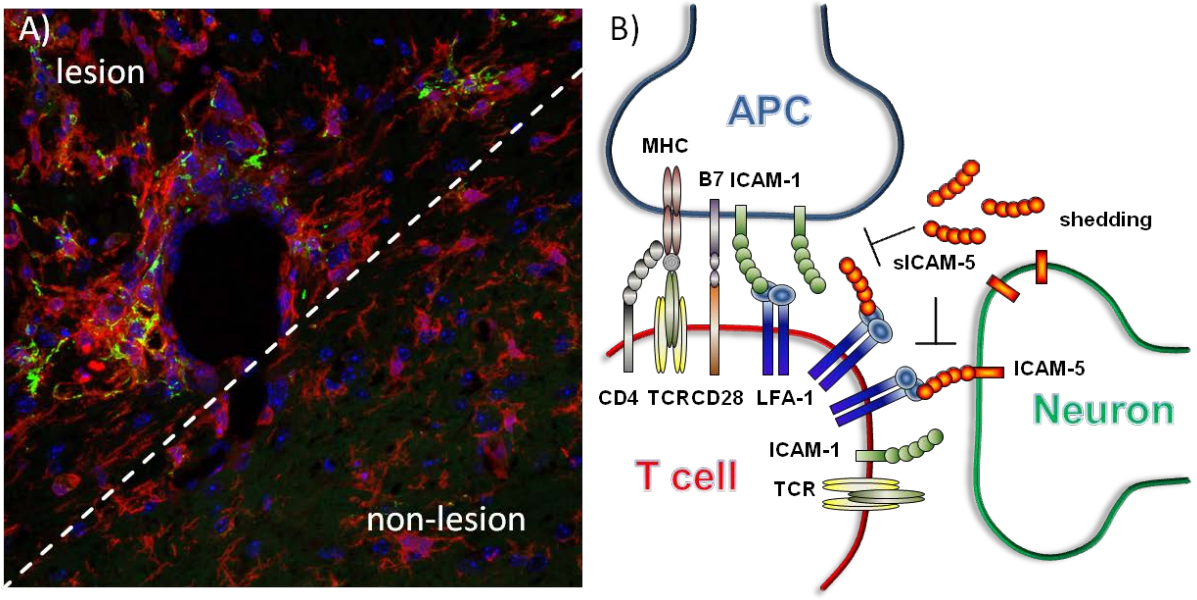

Figure 4: Ambivalent mechanisms of action of ICAM-5 in the CNS

(A) Lesion in the brainstem of an EAE mouse. An accumulation of cells (DAPI: blue, nuclei) indicating immune cell infiltration can be seen around a blood vessel. Neuroinflammation is accompanied by the activation of resident microglia (Iba1: red) and destruction of neurons (DAPI, huge, inhomogeneous nuclei). CD11c^{+} cells (green) serving as APCs are located closely to the blood vessel presumably influencing T cell entry and restimulation in the CNS.

(B) In its soluble form, ICAM-5, a ligand for LFA-1 on neuronal side, inhibits activation and proliferation of T cells in the presence of APCs and antigens by blocking ICAM-1 and LFA-1 interaction. Furthermore, sICAM-5 is considered to block contact formation between T cells and neurons. The blockade of T cell-neuronal interaction is probably realized by inhibiting the interaction of LFA-1 with membrane bound neuronal ICAM-5 or other LFA-1 ligands. Therefore, shedding of ICAM-5 on neurons might be a neuronal defense mechanism to limit the immune response and destructive T cell-neuronal interactions in inflamed CNS regions. In contrast membrane bound neuronal ICAM-5 serves as an adhesion molecule for the attachment of T cells on neurons potentially leading to neuronal dysfunction.

However, the potentially relevant immunofunctional role of ICAM-5 in the CNS is ambivalent (Figure 4). Through cleavage by matrix metalloproteinase (MMP)-2 and 9 the extracellular domain of ICAM-5 can be shedded from neuronal membranes resulting in soluble ICAM-5 (sICAM5) fragments (Tian et al., 2007). Under homeostatic conditions

sICAM-5 acts in an autoregulatory feedback loop on neuronal excitability and glutamatergic transmission (Lonskaya et al., 2013; Niedringhaus et al., 2012). Most interestingly, in the context of CNS inflammation, shedded ICAM-5 attenuated T-cell receptor-mediated activation of T cells via APCs *in vitro* (Tian et al., 2008). Interaction between T cells and APCs led to the recruitment and reactivation of T cells in the CNS and triggers the perpetuation of inflammation (Siffrin et al., 2015a). The immunosuppressive effect of sICAM5 is achieved by blockage of ICAM-1 and LFA-1 interaction at the immunologic synapse between T cells and APCs (Tian et al., 2008). Moreover activation of NMDA receptors, which might occur during T cell attacks on neurons leads to an enhanced MMP-mediated ICAM-5 cleavage (Siffrin et al., 2010b; Tian et al., 2007). This led to the second hypothesis that sICAM-5 is involved in neuronal regulation of ongoing neuroinflammation and acts as an anti-inflammatory agent by inhibiting T cell-APC interaction.

To address the two hypotheses of the significance of membrane bound ICAM-5 and in particular sICAM-5 in the context of neuroinflammation we performed EAEs with ICAM-5 KO animals and T cell-APC co-cultures in this thesis. Interestingly, we could demonstrate a more severe disease progression in ICAM-5 KO mice and an anti-inflammatory potential of sICAM5 *in vitro* and *in vivo*.

1.3 Preventing neurodegeneration in neuroinflammation by ion channel blocking

As soon as activated encephalitogenic T cells form contact with neurons they induce neuronal dysfunctions potentially leading to damage of neuroaxonal structures as a final consequence of T cell-mediated neuroinflammation.

Early damage of neuroaxonal structures has been recognized as a major aspect of MS pathology (Trapp et al., 1998). Spinal cord atrophy correlates with disability in MS (Bjartmar et al., 2000) and was already found in patients with clinically isolated syndrome - a very early phase preceding MS. However, also grey matter involvement, i.e. significant focal cortical thinning and thalamic neurodegeneration, was demonstrated even early in the disease course of MS patients (Chard et al., 2002). Magnetic resonance spectroscopic imaging (MRSI) has confirmed that atrophy is associated with loss of the neuronal marker, N-acetylaspartate (Wylezinska et al., 2003).

In order to be able to develop targeted therapies, the underlying causes need to be fully understood. Neuronal damage and axonal damage may not have the same causes and may be addressed differently (Herz et al., 2010). The knowledge about the actual mode of damage of the distinct parts of the neuronal compartment is of great interest as current therapy regimen addresses the neurodegenerative part of the disease only unsatisfactorily, in particular in patients with advanced disease.

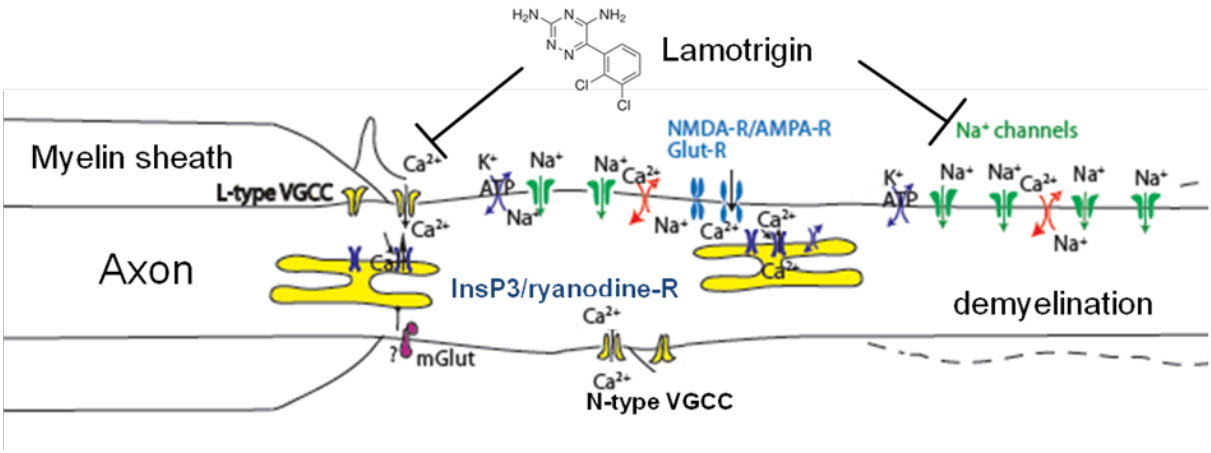

Figure 5: Mechanisms of neurodegeneration in neuroinflammation

The inflammatory milieu in neuroinflammation triggers a cascade of detrimental events finally leading to neurodegeneration. Initiating events like the CNS invasion of T cells promote demyelination of axons causing a redistribution of sodium channels to restore electrical nerve conduction. As a side effect, intracellular sodium accumulation occurs challenging the Na^+/K^+ ATPase to buffer increasing intracellular Na^+ levels. However, this compensation mechanism is disturbed due to energy failure caused by dysfunctional mitochondria accompanying neuroinflammation. Moreover, an upregulation of Na^+/Ca^{++} exchanger kicks in to partially stabilize intracellular sodium concentrations. Consequently, as a substitute for sodium, intracellular calcium accumulates. Furthermore, sensitized NMDA/AMPA receptors and voltage-gated calcium channels contribute to sustained elevated calcium levels, which finally lead to neurodegeneration. Lamotrigine as a blocker of sodium and voltage gated calcium channels (VGCC) might counteract this cascade and prevent neuronal cell death in neuroinflammation.

Various mechanisms, which may contribute to axonal and neuronal damage in chronic inflammation of the CNS, have been proposed. The primary role of intracellular increase of free $[Ca^{2+}]$ has been the center of many hypotheses of neurodegeneration (DeCoster, 1995). Several mechanisms have been described to be potentially responsible for this first step of neuronal damage formation. The role of excitotoxicity by extracellular glutamate, the main excitatory neurotransmitter in the CNS, has been investigated and supported by us and others (Basso et al., 2008; Kanwar et al., 2004; Pitt et al., 2000; Sühs et al., 2014). The modulation of this pathway is however difficult to translate into clinical settings, where side effects limit the use of related drugs (Muir and Lees, 1995; Villoslada et al., 2009). A second - indirect -

mechanism of intracellular free [Ca^{2+}] elevation relies on the increase of intracellular Na^+ through voltage-gated Na^+ channels for axon potential propagation and secondary reversal of the Na^+/Ca^{2+} antiporter due to a lack of ATP which is needed for this antiporter (Ellwardt and Zipp, 2014; Figure 5). Several Na^+-blocking drugs have been investigated for their effect on clinical signs in EAE. In particular, phenytoin and lamotrigine (LTG) have been described to be protective in models of MS (Bechtold et al., 2006; Lo et al., 2003). However, clinical studies have been - so far - disappointing (Hayton et al., 2012; Kapoor et al., 2010).

The knowledge about the actual mode of the damage processes of the axono-glial unit in autoimmune neuroinflammation is of critical importance to therapeutically target the loss of neurons in the disease. Therefore, a better understanding of the processes leading to the axonal damage formation is needed. Since its development in 1990 two-photon laser scanning microscopy (TPLSM) has tremendously contributed to understanding pathologic processes within the inflamed brain, in particular with respect to immune cell invasion into the CNS (Kawakami et al., 2005; Leuenberger et al., 2013; Odoardi et al., 2007; Schulze-Topphoff et al., 2009; Siffrin et al., 2009), but also tissue damage (Nikić et al., 2011; Siffrin et al., 2010b). We showed that imaging [Ca^{2+}] dynamics in axons and neurons by genetically expressed [Ca^{2+}] sensors is possible *in vivo* in the brainstem of living anesthetized mice (Siffrin et al., 2015b) and that intraaxonal and intraneuronal free [Ca^{2+}] are altered in EAE.

Here, we investigated the role of LTG - an antiepileptic drug with different effector mechanisms - on different aspects of neuronal damage formation by using intravital TPLSM in EAE. We dissected the role of different doses on distinct parts of the neuronal compartment, i.e. myelinated axons and neuronal somata, and on the immune system. We identified a reduction of intraneuronal free [Ca^{2+}] in low-dose LTG conditions but not in axons or if given in high-dose. A clinical study in mice supported our findings that low-dose LTG is superior to high-dose regimen for the improvement of clinical deficits during an attack of EAE.

1.4 Summary and aim of the thesis

Taken together the aim of this thesis was to give new insights into the mechanisms of T cell-mediated neuroinflammation. This includes a definition of the contribution of distinct Th cells towards the perpetuation of CNS inflammation, followed by the description of a potential neuronal defense mechanism as a response to harmful inflammatory conditions, and finally to test novel approaches to prevent neuronal degeneration as a consequence of the detrimental cascade of T cell-mediated neuroinflammation (Figure 2).

2. Materials & Methods

2.1 Materials

2.1.1 Buffers & Chemicals & Medications

Compound	Company
4′,6-Diamidino-2-phenylindole dihydrochloride (DAPI)	Sigma-Aldrich Corp., St Louis (USA)
Albumin bovine, cell culture grade (BSA)	Serva Electrophoresis GmbH, Heidelberg (Germany)
Aqua bi. dest. sterile	B. Braun AG, Melsungen (Germany)
Brefeldin A	Sigma-Aldrich Corp., St Louis (USA)
Dimethyl Sulfoxide (DMSO)	Sigma-Aldrich Corp., St Louis (USA)
Dulbeccos PBS w/o Ca2+ & Mg2+ (PBS [-])	Gentaur, Kampenhout (Belgium)
Dulbeccos PBS with Ca^{2+} & Mg^{2+} (PBS [+])	Gentaur, Kampenhout (Belgium)
Ethanol 70% + 100 % (v/v) (EtOH)	AppliChem GmbH, Darmstadt (Germany)
Fetal Bovine Serum, heat inactivated (FBS)	Biochrom AG, Berlin (Germany)
Fixation/Permeabilization Concentrate and Diluent	eBioscience Inc., San Diego (USA)
Fluorescent Mounting Medium	Dako, Carpinteria (USA)
General Chemicals	Merck KGaA, Darmstadt, (Germany), Sigma-Aldrich Corp., St Louis (USA)
Hank's Balanced Salt Solution w/o Ca^{2+} and Mg^{2+} (HBSS [-])	Life Technologies Corp., Grand Island (USA)
Hank's Balanced Salt Solution with Ca^{2+} and Mg^{2+} (HBSS [+])	Life Technologies Corp., Grand Island (USA)
HEPES	Life Technologies Corp., Grand Island (USA)
Isoflurane	Abbot, Wiesbaden (Germany)
Isotonic Ringer solution	B. Braun AG, Melsungen (Deutschland)
Ketamin	Curamed (Germany)
Lamotrigine	Sigma-Aldrich Corp., St Louis (USA)
Percoll	Sigma-Aldrich Corp., St Louis (USA)
Permeabilization Buffer (10x)	eBioscience Inc., San Diego (USA)
Poly-D-lysine hydrobromide, average mol wt 30,000-70,000, lyophilized powder	Sigma-Aldrich Corp., St Louis (USA)
Propidium iodide (PI)	Sigma-Aldrich Corp., St Louis (USA)
Saponine	Carl Roth GmbH & Co. KG, Karlsruhe (Germany)
Triton-X	Sigma-Aldrich Corp., St Louis (USA)
Trypan blue	Sigma-Aldrich Corp., St Louis (USA)

Compound	Company
Urbason® (dry ampoule, 16 mg) active substance: Methylprednisolone	Sanofi-aventis GmbH, Wien (Austria)
Xylazinhydrochloride (2 %)	Bayer Health Care, Leverkusen (Germany)
β-Mercaptoethanol	Sigma-Aldrich Corp., St Louis (USA)

Self-made Buffer	Ingredients
FACS Buffer	0.5 % BSA (i.e. 5 g/l) in PBS [+]
Lysis Buffer	NH_4Cl (8.29 g/l) $KHCO_3$ (i.e. 1 g/l) NA_2EDTA (i.e. 37.2 mg/l) in dH_2O
MACS Buffer	0.5 % BSA (i.e. 5 g/l) 0.5 M EDTA (i.e. 4 ml/l) in PBS
Paraformaldehyde (PFA) buffer 4 %	40 g Paraformaldehyde + 1000 ml 0,1 M PBS buffer, pH 7.0 – 7.4
Saponine Buffer	0.5% Saponine 0.5 % BSA in PBS [+]

2.1.2 Labware & Equipment

Product	Company
Cell Culture Dish, polystyrene, Ø 60 mm + 100 mm	Greiner Bio-One GmbH, Frickenhausen (Germany)
Cell strainer, nylon mesh, 100 µm	BD Bioscience, Franklin Lakes (USA)
Centrifuge Tubes, polyethylene-terephthalate (PET), 15 ml + 50 ml	Corning Inc., Corning (USA)
Centrifuge Tubes, polypropylene (PP), 15 ml + 50 ml	Greiner Bio-One GmbH, Frickenhausen (Germany)
Cryo tubes	Thermo Fisher Scientific Inc., Waltham (USA)
Eppendorf Tubes 1.5 ml + 2 ml	Eppendorf GmbH, Wesseling-Berzdorf (Germany)
Glass Coverslips Ø 10 mm	Menzel GmbH, Braunschweig Germany
MACS LS Columns	Miltenyi Biotec GmbH, Bergisch Gladbach (Germany)
Microscope glass slides	Thermo Fisher Scientific Inc., Waltham (USA)

Product	Company
Multiwell Plate, tissue-culture treated polystyrene, 24-well, 48-well, 96-well	BD Bioscience, Franklin Lakes (USA)
Pasteur pipettes, cotton plugged, L 9-in.	Sigma-Aldrich Corp., St Louis (USA)
Petri Dish, glass, 150x160x30mm	Sciencelab.com, Inc. Houston (USA)
Pipette tips	VWR International GmbH, Darmstadt (Germany)
Polystyrene Round Bottom Test Tubes 5 ml (FACS tubes)	BD Bioscience, Franklin Lakes (USA)
Pre-Separation Filters, 30 µm	Miltenyi Biotec GmbH, Bergisch Gladbach (Germany)
Scalpels	B. Braun AG, Melsungen (Deutschland)
Serological Pipettes, polystyrene, 5 ml + 10 ml + 25 ml	Greiner Bio-One GmbH, Frickenhausen (Germany)
Syringe, 2 ml	B. Braun AG, Melsungen (Deutschland)

2.1.3 Cell Culture Reagents & Supplements

Reagent	Company
B-27 Serum-Free Supplement (50X), liquid	Life Technologies Corp., Grand Island (USA)
Collagenase	R&D Systems, Inc., Minneapolis (USA)
Dispase	R&D Systems, Inc., Minneapolis (USA)
DNase I, recombinant grade I from bovine pancreas, expressed in Pichia pastoris	F. Hoffmann-La Roche AG, Basel
huTGF-β	R&D Systems, Inc., Minneapolis (USA)
IL-12	R&D Systems, Inc., Minneapolis (USA)
IL-18	R&D Systems, Inc., Minneapolis (USA)
IL-2	R&D Systems, Inc., Minneapolis (USA)
IL-23	R&D Systems, Inc., Minneapolis (USA)
IL-4	R&D Systems, Inc., Minneapolis (USA)
IL-6	R&D Systems, Inc., Minneapolis (USA)
IMDM	Life Technologies Corp., Grand Island (USA)
L-Glutamine	Life Technologies Corp., Grand Island (USA)
MOG_{35-55}, sequence: M E V G W Y R S P F S R V V H L Y R N G K	Pepceuticals Ltd., Leicestershire (UK)
Neurobasal Medium, w/o Glutamine (NBM [-])	Life Technologies Corp., Grand Island (USA)
Penicillin / Streptomycin (P/S)	Life Technologies Corp., Grand Island (USA)
RPMI 1640	Life Technologies Corp., Grand Island (USA)
Trypsin 2.5 %, w/o phenol red	Life Technologies Corp., Grand Island (USA)
Trypsin-EDTA 0.05 %, with phenol red	Life Technologies Corp., Grand Island (USA)

Medium	Ingredients
Artificial Cerebrospinal Fluid (ACSF)	124 mM NaCl (i.e. 7.247 g/l) 138 mM NaH2PO4*H2O (i.e. 172 mg/l) 198 mM Glucose*H2O (i.e. 1.982 g/l) 120 mM MgSO4 (i.e. 217 mg/l) 147 mM CaCl2*2H2O (i.e. 235 mg/l) 75 mM KCl (i.e. 224 mg/l) 26 mM NaHCO3 (i.e. 2.184 g/l)
Cell Freezing Medium	90% FCS 10 % DMSO
Mouse Medium (MM)	10 % FCS 1 % P/S (100U/ml / 100 µg/ml) 1% L-Glutamine (2 mM) 0.1 % β-Mercaptoethanol 1 % HEPES (1 M) in RPMI 1640
Neurobasal Medium + supplements (NBM [+])	1 % L-Glutamine (2 mM) 1% P/S (100U/ml / 100 µg/ml) 2% B-27 in Neurobasal Medium
Wash Medium (WM)	5 % FCS 1 % P/S (100U/ml / 100 µg/ml) 1 % HEPES (1 M) in RPMI

2.1.4 Kits & Assays

Kit system	Company
CD4 T Cell Isolation Kit	Miltenyi Biotec GmbH, Bergisch Gladbach (Germany)
$CD4^+CD62L^+$ T Cell Isolation Kit	Miltenyi Biotec GmbH, Bergisch Gladbach (Germany)
Hooke Kit™ MOG_{35-55}/CFA Emulsion + PTX	Hooke Laboratories, Inc. Lawrence (USA)
In Situ Cell Death Detection Kit, TMR red	F. Hoffmann-La Roche AG, Basel, (Switzerland)

2.1.5 Antibodies & MicroBeads

Antibody	Isotype	Concentration	Company
CD16/CD32 (FC-block) clone: 2.4G2	rat-α-mouse monoclonal IgG2b κ	0.5 mg	BD Bioscience, Franklin Lakes (USA)
CD25-PE-Cy7 clone: PC61	rat-α-mouse monoclonal IgG1, λ	0.2 mg/ml	BD Bioscience, Franklin Lakes (USA)
CD28 clone: H57-597	hamster-α-mouse monoclonal IgG2, λ1	0.5 mg/ml	BD Bioscience, Franklin Lakes (USA)
CD3-APC clone: 1452-C11	hamster-α-mouse monoclonal IgG1, κ	0.2 mg/ml	BD Bioscience, Franklin Lakes (USA)
CD3e clone: 1452-C11	hamster-α-mouse monoclonal IgG1 κ	0.5 mg/ml	BD Bioscience, Franklin Lakes (USA)
CD3e-FITC clone: 1452-C11	hamster-α-mouse monoclonal IgG1, κ	0.2 mg/ml	BD Bioscience, Franklin Lakes (USA)
CD3-PE clone: 1452-C11	hamster-α-mouse monoclonal IgG1, κ	0.2 mg/ml	BD Bioscience, Franklin Lakes (USA)
CD45-eFluor605 clone: 30-F11	rat-α-mouse polyclonal IgG	0.5 mg/ml	BD Bioscience, Franklin Lakes (USA)
CD4-AF647 clone: RM4-5	rat-α-mouse monoclonal IgG2a	0.1 mg/ml	Life Technologies Corp., Grand Island (USA)
CD4-FITC clone: RM4-5	rat-α-mouse monoclonal IgG2a, κ	0.5 mg/ml	BD Bioscience, Franklin Lakes (USA)
CD4-Horizon(V450) clone: RM4-5	rat-α-mouse monoclonal IgG2a, κ	0.2 mg/ml	BD Bioscience, Franklin Lakes (USA)
CD4-PE-Cy7 clone: RM4-5	rat-α-mouse polyclonal IgG	0.2 mg/ml	BD Bioscience, Franklin Lakes (USA)
CD62L-APC clone: MEL-14	rat-α-mouse monoclonal IgG2a, κ	0.2 mg/ml	BD Bioscience, Franklin Lakes (USA)
Cleaved Caspase-3 (Asp175)	rabbit-α-mouse polyclonal IgG	n/a	.Cell Signaling Technology Inc., Danvers (USA)
Foxp3-PE clone: FJK-16s	rat-α-mouse monoclonal IgG2a, κ	0.1 mg/ml	eBioscience Inc., San Diego (USA)
FoxP3-PeCy7 clone: FJK-16s	rat-α-mouse monoclonal IgG2, κ	0.1 mg/ml	eBioscience Inc., San Diego (USA)
Gata-3-PE clone: TWAJ	rat-α-mouse monoclonal IgG2b, κ	0.1 mg/ ml	eBioscience Inc., San Diego (USA)
Glial Fibrillary Acid Protein (GFAP)	rabbit-α-mouse polyclonal IgG	n/a	Life Technologies Corp., Grand Island (USA)
IFN-γ clone: XMGl.2	rat-α-mouse monoclonal IgG1, κ	1 mg/ml	eBioscience Inc., San Diego (USA)

Antibody	Isotype	Concentration	Company
IFN-γ-Horizon (V450) clone: XMG1.2	rat-α-mouse monoclonal IgG1, κ	0.2 mg/ml	BD Bioscience, Franklin Lakes (USA)
IL-10-APC clone: JES5-16E3	rat-α-mouse monoclonal IgG	0.2 mg/ml	BD Bioscience, Franklin Lakes (USA)
IL-12/23 p40 clone: C17.8	rat-α-mouse monoclonal IgG1, κ	1 mg/ml	eBioscience Inc., San Diego (USA)
IL-17A-AF647 clone: TC11-18H1O	rat-α-mouse monoclonal IgG1, κ	0.2 mg/ml	BD Bioscience, Franklin Lakes (USA)
IL-17A-PE clone: TC11-18H1O	rat-α-mouse monoclonal IgG1, κ	0.2 mg/ml	BD Bioscience, Franklin Lakes (USA)
IL-17-FITC clone: eBio 17B7	rat-α-mouse monoclonal IgG1, κ	0.2 mg/ml	eBioscience Inc., San Diego (USA)
IL-4 clone: 11B11	rat-α-mouse monoclonal IgG1, κ	1 mg/ml	eBioscience Inc., San Diego (USA)
IL-4-PE clone: 11b11	rat-α-mouse monoclonal IgG1, κ	0.2 mg/ml	BD Bioscience, Franklin Lakes (USA)
Neuronal Nuclei (NeuN)	mouse-α-mouse monoclonal IgG	1 mg/ml	Millipore, Billerica (USA)
RoRγ(t)-APC clone: B2D	rat-α-mouse monoclonal IgG2a	0.1 mg/ml	eBioscience Inc., San Diego (USA)
T-bet-Horizon (V450) clone: 4BIO	rat-α-mouse monoclonal IgG2a	0.5 mg/ml	BD Bioscience, Franklin Lakes (USA)
TNF-α-AF700 clone: MP6-XT22	rat-α-mouse monoclonal IgG1, κ	0.2 mg/ml	BD Bioscience, Franklin Lakes (USA)
α-mouse-AF488	goat-α-mouse polyclonal IgG	2 mg/ml	Life Technologies Corp., Grand Island (USA)
α-rabbit-AF568	goat-α-rabbit polyclonal IgG	2 mg/ml	Life Technologies Corp., Grand Island (USA)

MicroBeads	Isotype	Company
CD8a (Ly-2) MicroBeads	mouse-α-mouse monoclonal IgG2a	Miltenyi Biotec GmbH, Bergisch Gladbach (Germany)
CD90.2 MicroBeads	rat-α-mouse monoclonal IgG2b	Miltenyi Biotec GmbH, Bergisch Gladbach (Germany)
CD4 (L3T4) MicroBeads (mouse)		

2.1.6 Instruments

Instrument	Company
Analog Vortex Mixer	VWR International GmbH, Darmstadt (Germany)
BD FACS Canto II	BD Bioscience, Franklin Lakes (USA)
Binocular Microscope Leica 56D	Leica Mikrosysteme Vertrieb GmbH, Wetzlar (Germany)
Cell Counting Chamber Neubauer improved	Brand , Wertheim (Germany)
Cell Culture Incubator	Binder GmbH, Tuttlingen (Germany)
Cell Culture Microscope, bright field	Hund, Wetzlar (Germany)
Centrifuge Heraeus Fresco 21	Thermo Fisher Scientific Inc., Waltham (USA)
Confocal Laser Scanning System SP8	Leica GmbH, Wetzlar, (Germany)
Eppendorf Research Adjustable-volume Pipettes	Eppendorf GmbH, Wesseling-Berzdorf (Germany)
Fluorescence Microscope IX5I, invert	Olympus Soft Imaging Solutions GmbH, Münster (Germany)
Horizontal Laminar Flow Hood Heraguard	Thermo Fisher Scientific Inc., Waltham (USA)
MidiMACS and QuadroMACS Separators	Miltenyi Biotec GmbH, Bergisch Gladbach (Germany)
Multifuge Heraeus XIR	Thermo Fisher Scientific Inc., Waltham (USA)
Pipetus	Hirschmann Laborgeräte GmbH & Co.KG, Eberstadt (Germany)
Surgery Instruments	Fine Science Tools Inc., Heidelberg (Germany)
Vertical Laminar Flow Hood SAFE 2020	Thermo Fisher Scientific Inc., Waltham (USA)
Water bath Aqualine AL18	Lauda GmbH & CO. KG, Lauda-Königshofen (Germany)
Two-Photon Laser Scanning microscopy (TPLSM) system including:	
Harvard Apparatus Advanced	Hugo Sachs, March-Hugstetten (Germany)
MaiTai Laser	Spectra Physics, Irvine (USA)
Olympus BX51 WI upright microscope	Olympus Soft Imaging Solutions GmbH, Münster (Germany)
Optical Parametric Oscillator (OPO)	APE, Berlin (Germany)
Scan Head	La Vision BioTec GmbH, Bielefeld (Germany)

2.1.7 Software

Software	Company
analySIS 5.0	Olympus Soft Imaging Solutions GmbH, Münster (Germany)
FlowJo	Tree Star, Ashland (USA)
GraphPad Prism 5	GraphPad Software, Inc., La Jolla (USA)
Illustrator CS5	Adobe Systems Inc., San Jose, (USA)
ImageJ	National Institutes of Health, Bethesda (USA)
MacBiophotonics ImageJ	MacMaster Biophotonics Facility, Hamilton (Canada)
Neurolucida	MBF Bioscience, Williston (USA)
Office 2007/2010	Microsoft Corp., Redmond (USA)
Photoshop CS5	Adobe Systems Inc., San Jose, (USA)
Volocity 3D Image Analysis Software	PerkinElmer, Inc. - Improvision, Waltham (USA)
FACSDiva	BD Bioscience, Franklin Lakes (USA)
Origin	OriginLab Software Corp., Northampton (USA)

2.1.8 Mouse strains

Strain	Laboratory
B6.2d2 CD90.1	Waisman Laboratory, Mainz (Germany)
B6.2d2 CD90.2	Kuchroo Laboratory, Boston (USA)
B6.ICAM5-KO	Gahmberg Laboratory, Helsinki (Finland)
B6.IL17EGFP.acRFP.2d2	Max-Delbrück-Centrum für Molekulare Medizin, Berlin (Germany)
B6.Rag2-KO	Max-Delbrück-Center for Molecular Medicine (Germany)
B6.Thy1.TNXXL	Max Planck Institute of Neurobiology, Martinsried (Germany)
C57BL/6J (B6)	Janvier Labs, Laval (France)

All animals were raised and kept under specifically pathogen free (SPF) conditions in individually ventilated cages during experiments at the University Medical Center of the Johannes Gutenberg-University Mainz. C57BL/6 mice were purchased from Janvier (France). B6.Rag2$^{-/-}$ (B6(Cg)-Rag2$^{tm1.1Cgn}$/J) mice, which do not have any B or T cells, were originally derived from the Max-Delbrück-Center for Molecular Medicine in Berlin. B6.2d2 (C57BL/6-Tg$^{(Tcra2d2,Tcrb2d2)1Kuch}$/J) are C57BL/6J CD90.1^{+} or CD90.2^{+} mice, in which all CD4^{+} T cells are MOG_{35-55} specific, were originally generated by the Kuchroo laboratory and obtained from the Waisman laboratory. The use of the C57BL/6J CD90.1^{+} or CD90.2^{+} congenic strains is useful

because they carry two distinct T lymphocyte specific Thy1a (Thy1.1) alleles. CD90.1+ T cells can be easily distinguished from CD90.2+ T cells during passive EAE experiments (2.2.13.2) by both flow cytometry (2.2.4). B6.IL17EGFP.acRFP.2d2 mice are B6.2d2 mice with ubiquitous tdRFP-expression under a ROSA26 promotor and EGFP-expression under the IL-17 promotor, thus serving as IL-17-reporter mice. B6.thy1-TN-XXL mice neuronally express the TN-XXL construct, as originally described by Mank et al., 2008. Those mice specifically express the genetically encoded ratiometric calcium sensor TN-XXL in neurons via the thy1 promoter. Conformational changes within the protein, which are induced by Ca^{2+}, increase Fluorescence Resonance Energy Transfer (FRET) from donor to acceptor and can be visualized by 2-photon laser scanning microscopy to measure changes in neuronal calcium concentrations (2.2.17). All animal experiments were approved by local authorities and conducted according to the German Animal Protection Law.

2.2 Methods

2.2.1 Cell culture

Cells were cultured and handled under a laminar flow hood under sterile conditions. Murine cells were cultured in mouse cell culture medium (MM) in incubators at 37 °C in a 5 % CO_2 atmosphere and 95 % humidity. All material for cell culturing was sterilized or disinfected with 70 % alcohol before use. Waste was autoclaved at 121 °C for 20 min at 1 bar.

2.2.2 Cell counting

In order to determine cell numbers, cells had to be taken up in a defined volume. An aliquot of the cell suspension was mixed with trypan blue in a ratio of 1:1, 1:5 or 1:10. The mixture was applied to a Neubauer hemocytometer and the cells in the 16 fields of one quadrant (n) were counted under a light microscope. Due to the uptake of trypan blue, dead cells could be excluded. They can be distinguished from viable cells by their blue appearance under the light microscope. The total number of living cells was calculated as follows:

Total cell number = n x dilution factor (trypan blue) x ml cell suspension x 10^4 (chamber coefficient)

2.2.3 Isolation of immune cells by magnetic sorting

For the isolation of immune cell subsets from mouse spleen and lymph node cells magnetic cell sorting (MACS) was used. Kits from Miltenyi Biotec were utilized mainly according to the manufacturer's instructions. Two basic principles can be distinguished when applying the magnetic cell sorting technique. There is either the direct labeling of the target cells, which is also called a positive sort, or the indirect or negative sort, in which everything but the target cells are labeled. When applying the direct labeling technique, antibodies that are directly coupled to magnetic beads are used. Those are specific for the wanted cell population. After coupling the cells with the magnetically labeled antibodies, they are put on a MACS column in the magnetic field of a MACS separator. After rinsing the column, it contains only the magnetically labeled target cells within its magnetic field. Subsequently, the target population can be eluted. The target population is still labeled with the magnetic beads on its surface; however, the beads fall off of the cells after several days in culture. For the indirect or negative sort, all unwanted cells are labeled with magnetic beads and the target population stays "untouched". In order to achieve this, a mixture of biotinylated antibodies labeling all

cells except the target cell population is applied. In a second labeling step, an anti-biotin antibody coupled to magnetic beads is added. This magnetically labeled secondary antibody binds to the primary antibodies. After running the cell suspension over the column and rinsing it, all unwanted cells are retained in the magnetic field of the MACS separator, whereas the unlabelled target cells pass through the column and can be collected. This results in an untouched target cell population, with no bead-coupled antibodies on its surface.

2.2.4 Flow cytometry

Flow cytometry (FACS = fluorescence activated cell sorting) is a technique for characterizing and examining individual immune cell populations.

When using flow cytometry, two aspects can be utilized. Firstly, the natural scattering of light by the cell structures and secondly, the fluorescence of molecules bounded to specific antibodies that can bind to the cells. Therefore, it is possible to analyze morphological characteristics, such as cell size and granularity, but also the expression of specific molecules on the cell surface or within the cells. For this purpose either monoclonal antibodies that are coupled with fluorochromes can be used or biotinylated monoclonal antibodies. With the directly coupled antibodies it is possible to mark individual cell populations by them binding to specific molecules immediately. When utilizing the biotinylated monoclonal antibodies, they have to be combined with a secondary fluorescently labeled streptavidin antibody that binds to the primary biotinylated antibody. When measured at a flow cytometer (e.g. FACS Canto II), the cells pass several laser beams with different wavelengths in a single-cell stream. The fluorescent molecules bound to each cell are excited by the corresponding laser beam and emit a signal that is detected by the flow cytometer. The detected signal intensity is proportional to the concentration of the fluorescent molecules present. Depending on the number of lasers within the flow cytometer, the simultaneous detection of a certain number of parameters on each cell is possible. A FACS Canto II (3 lasers) allows the simultaneous detection of 8 different fluorochromes in addition to cell size (FSC = forward scatter) and cell granularity (SSC = sideward scatter). The analysis of flow cytometric data was performed using the FlowJo analysis software.

2.2.5 Isolation of naïve $CD4^+/CD62L^+$ T cells (Naïve Sort)

Obtaining cells: Surgical instruments were disinfected with 70% EtOH and 15 ml PP-tube(s) prepared with 5 ml WM. 5-8 week old C57BL/6-2d2 mice were sacrificed by neck dissection. Spleens and/or lymph nodes (LN; inguinal + axial + brachial) were isolated and separated by gender and genotype. All following operations were performed in a vertical laminar flow sterile hood.

A cell suspension was generated by smashing the spleens and LNs through a 100 µl-cell strainer into a 50 ml PP-tube using a syringe stamp (2 ml). The strainer was washed 3-4 times with 10 ml WM. The cells were then centrifuged for 5 min at 550 g at 4 °C, the supernatant was removed, and the cells resuspended in 2 ml lysis buffer to remove red blood cells. Another 8 ml lysis buffer and 5 ml WM were added, followed by a centrifugation step for 5 min at 550 g at 4 °C and uptake of the cells in an appropriate amount of MACS buffer (10 -30 ml). Any fatty clumps were removed with a 1 ml pipette and cells were counted (2.2.2). The expected yield was approximately 130 Mio cells/mouse or 60 -120 Mio cells/spleen.

All following operations were performed on ice and by using the MidiMACS and QuadroMACS Separators for magnetic sorting of immune cells (2.2.3).

MACS Sort No. I (CD4 untouched, CD8 positive sort): Cells were taken up in 50 ml MACS buffer, centrifuged for 5 min at 550 g, at 4 °C the supernatant was removed. 40 µl MACS buffer and 10 µl of the CD4 T cell biotin antibody cocktail (CD4 T-cell Isolation Kit, 2.1.5.) were used for 10^7 cells. The pellet was resuspended in the corresponding volume and incubated for 10 min at 4°C in the dark. 30 µl MACS buffer and 20 µl anti-biotin microbeads as well as 5 µl CD8 microbeads were added subsequently to reduce contamination with $CD8^+$ cells. Cells were incubated for 15 min at 4°C in the dark and washed with 50 ml MACS buffer afterwards. After centrifugation for 5 min at 550 g at 4 °C cells were taken up in 0.5 ml MACS-buffer for every 10^8 cells; but at least in 1 ml MACS-Buffer.

MACS columns with Pre-Separation Filters (30 µm) on top were equilibrated using 3 ml of MACS buffer and up to 300 Mio cells per column were added. The pipette tip was resuspended in a 1.5 ml tube with 1 ml FACS buffer as a pre-sort control for the quality determination of the sort, so called MACS check. The cell tube was washed twice with 3 ml MACS buffer, which was added to the column followed by another 3 ml of MACS buffer.

The flow through with enriched $CD3^+/CD4^+/CD8^-$ cells was collected in 50 ml PP-tubes. 100 µl of the cell suspension was transferred to a 1.5 ml tube with 900 µl FACS as a post-CD4-sort control for the MACS check.

MACS check #1: The pre- and post-$CD4^+$-sort control tubes were centrifuged for 5 min at 600g at 4 °C and washed with 1 ml FACS buffer. 100 µl of an antibody solution of CD4-Horizon (1:400) and CD3-APC (1:600) in FACS buffer were added per tube and incubated for 10 min at 4°C. Subsequently the cells were washed with 1 ml FACS buffer, the supernatant was discarded and the cells were resuspended in 300 µl FACS buffer. The cell solution was transferred in FACS tubes and 5.000-30.000 cells were analyzed via flow cytometry. $CD3^+/CD4^+$ purity was about > 90 % of the lymphocytes.

MACS sort No. II (CD62L positive sort): The flow through of the first sort was centrifuged for 5 min at 550 g at 4 °C and 960 µl of MACS buffer and 40 µl of CD62L microbeads were added. Cells were incubated for 15 min at 4°C in the dark and the tube was filled with MACS buffer afterwards. The cells were centrifuged for 5 min at 550 g at 4 °C, resuspended in 1 ml MACS buffer and added to a new column (without filter) equilibrated using 3 ml MACS buffer. The cell tube twice was washed with 3 ml MACS buffer, which was added to the column followed by additional 3 ml MACS-buffer.

The enriched $CD4^+/CD62L^+$ cells were collected by squeezing 2x 5 ml MACS buffer through the column into a new tube. 100 µl of the cell suspension was transferred in a 1.5 ml tube with 900 µl FACS buffer as a post-$CD62L^+$-sort control for the second MACS check.

MACS check #2: The post-$CD62L^+$-sort control tube was centrifuged for 5 min at 600 g at 4 °C and washed with 1 ml FACS buffer. 100 µl of an antibody solution of CD4-Horizon (1:400) and CD62L-APC (1:200) in FACS-Buffer were added. The cells were incubated for 10 min at 4°C, followed by a washing step with 1 ml FACS-buffer, and resuspended in 300 µl of FACS buffer. The solution was transferred in FACS tubes and 5.000-30.000 cells were analyzed via flow cytometry. $CD4^+/CD62L^+$ purity of $CD4^+$ population was about > 97%.

The sorted cells were centrifuged for 5 min at 550g at 4 °C and taken up in 5 - 10 ml MM. T cell number was determined (2.2.2). The expected yield was approximately 3-5 Mio naïve T cells/mouse.

2.2.6 Isolation of Antigen Presenting Cells (APCs)

Obtaining cells: The surgical instruments were disinfected with 70% EtOH. C57BL/6 mice were sacrificed by neck dissection. Spleens were taken out and separated by gender and genotype. Two spleens were collected in every prepared 15 ml PP-tube tube with 5 ml WM. All following operations were performed in a vertical laminar flow sterile hood.

A cell suspension was generated by smashing the spleens through a 100 µl-cell strainer into a 50ml PP-tube using a syringe stamp (2 ml). The strainer was washed 3-4 times with 10 ml of WM and the cells were centrifuged for 5 min at 550 g at 4 °C. The supernatant was removed and the cells were resuspended in 2 ml of lysis buffer to remove red blood cells. Another 8 ml of lysis buffer and 5 ml of MW were added, the cells were centrifuged for 5 min at 550 g at 4 °C and taken up in an appropriate amount of MACS buffer (10 -30 ml). Any fatty clumps were removed with the 1 ml pipette and the cells were counted. The expected yield was approximately 130 Mio cells/mouse or 60 -120 Mio cells/spleen.

All following operations were performed on ice and by using the MidiMACS and QuadroMACS Separators for magnetic sorting of immune cells (2.2.3).

MACS sort (CD90.2 depletion): The cells were taken up in 50 ml MACS buffer and centrifuged for 5 min at 550 g at 4 °C. The supernatant was removed and 95 µl of MACS buffer and 5 µl of CD90.2 beads for every 10^7 cells were added. The pellet was resuspended in the corresponding volume and incubated for 15 min at 4°C in the dark. Afterwards the tube was filled up to 50 ml with MACS buffer and centrifuge for 5 min at 550 g at 4 °C. The cells were taken up in 0.5 ml MACS buffer per 10^8 cells, but at least in 1 ml MACS-Buffer.

MACS columns with Pre-Separation Filters (30 µm) on top were equilibrated using 3 ml of MACS buffer and up to 300-400 Mio cells were added per column. The pipette tip was resuspended in 1.5 ml tube with 1 ml FACS buffer as a pre-sort control for the quality determination of the sort (MACS check). The cell tube was washed twice with 3 ml MACS buffer, which was added to the column followed by another 3 ml of MACS-buffer. The flow through with enriched $CD90.2^-$ cells was collected in 50 ml PP-tubes. 100 µl of the cell suspension was transferred to a 1.5 ml tube with 900 µl FACS as a post-sort control for the MACS check.

MACS check: The pre- and post-sort control tubes were centrifuged for 5 min at 600 g at 4 °C and washed with 1 ml FACS buffer. 100 µl of an antibody solution of CD3-PE (1:100) in FACS buffer were added per tube and incubated for 10 min at 4°C. Subsequently cells were washed with 1 ml FACS buffer, the supernatant discarded and the cells resuspended in 300 µl FACS buffer. The cell solution was transferred in FACS tubes and 5.000-30.000 cells were analyzed via flow cytometry. The frequency of the $CD3^+$ population was less than 5 % of the cells alive.

The sorted cells were centrifuged for 5 min at 550 g at 4 °C and taken up in 10 ml MM. The cell number was determined (2.2.2). The expected yield was approximately half of the original number of cells.

The purified APCs were irradiated at 30 Gy/3000 rad to stop cell proliferation as well as to limit APC lifetime during culturing and used for T cell stimulations.

2.2.7 Differentiation of naïve B6.2d2- $CD4^+$/$CD62L^+$ cells to Th cell subsets

Obtain B6.2d2 $CD4^+CD62L^+$ T cells and APCs as described in 2.2.5 and 2.2.6. T cells from B6.2d2 mice expresses MOG_{35-55} specific T cell receptors which allow antigen-specific stimulation via antigen presenting cells during culturing.

The differentiation of naïve T cells from these transgenic mice strains to 2d2 Th17, Th1 or Th2 cells is therefore driven by three antigen-specific stimulations via APCs and specific cytokine treatments within 13 (for Th1 and Th2) or 17 days (for Th17). As a tool to define the current differentiation state of each culture during this period, the culture is named after the previous restimulation “re0, re1 or re2” and the days “d1-d7” that passed since the last stimulation. For each stimulation the APCs were loaded with antigen as follows:

- In case of 2d2 Th1 and Th2 cells: 25 µg/ml MOG_{35-55} (stock 2.5 mg/ml) were added to the APC (final concentration 12.5 µg/ml) and preincubated for 10-30 min in the cell culture incubator before co-culturing with T cells
- In case of 2d2 Th17 cells: 12.5 µg/ml MOG_{35-55} (stock 2.5 mg/ml) were added to the APC (final concentration 6.25 µg/ml) and preincubated for 10-30 min in the cell culture incubator before co-culturing with T cells

Initial Stimulation (re0d0):

B6.2d2 $CD4^+CD62L^+$ T cells were co-cultured with antigen loaded APCs in a 1:5 (for Th1 and Th2) or 1:10 (for Th17) ratio in a concentration of 6 Mio cells in 2 ml MM per well on a 24-well plate. The following T cell subset specific cytokines were added:

Table 1: Cytokine treatment for Th cell differentiation during initial stimulation

Th cell subset	(α-)Cytokine	Stock solution	Final concentration
Th1	IL-12	10 µg/ml	50 ng/ml
	IL-18	25 µg/ml	25 ng/ml
	α-IL-4	1 mg/ml	10 µg/ml
Th2	IL-4	10 µg/ml	10 ng/ml
	α-IL-12	1 mg/ml	10 µg/ml
	α-IFN-γ	1 mg/ml	10 µg/ml
Th17	huTGF- β	2 µg/ml	3 ng/ml
	IL-23	10 µg/ml	20 ng/ml
	IL-6	5 µg/ml	20 ng/ml

Maintenance (re0d3 and re0d5):

The maintenance of the T cell culture included culturing at constantly 5 % CO_2 and 37 °C, splitting at high cell densities and feeding with fresh MM with cytokines, which was crucial for a good yield and to prevent the culture from shifting to other T cell subsets. The regular time point to split the culture varied between the cultures, but was in general on d3 and d5 after stimulation.

The cultures were splitted by adding the following cytokines:

- Th1: 100 U/ml IL-2 were added when splitted on day 2 or 3.
- Th2: 100 U/ml IL-2 and 10 ng/ml IL-4 were added when splitted on day 2 or 3.
- Th17: 50 U/ml IL-2 and 10 ng/ml IL-23 were added when splitted cells on day 3; 25 U/ml IL-2 and 10 ng/ml IL-23 were added when splitted cells on day 5

For Th17-skewing condition IL-2 concentration counteracting IL-17 expression was kept as low as possible. CD3/28 stimulation (2.2.8) was performed on day 4-6 to test for an adequate cytokine production:

- Th1: IFN-γ ↑ / IL-17 ↓ / TNF-α ↑ / IL-4 ↓
- Th2: IFN-γ ↓ / IL-17 ↓ / TNF-α ↑ / IL-4 ↑
- Th17: IFN-γ / IL-17 ↑ / TNF-α ↑ / IL-4 ↓

First restimulation (re1d0):

T cells were harvested, washed with WM and taken up in MM. Subsequently, T cells were co-cultured with antigen loaded APCs in a 1:3 (for Th1 and th2) or 1:5 (for Th17) ratio in a concentration of 6 Mio cells in 2 ml MM per well on a 24-well plate. The following T cell subset specific cytokines were added:

Table 2: Cytokine treatment for Th cell differentiation during first restimulation

Th cell subset	(α-)Cytokine	Stock solution	Final concentration
Th1	IL-12	10 µg/ml	10 ng/ml
	IL-18	25 µg/ml	10 ng/ml
	IL-2	100.000 U/ml	100 U/ml
	α-IL-4	1 mg/ml	5 µg/ml
Th2	IL-4	10 µg/ml	10 ng/ml
	IL-2	100.000 U/ml	100 U/ml
	α-IL-12	1 mg/ml	5 µg/ml
	α-IFN-γ	1 mg/ml	5 µg/ml
Th17	huTGF-β	2 µg/ml	0.75 ng/ml
	IL-23	10 µg/ml	20 ng/ml
	IL-6	5 µg/ml	10 ng/ml

T cells were maintained as after the initial stimulation and CD3/CD28 stimulation (2.2.8) was performed on day re1d4-6 to test for adequate cytokine production.

Second restimulation (re2d0):

T cells were harvested, washed with WM and taken up in MM. Subsequently, T cells were co-cultured with antigen loaded APCs in a 1:3 ratio in a concentration of 6 Mio cells in 2 ml MM per well on a 24-well plate. The following T cell subset specific cytokines were added:

Table 3: Cytokine treatment for Th cell differentiation during second restimulation

Th cell subset	(α-)Cytokine	Stock solution	Final concentration
Th1	IL-12	10 µg/ml	5 ng/ml
	IL-18	25 µg/ml	10 ng/ml
	IL-2	100.000 U/ml	100 U/ml
	α-IL-4	1 mg/ml	2.5 µg/ml
Th2	IL-4	10 µg/ml	10 ng/ml
	IL-2	100.000 U/ml	100 U/ml
	α-IL-12	1 mg/ml	2.5 µg/ml
	α-IFN-γ	1 mg/ml	2.5 µg/ml
Th17	IL-23	10 µg/ml	20 ng/ml
	IL-6	5 µg/ml	5 ng/ml

T cells were used on day 3 after the second restimulation for transfer in recipient animals (2.2.14) and for co-culture with primary neurons *in vitro* (2.2.12), after confirmation of adequate cytokine expression (2.2.8) according to polarizing condition (Th17 cells: 15%–30% IL-17$^+$, Th1 cells: >50% IFN-γ$^+$, Th2 cells: >15% IL-4$^+$).

2.2.8 Analysis of cytokine profile of T cell cultures (CD3/CD28 Stimulation)

Prearrangement: All following operations were performed under sterile conditions. For antigen unspecific stimulation of T cells one well per culture was coated on a 48-well plate with α-CD3e and α-CD28 antibodies. 120 µl per well of an α-CD3e / α-CD28 solution with a concentration of 3 µg/ml and 2.5 µg/ml in PBS [+], respectively, was applied. As an unstimmulated control one well per culture was covered only with PBS [+]. The plate was shacked to distribute coating solution evenly, covered with 70 % EtOH sprinkled cling film and incubated overnight at 4°C.

Stimulation: The coating solution from the prearranged plate was removed. 2 ml of each T culture (1 well, 3-8 Mio cells) was resuspended carefully and 1 ml cell suspension was transferred to both the coated and control well. The plate was incubated for 2 hr at 37 °C. Cytokine secretion was blocked by using the secretory pathway blocker Brefeldin A with a final concentration of 5 µg/ml. T cells were incubated again for 2 hr at 37 °C and harvested subsequently.

Staining: All following operations were performed under on ice. Cells were centrifuged for 5 min at 600 g at 4° C and the supernatant removed. For the extracellular staining 90 µl antibody solution of CD4-FITC (1:400) in FACS buffer was added. T cells were incubated for 10 min at 4 °C, washed with 2 ml FACS buffer and 2 ml PBS subsequently. Cells were fixated by adding 500 µl 4% PFA solution and 500 µl PBS to each tube and incubated for 20 min at 4 °C followed by addition of 1 ml PBS subsequently.

Tubes were centrifuged for 5 min at 600 g at 4°C and the supernatant was removed. For membrane perforation 2 ml Saponine buffer was added followed by a centrifugation step for 5 min at 600 g at 4°C. The supernatant was removes and for Fc-Blocking 70 µl Fc-blocking solution (1:100) in Saponine buffer was added and incubated for 10 min at 4°C.

For the intracellular staining an antibody solution of 20 µl IFN-γ-Horizon (1:200) and IL-17-AF647 (1:200) in Saponine buffer was added and incubated for 20 min at 4 °C. Cells were washed with 2 ml Saponine buffer and 2 ml FACS buffer and resuspended in 300 µl FACS buffer. The solution was transferred in FACS tubes and 5.000-30.000 cells were analyzed via flow cytometry. The frequency of the $CD4^+$ population and cytokine producers gave insights into the purity and differentiation state of the T cell culture.

2.2.9 Analysis of transcription factor (TF) expression of Th cell cultures

Prearrangement: The Fixation/Permeabilization Concentrate (1 part) was diluted with the Fixation-Permeabilization Diluent (3 parts) to gain the desired volume of Fix/Perm working solution. 10x Permeabilization Buffer was diluted 1:10 with dH_2O. It was always centrifuged for 5 min at 550 g at 4 °C and worked on ice during the following procedures.

Staining: 2 ml of each Th17 culture (1 well, 3-8 Mio cells) was resuspended carefully and 1 ml cell solution was transferred to a 1.5 ml tube. The second 1 ml was used as an unstained control for the following staining. The tubes were centrifuged and the supernatant removed.

For the extracellular staining 100 µl of an antibody solution of CD4-FITC (1:400) and CD25-PE-Cy7 (1:400) in FACS-Buffer was added. Cells were incubated for 10 min at 4 °C and washed with FACS buffer subsequently. The cell pellet was resuspended in 500 µl freshly prepared Fix/Perm working solution and incubated for 2-18 hrs at 4 °C in the dark.

Cells were washed twice by directly adding 1 ml 1x Permeabilization Buffer followed by a centrifugation step and by discarding the supernatant. For the intracellular TF staining 100 µl of an antibody solution of T-bet-Pacific blue (1:400), RORγt-APC (1:400) and Foxp3-PE (1:200) in 1x Permeabilization Buffer was added and incubated for 30 min at 4 °C. Again cells were washed twice by directly adding 1 ml 1x Permeabilization Buffer followed by a centrifugation step and by discarding the supernatant. Cells were taken up in 300 µl FACS buffer, transferred in FACS tubes 5.000-30.000 cells were analyzed via flow cytometry. The frequency of the $CD4^+$ population and expression of the transcription factors gave insights into the purity and differentiation state of the T cell culture.

2.2.10 CFSE proliferation assay

To measure murine T cell proliferation, T cells were labeled with the fluorescent dye carboxyfluorescein succinimidyl ester (CFSE). Therefore, T cells were preincubated for 15-30 min at 37°C in MM and subsequently washed twice in pre-warmed RPMI+1% Hepes. Cells were then resuspended in 10 ml pre-warmed RPMI+1% Hepes containing 2.5 µM CFSE and incubated for 10 min at 37°C in the dark. The labeled cells were washed twice with cold MM, counted, and cultured in 48-well plates for 3-4 days. Target cells were thereby stimulated either polyclonally with anti-CD3 and anti-CD28 antibodies or with APC and the corresponding antigen (ratio targets to APC 1:3). After this culture period, cells were harvested, washed with FACS buffer, stained with FACS antibodies for T cell markers and measured at a FACS Canto II.

2.2.11 Isolation of cortical neurons from fetal murine brains

Prearrangement: For the preparation of cortical neurons followed by co-culturing with T cells glass coverslips were degreased and disinfected in a glass petri dish by washing 1 hr with PBS, 70% and 100% ethanol, respectively. Overlapping of coverslips during these washing procedures was avoided. Coverslips were sterilized in the drying cabinet for at least 1 hr at 200 °C and added to a 24 well plate subsequently (one coverslip/well).

Coverslip were coated by adding 80 µl of poly-D-Lysine substrate diluted in sterile Aqua bidest (20 µg/ml) and incubated for at least 2 hr at RT or overnight at 4 °C. Plate was washed 3x with Aqua bidest and air dried it under a vertical laminar flow sterile hood. Surgical instruments were sterilized in a drying cabinet at 200 °C for 1 hr and with 70% EtOH.

Preparation: Pregnant C57BL/6J donor mice were sacrificed at state E16 by neck dissection. Abdomen was disinfected with 70 % EtOH and the uterus containing the embryos (usual 6-8) was taken out and transferred into a 10 cm Petri dish with 10 ml HBSS [-] on ice. All following operations were performed in a horizontal laminar flow sterile hood using a Leica 56D binocular microscope. Liquids were kept cool on ice.

Embryos were separately transferred to another 10 cm Petri dish with 10 ml HBSS medium [-]. The uterus was opened and the head was exposed subsequently. Subsequently, the embryo was decapitated and fixated by pricking forceps through its eyes. The skin was cut from the occipital to the eyes using a pair of scissors and removed with a forceps. To remove the bone the procedure was repeated and a spatula was used to transfer the brain gently into a 6 cm Petri dish with 3 ml HBSS medium [+]. The brain was fixated by putting a scalpel through the cerebellum and cortex halves were cut off from the hypothalamus with another scalpel (Figure 6 A+B). Olfactory bulbs, meninges, hippocampus and remaining parts of the thalamus were precisely removed with a forceps (Figures 6 C-F). The cortex was transferred into a 15 ml PET-tubes with 5 ml HBSS [+] and another embryo was processed equally. Up to 4 cortex halves were added to each tube and instruments were occasionally washed with 70 % ethanol. The preparation duration was limited to less than 6 min per embryo to minimize neuron cell death.

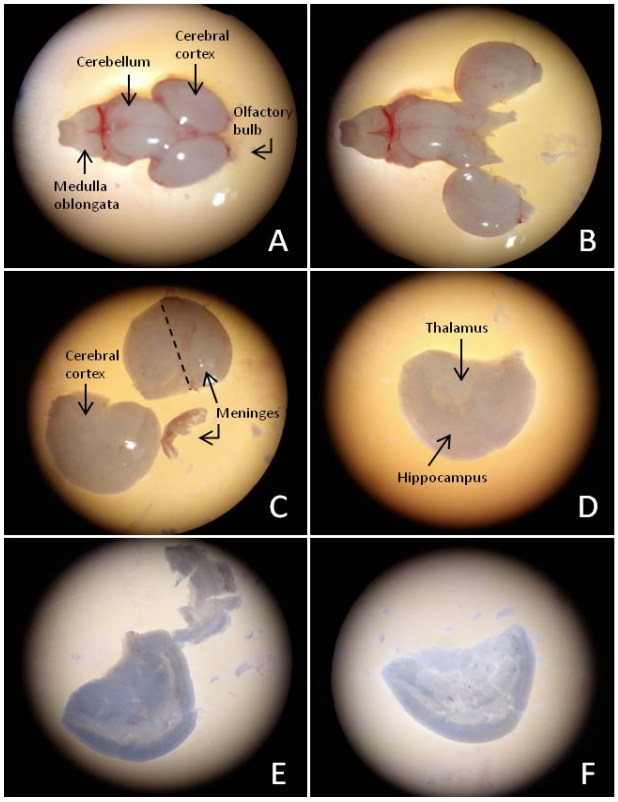

Figure 6: Preparation of cortex from fetal murine brain

(A) full brain (B) separated Hemispheres (C) removed meninges (D) cortex with Hippocampus (E) removed hippocampus (F) isolated cortex

Postprocessing: All following operations were performed in a vertical laminar flow sterile hood. Cortex halves were washed 3x with 5 ml HBSS [-] to remove inhibitory ions prior to Trypsin treatment. 3.5 ml medium were left in each tube, 500 µl Trypsin (2.5 %) were added and incubated for 15-20 min in a water bath at 37 °C until the tissue was slightly swollen. Tubes were shacked every 5 min and the protease activity was neutralized by adding 2 ml of heat inactivated FCS to each tube. Tissue was washed 3x with 5 ml NBM [-] and 2 ml medium was left in each tube to perform trituration. A 1 ml pipette was used to triturate 6 times until the cells were dissolved homogeneously during to keep the neuron survival rate and yield high. Subsequently, cells were resuspended in 10 ml NBM [+], centrifuged 5 min at 300 rpm at 4 °C and the supernatant was transferred into a new PET-tube. Tubes were pooled and pellets with cell debris were discarded. Subsequently, cells were taken up in an appropriate amount of warm NBM [+] and counted (2.2.2). 300.000 cells were plated in 2 ml NBM [+] per well on the prearranged 24-well plates either with or without coverslips depending on the experiment. Neurons were cultured in an incubator at 5% CO_2 and 37 °C.

24 hrs after plating neurons were fed by changing half of the medium. Growth of neuronal processes was monitored continuously during culturing by using a light microscope and the quality of the preparation in terms of survival rate and astrocyte contamination was analyzed regularly (2.2.13).

2.2.12 Co-culture of primary neurons and Th cells

Primary neurons and Th cells were obtained as described in 2.2.10 and 2.2.7, respectively. Both cultures had to be synchronized since the cells were taken at the same development status for each co-culture to ensure the results are comparable. Therefore the neurons were always used at day 4 after plating (day 0) and the Th17 cells 3 days after the second restimulation, i.e. re2d3.

For preparation T cells were harvested into a 50 ml tube, toped up with WM and centrifuged for 5 min at 600 g at 4 °C. Cells were taken up in an appropriate amount of NM [+] depending on the size of the pellet and counted with a Cell Counting Chamber and Trypan blue. T cell concentration was adjusted to 1 Mio/ml by adding additional NM [+]. 300.000 Th17 cells were added to the neuron culture by replacing 250 µl medium in each well with the prepared cell solution and incubated for 24 hrs at 5% CO_2 and 37 °C.

2.2.13 Analysis of neuron and co-cultures by immunocytochemistry

To test the quality of neuron preparations in terms of viability and astrocyte contamination as well as the impact of T cells on neurons immunocytochemistry was performed. For this purpose neurons were prepared and cultured on glass coverslips as described in 2.2.10.

The neuron or co-cultures were washed carefully with 1 ml PBS [+] after 24 hrs and fixated by adding freshly prepared 4 % PFA for 20 min at 4 °C. Cells were washed 3x with PBS [+] afterwards. For cell permeabilization 300 µl of 0.1 % Triton-X were added to each well and incubated for 2 min at 4 °C followed by three washing steps with PBS [+].

Immunocytochemistry stainings were performed following the procedure described below which either includes the staining with antibodies or the enzymatic staining of DNA double strand breaks via terminal deoxynucleotidyl transferase-mediated biotinylated UTPn nick end labeling, abbreviated as TUNEL staining (In Situ Cell Death Detection Kit, TMR red).

Table 4: Procedure of immunocytochemistry stainings

<table>
<tr><th>Antibody staining</th><th>TUNEL</th></tr>
<tr><td>Sample was incubated overnight at 4 °C in the dark with 80 µl antibody solution of rat-α-mouse-CD4-647 (1:500), mouse-α-mouse-NeuN (1:500) and rabbit-α-mouse-Cleaved Caspase-3 (1:500) or rabbit-α-mouse GFAP in PBS [+]</td><td>Sample was incubated overnight at 4 °C in the dark with 80 µl antibody solution of rat-α-mouse-CD4-647 (1:500) and mouse-α-mouse-NeuN (1:500) in PBS [+]</td></tr>
<tr><td colspan="2">Sample was washed 3x with PBS [+]</td></tr>
<tr><td rowspan="3">Sample was incubated for 2 hrs at RT in the dark with 80 µl antibody solution of goat-α-mouse-AF488 (1:1000) and goat-α-rabbit-AF568 (1:1000)</td><td>50 µl TUNEL reaction mixture (In Situ Cell Death Detection Kit) was added and incubate in a humidified atmosphere for 60 min at 37 °C in the dark</td></tr>
<tr><td>Sample was washed 3x with PBS [+]</td></tr>
<tr><td>Sample was incubated for 2 hrs at RT in the dark with 80 µl antibody solution of goat-α-mouse-AF488 (1:1000)</td></tr>
<tr><td colspan="2">Sample was washed 3x with PBS [+]</td></tr>
<tr><td colspan="2">Sample was incubated for 30 min at RT in the dark with DAPI (1:10000)</td></tr>
<tr><td colspan="2">Sample was washed 3x with PBS [+]</td></tr>
<tr><td colspan="2">Coverslips were mounted on microscopy slides and samples were dried overnight in the dark</td></tr>
</table>

A fluorescence microscope was used to detect the staining. Several pictures for every channel at a 10x optical magnification of each coverslip were taken to gain enough information from this co-culture for statistical purposes.

MacBiophotonics ImageJ software was used for automatic determination of NeuN distribution and counting of cleaved Caspase-3 and TUNEL signals. For this pictures were imported as an image sequence and converted into 8-bit files. The signal threshold for all images was adjusted and applied concurrently and the watershed algorithm was performed to separate adjacent signals. Particles of an appropriate size were counted or the area fractions were measured automatically. The neuron / astrocyte ratio was determined equally.

2.2.14 Experimental autoimmune encephalomyelitis (EAE)

2.2.14.1 Induction of active EAE

Active EAE in C57BL/6 mice was induced using the Hooke Kit™ MOG_{35-55}/CFA Emulsion + PTX (2.1.4) following the manufacturer's protocol. In short mice were actively immunized by subcutaneous injection of an emulsion of MOG_{35-55} in complete Freund's adjuvant (CFA), followed by the administration of two intraperitoneal doses of 400 ng of pertussis toxin (PTX) in PBS, first at the time of immunization and second 48 hrs later. The clinical outcome was monitored daily.

2.2.14.2 Induction of passive EAE

Passive EAE was induced in B6.Rag2$^{-/-}$ mice by intravenous injection of 2 Mio 2d2 CD90.1^{+} Th17 cells (first transfer). Seven days later PBS (control) or 10 Mio 2d2 CD90.2^{+} Th17, 2d2 Th1, or 2d2 Th2 cells were co-transferred intravenously (second transfer). The clinical outcome was monitored daily.

2.2.14.3 Anti-inflammatory treatment of EAE mice with corticosteroids

Using steroid pulses of 16 µg/g Urbason on three to five consecutive days, we induced a rapid remission of symptoms which was followed by a slow and chronic progressive deterioration of clinical disability. This model is ideal to investigate the progressive phase of the disease and to test the reversal of neuronal/axonal damage with the aim to reduce non-remitting disability.

2.2.14.4 Scoring

After induction of EAE, mice were scored daily starting from day 7 (active EAE) or day 10 (passive EAE). Clinical signs usually started on day 10-14 after induction of EAE, and in classical EAE manifested themselves as ascending paralysis, starting at the tail, then affecting the hind limbs, and in later stages also the forelimbs. Clinical signs of classical EAE were translated into clinical scores as follows:

0 = no detectable signs of EAE
1 = complete tail paralysis
2 = partial hind limb paralysis
3 = complete bilateral hind limb paralysis
4 = total paralysis of forelimbs and hind limbs
5 = death

In some cases an atypical clinical course was observed. These clinical signs were translated into scores as follows:

1 = tail paralysis, hunched appearance, unsteady walk
2 = ataxia, head tilt, hypersensitivity
3 = severe ataxia, spasticity or knuckling, severe proprioception defects
4 = moribund
5 = death
Mice with a score above 3 were killed, according to animal protection law.

2.2.15 Isolation of lymphocytes from the CNS of EAE animals

For isolation of lymphocytes from the central nervous system, mice were lethally anaesthetized with an intraperitoneal injection of a ketamine/xylazine-mixture (415 mg/kg / 9.7 mg/kg). For transcardial perfusion the animal was disinfected with 70 % EtOH and the fur was cut open. Next, the sternum was removed to expose the heart. Subsequently, the right atrium was opened, a 20-gauge needle was inserted into the left ventricle, and mice were transcardially perfused with 25 ml ice-cold PBS. Brain and spinal cord were removed and placed in a 15 ml Falcon tube on ice containing 5 ml IMDM. All the following steps were performed under a laminar flow hood. First, the brain and spinal cord were transferred along with the 5 ml IMDM into a petri dish. The CNS tissue was cut into small pieces using a

scalpel and retransferred along with the 5 ml IMDM into the 15 ml Falcon tube. The IMDM medium was then supplemented with 360 U/ml collagenase, 200 U/ml DNAse, and 5 µg/ml collagenase/dispase. After incubation for 30 min at 37 °C, tubes were inverted every 5 min, the CNS tissue was put through a cell strainer and washed with cold IMDM medium. Next, the gradient for the isolation of the lymphocytes was prepared. Therefore, the pellet was resuspended in 5 ml 40 % percoll-solution (percoll diluted in IMDM) and carefully layered on top of 5 ml 70 % percoll-solution (percoll diluted in PBS) in a 15 ml falcon tube. After centrifugation for 30 min at 750 g at room temperature without break, mononuclear cells were collected from the interphase of the gradient, washed with WM, and counted. To examine the cytokine and transcription factor expression the cells were stimulated with αCD3/αCD28 (2.2.8 / 2.2.9) followed by FACS analyses (2.2.4).

2.2.16 Generation and purification of ICAM-5 D1-2-Fc fusionprotein

The sequence for ICAM-5 D1-2-Fc was kindly provided by the Gahmberg Laboratory, University of Helsinki, Finland, while the generation and purification of ICAM-5 D1-2-Fc fusionprotein was done in co-operation with the Koch-Brandt Laboratory, University Mainz, Germany. In short, the ICAM-5 D1-2-Fc construct were cloned in pcDNA6/V5-HisB und stably transfected into HEK-293 cells. Subsequently, HEK-293 cells overexpressing ICAM-5 D1-2-Fc were cultivated to a confluency of about 100% and subsequently serum-starved for 60 h. Detached cells were removed from supernatant by centrifugation (1000g, 30 min, 4°C). The DMEM-based buffer of the cleared ICAM-5 D1-2-Fc enriched supernatant was substituted by binding buffer (20 mM Na_2HPO_4/NaH_2PO_4 [pH 7]) via a MinimateTM TFF Capsule 30 K (PALL). The obtained solution was subjected to a 1 ml HiTrapTM rProtein A FF column (GE Healthcare). After washing with at least ten bed volumes of binding buffer, the bound ICAM-5 D1-2-Fc was eluted three times with 1 ml 100 mM sodium citrate (pH 4) into 5 ml neutralization buffer (1 M Tris [pH 9]). Subsequently, the binding buffer/sodium citrate solution was removed by PBS with an Amicon Ultra-15 Centrifugal Filter Unit, 50 NMWL (Millipore). The final protein concentration was determined by Bradford assays.

2.2.17 Intrathecal injection of ICAM-5 D1-2-Fc by lumbar puncture

ICAM-5 D1-2-Fc was delivered intrathecally by lumbar puncture in awake mice as described by Lu and Schmidtko, 2013 and Vulchanova et al., 2010. In short, the mouse was shaved on the back and grasped at the iliac crest, so that both hind legs move outward and downward.

Then the Hamilton syringe/needle was inserted at about a 45° angle between the L5 and L6 spinous process and 5 µl injection solution is applied. A reflexive flick of the tail indicated puncture of the dura. In passive EAE mice 0,2 µg of ICAM-5 D1-2-Fc was applied seven times in 48 hrs intervals from a score of 2 on to induce a ICAM-5 D1-2-Fc concentration in the CSF of 5 µg/ml.

2.2.18 TPLSM live imaging of neuronal Ca^{2+} fluctuations *in vivo*

Operation procedures and two-photon laser scanning microscopy (TPLSM) live imaging of neuronal Ca^{2+} fluctuations were performed as previously described by Siffrin et al., 2015. In short, mice were anesthetized with 1.5% isoflurane in oxygen/nitrous oxide (2:1) via a facemask. The mice were then tracheotomized and continuously respirated with a Harvard Apparatus Advanced Safety Respirator. The anesthetized animal was transferred to a custom-built operation and microscopy table, and fixed in a hanging position. The preparation of the imaging field was performed according to adapted protocols for cortical imaging. In brief, the brain stem was exposed by carefully removing musculature above the dorsal neck area and removing the dura mater between the first cervical vertebra and occipital skull bone. The head was inclined for access to deeper brain stem regions, and the brain stem was superfused with isotonic Ringer solution or a treatment solution. A sterile agarose patch (0.5% in 0.9% NaCl solution) was installed on the now-exposed brain surface to reduce heartbeat and breathing artifacts. During surgery and microscopy, body temperature was maintained at 37°C. The depth of anesthesia was controlled by continuous CO_2 measurements of exhaled gas and recorded with a CI-240 Microscapnograph.

We employed dual near-infrared (NIR) and infrared (IR) excitation, i.e., two-photon excitation of the sample at 850 nm by an automatically tunable Ti:Sa laser (Mai Tai HP, Spectra Physics, USA) and 1110 nm by an optical parametric oscillator (OPO) pumped by the Ti:Sa laser. The co-localized excitation beams are coupled into a commercially available scan head (2.1.6) via routing mirrors. The Ti:Sa beam is coupled into an upright microscope (BX-51WI) through the scan–tube lens combination (SL, TL). A dichroic mirror (DM) reflects the excitation beams toward the objective lens (20×, NA 0.95, Olympus Europe, Hamburg, Germany), which focuses them onto the sample at the same spot. Laser-beam scanning is done using a conventional pair of galvanometer scanners that allow free selection of the position and the size of the field of view. In combination with the motorized microscope z-

drive, three-dimensional objects can be visualized. In order to increase the penetration depth within tissue, the detection unit is placed in the vicinity of the sample, so that a maximum detection efficiency of the scattered fluorescence photons is achieved.

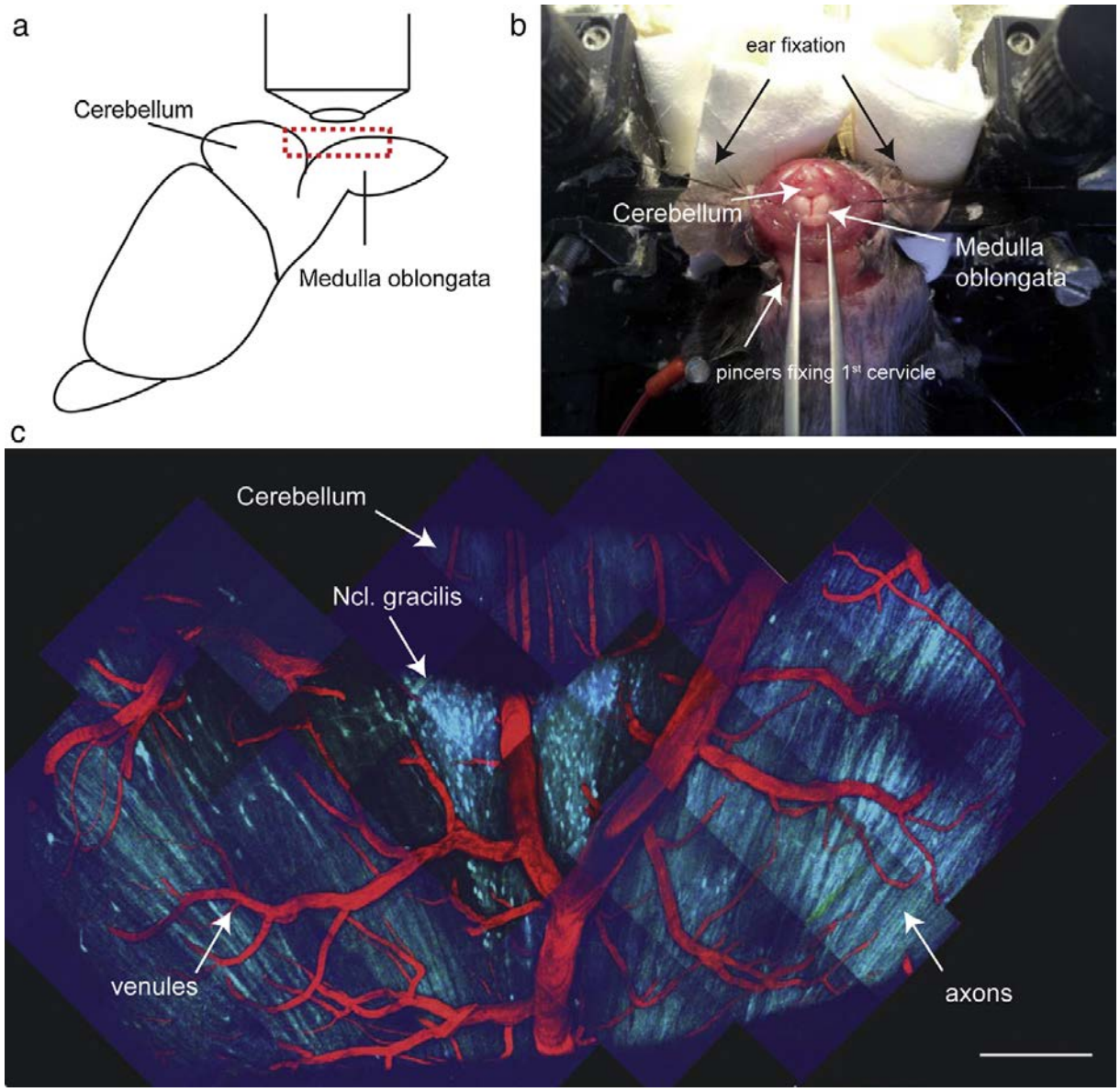

Figure 7: Intravital imaging of the brainstem of living anesthetized mice (Figure from Siffrin et al., 2015)

(a) Schematic representation of a mouse brain (sagittal view) illustrates the area of microscopy, which comprises the medulla oblongata, the caudal part of the cerebellum and the upper spinal cord. This imaging area is confined in the x-y direction by the first cervical and the skull bone. The z direction is limited by the maximal penetration depth (ca. 150 µm). (b) Animal preparation of the living anesthetized mouse with exposed brainstem. (c) Two-photon laser scanning microscopy of imaging areas of 300 × 300 × 70 - 140 µm (xyz). Neighboring regions have been scanned consecutively and image stacks have been combined to a photo mosaic to give an overview of the micro anatomical structures (scale bar: 300 µm).

xyz-stacks were typically collected within a scan field of 300 m × 300 m at 512 × 512 pixel resolution and a z-plane distance of 2 m at a frequency of 400 or 800 Hz. Applied laser powers ranged from 2 to 6 mW at the specimen surface, which allowed for imaging depths up to 150 m at low photobleaching and with negligible tissue photodamage. Time-lapse series of xyz stacks were acquired over several hours, each 60 s.

2.2.19 TPLSM data analysis

Acquired z-stacks were exported as TIF files and post-processed by the Volocity® software. Noise reduction was achieved by the software's "medium filter". Ratiometric channels were generated using the "ratio" function, which yields a ratiometric channel and an intensity modulated ratio channel (IMR). The latter was used for further [Ca^{2+}] analysis. False-color images of relative Ca^{2+}-concentration were generated with ImageJ. Statistical and mathematical analysis was carried out with Origin. Graphical presentation was performed with GraphPad Prism 6.

2.2.20 Statistical analysis

All FACS data were analyzed using FlowJo (Tree Star software, USA). Statistical analysis was carried out with GraphPad Prism 6. Data are usually presented as mean ± SEM. To compare two means, the paired *t* test or Mann–Whitney *U* test was used. To compare multiple means the one-way ANOVA test was used.

3. Results

3.1 Impact and fate of distinct T cell subsets in the course of autoimmune neuroinflammation

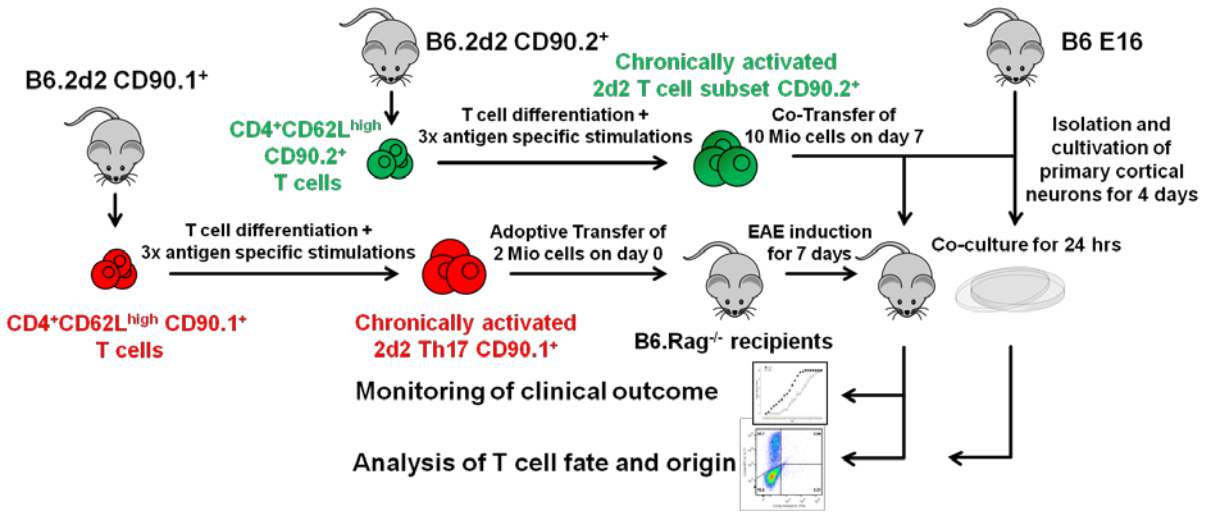

Figure 8: Experimental design project I

To gain insights into the impact and fate of distinct T cell subsets in the course of autoimmune neuroinflammation the following experiments were performed: Passive EAE was induced in lymphopenic Rag2$^{-/-}$ mice by adoptive transfer of chronically activated Th17 cells from MOG_{35-55} TCR transgenic 2d2 CD90.1^{+} mice. After seven days Th1, Th2 and Th17 cells generated from CD90.2^{+} mice were co-transferred. The clinical outcome was monitored daily. T cells were recovered from the CNS on the peak of the disease for detailed analysis of their phenotype and origin. In parallel T cell subsets were co-cultured with primary neurons to investigate changes in their cytokine profile after contact with neurons.

3.1.1 Subsequent co-transfer of distinct T helper subsets can alter the course of Th17-driven EAE

The capacity of distinct Th cell subsets to initiate neuroinflammatory processes such as EAE has been extensively studied. We sought to investigate their potential to perpetuate or control ongoing inflammation, using a model of co-transfer of a second subset of myelin-specific (2d2) effector CD4^{+} T lymphocytes (Th1, Th17, Th2) or PBS (control) seven days after EAE induction by 2d2 Th17 cells. The initial transfer of MOG_{35-55}-specific Th17 cells induced clinical symptoms after 14.96 ± 2.62 days, leading to a severe disease progression until sacrifice was required on day 22.09 ± 3.14 days (Figure 9 A). Co-transfer of 2d2 Th17 cells did not change the clinical outcome as compared to control (Figure 9 A). In contrast, the co-transfer of 2d2 Th1 or of 2d2 Th2 cells led to a significantly less aggressive disease course, as compared to co-transfer of 2d2 Th17 cells or to the control condition (Figure 9 A-C).

Furthermore, the co-transfer of Th2 cells significantly delayed the onset of EAE as compared to all other conditions (Figure 9 D). Our data therefore show that while the disease cannot be aggravated by a second wave of Th17 cells, Th1 and Th2 cells can both attenuate the neurological deficits induced by MOG_{35-55}-specific Th17 cells.

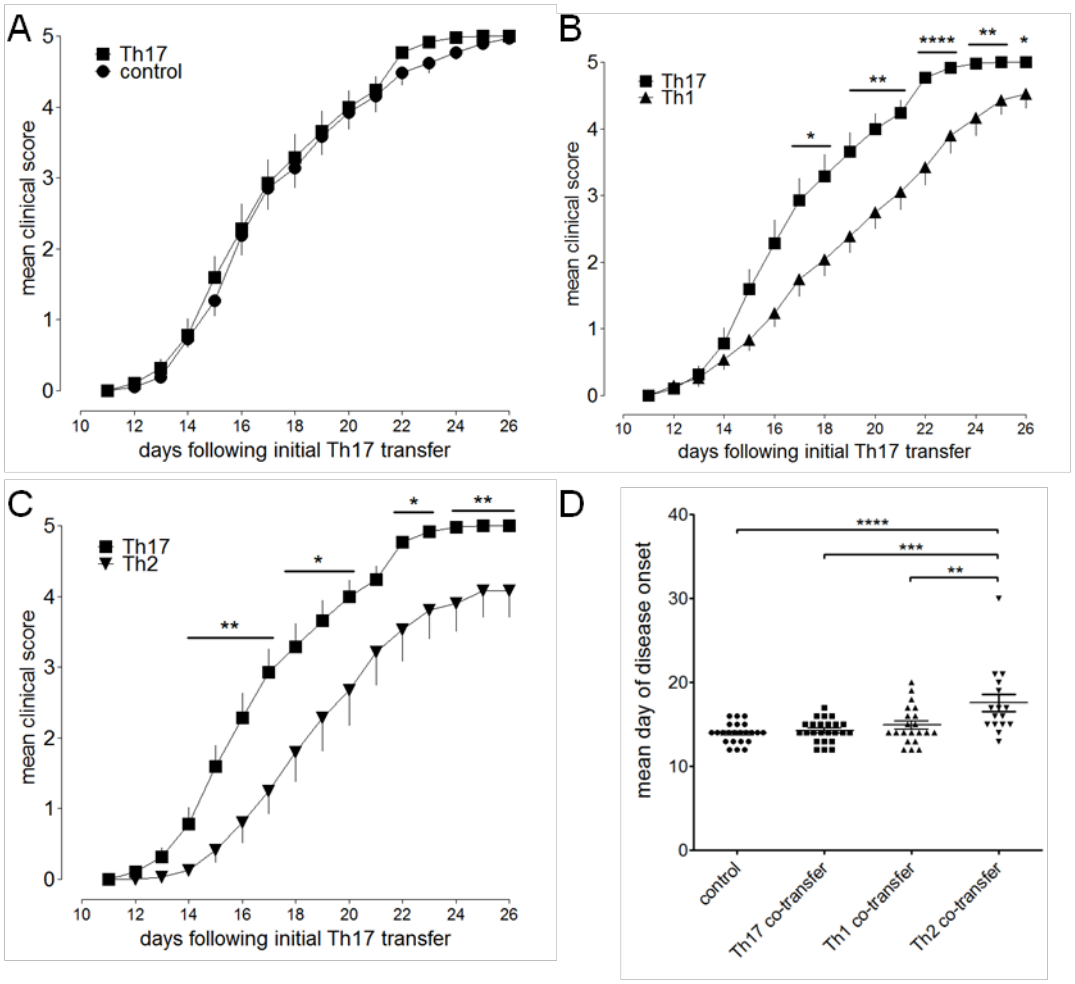

Figure 9: Subsequent co-transfer of distinct T helper subsets can alter the course of Th17-driven EAE
EAE was induced by adoptive transfer of $CD90.1^+$ 2d2 Th17 cells in $Rag2^{-/-}$ mice. After seven days $CD90.2^+$ 2d2 Th17, 2d2 Th1, or 2d2 Th2 cells were co-transferred. Clinical course of Th17-induced EAE with control co-transfer (PBS) in comparison to co-transfer of Th17 (A). Clinical course of Th17-induced EAE following co-transfer of Th17 cells as compared to co-transfer of Th1 (B) or Th2 (C). Mean day of disease onset (D). Pooled data from four independent experiments. Control n = 23 animals, co-transfer of Th17 n = 24, Th1 n = 21, or Th2 n = 16. Mann-Whitney U test (A-C) and one-way ANOVA with Bonferroni's Multiple Comparison Test (D); * $p < 0.05$, ** $p < 0.01$, *** $p < 0.001$, **** $p < 0.0001$. Data shown are mean ± SEM.

3.1.2 Analysis of T helper cell populations

To discriminate between the disease-inducing 2d2 T cells and the co-transferred 2d2 T cells we used the congenic CD90 (Thy1) marker expressed by thymocytes. The disease-inducing Th17 culture was generated from naïve T cells of CD90.1^{+} mice, while the co-transferred Th1, Th2 and Th17 cells were derived from naïve T cells of CD90.2^{+} mice. Thus, we were able to identify both populations in RAG2$^{-/-}$ mice during EAE by isolation of lymphocytes from the CNS and spleen (2.2.15) followed by FACS analysis (2.2.4). Additionally, we measured cytokine and transcription factor expression of both populations (2.2.8 / 2.2.9). This FACS gating strategy was used to determine frequency and absolute numbers of lymphocyte populations in the following experiments (Figure 10).

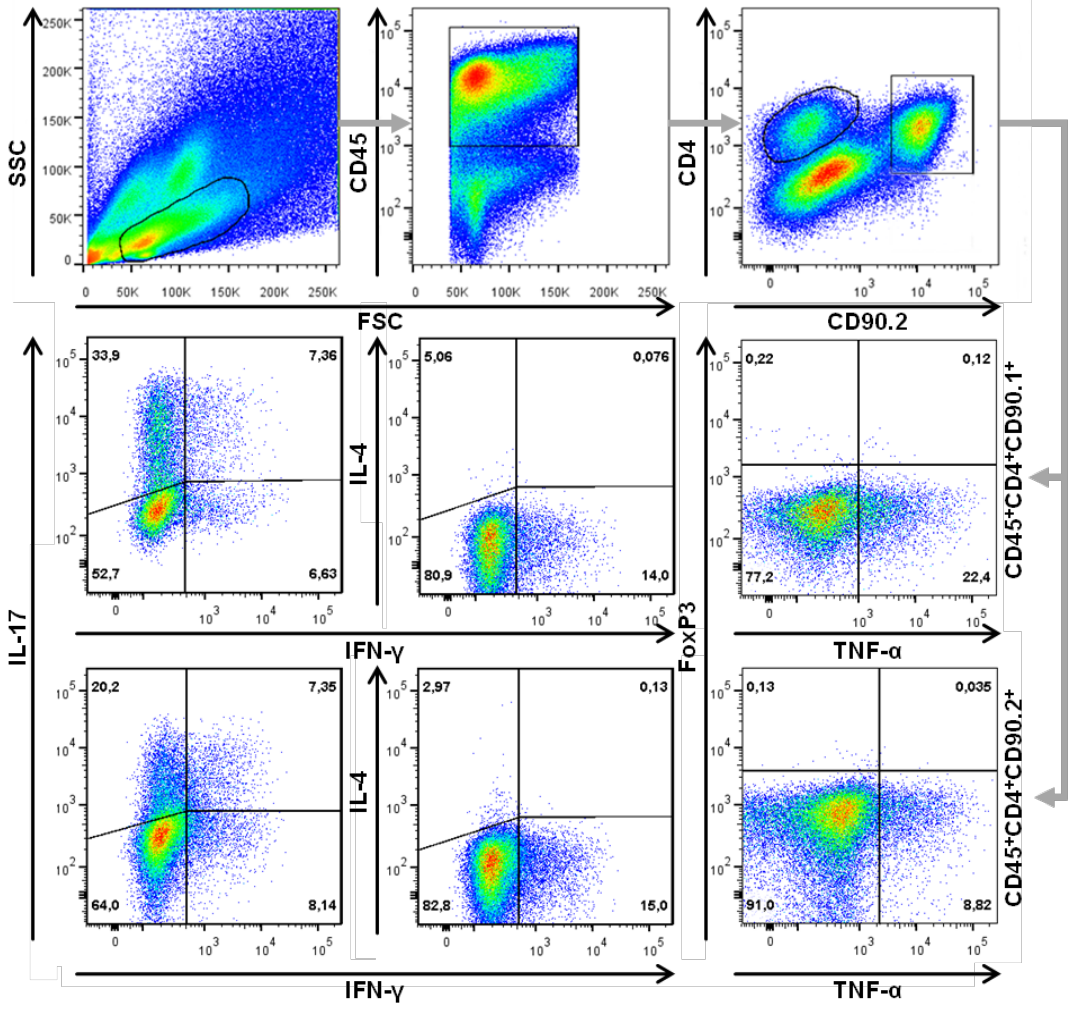

Figure 10: FACS gating strategy to investigate cytokine profiles of transferred T cell populations

Using FACS, the disease-inducing 2d2 T cells and the co-transferred 2d2 T cells we discriminated via the congenic CD90 (Thy1) marker after gating on CD45^{+}CD4^{+} cells (first row). Subsequently, the cytokine expression of the CD45^{+}CD4^{+}CD90.1^{+} (second row) and CD45^{+}CD4^{+}CD90.2^{+} (third row) was determined. The example shows lymphocytes from the CNS of a RAG$^{-/-}$ mouse, which received CD90.1^{+} and CD90.2^{+} Th17 cells.

3.1.3 Co-transfer of Th1 or Th2 cells before onset of the disease decreases lymphocyte numbers in the peak of the disease in the CNS

The pathogenicity of the different T cell subsets in MS and EAE is dependent on their capacity to invade the CNS compartment. It was previously demonstrated that Th17 cells can destabilize the blood-brain barrier and enhance recruitment of CD4 T cells to the CNS (Kebir et al., 2007). We therefore aimed to evaluate if the clinical impact observed upon co-transfer of different Th cell populations was dependent on the capacity of the distinct T cells subsets to modify the infiltration of the CNS by the disease-inducing Th17 cell population. Secondly, we were interested if the co-transferred T cell population differently homed to the CNS in the presence of ongoing Th17 inflammation.

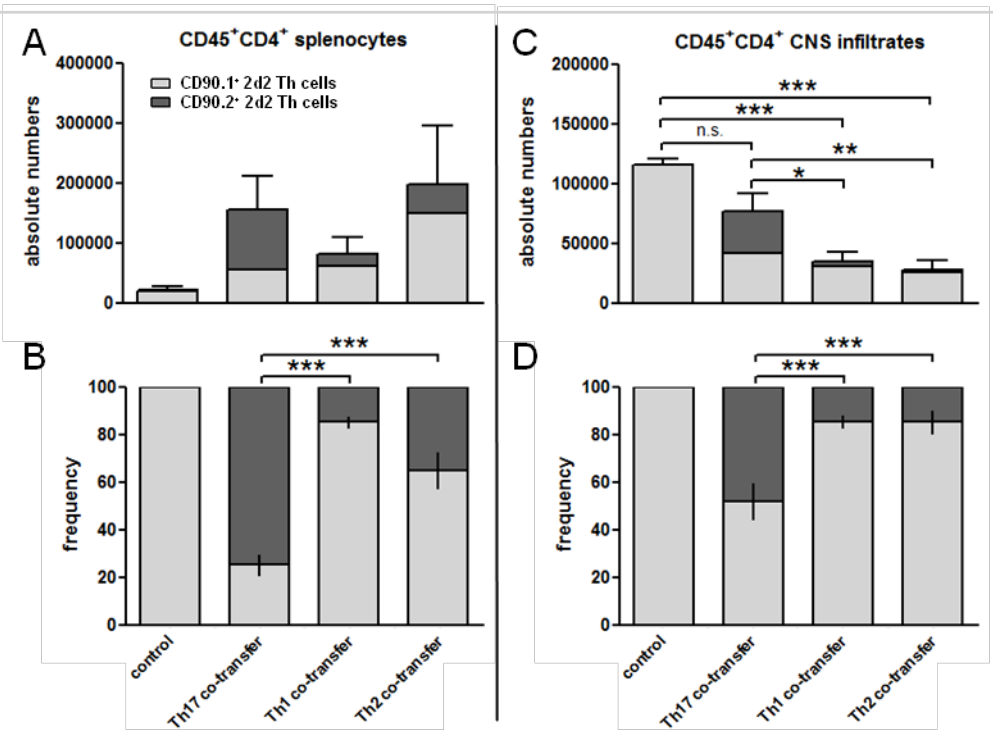

Figure 11: Th17 cells infiltrate the CNS more efficiently than Th1 or Th2 cells upon co-transfer at the onset of the disease

EAE was induced by adoptive transfer of CD90.1$^+$ 2d2 Th17 cells in Rag2$^{-/-}$ mice. Seven days later a second (co-) transfer of either 2d2 Th17, 2d2 Th1, or 2d2 Th2 cells derived from CD90.2$^+$ mice was performed. Both populations were isolated from the CNS and spleen at the peak of the disease for subsequent flow cytometry analysis. Absolute numbers (A) and percentages (B) of CD45$^+$ CD4$^+$ cells in the spleen, gating on CD90.1$^+$ versus CD90.2$^+$ populations. Absolute numbers (C) and percentages (D) of CNS-infiltrating CD45$^+$ CD4$^+$ cells, gating on CD90.1$^+$ versus CD90.2$^+$ populations. Pooled data from three independent experiments. Control n = 5 animals, co-transfer of Th17 n = 8, Th1 n = 7, or Th2 n = 8. One-way ANOVA with Dunnett's Multiple Comparison Test; * $p < 0.05$, ** $p < 0.01$, *** $p < 0.001$, **** $p < 0.0001$. Data shown are mean ± SEM.

In accordance with the observed clinical course, the absolute number of CD4 T cells did not differ significantly in the CNS at peak of the disease if 2d2 Th17 cells were co-transferred compared to PBS injection. The disease-inducing and the co-transferred 2d2 Th17 populations were present in similar proportion in the CNS. However, co-transferred Th1 or Th2 cells infiltrated the CNS in significantly lower proportions and numbers compared to co-transferred Th17 or controls, although they were still present in the spleen of recipients at the peak of the disease (Figure 11 A+C). Most importantly, as compared to controls or Th17 co-transfer, they caused a significant reduction of the number of CD90.1$^+$ Th17 cells present in the CNS, but not in the spleen of recipient animals. Our data show that co-transferred 2d2 Th17 cells infiltrate the CNS more efficiently than 2d2 Th1 or 2d2 Th2 in ongoing CNS inflammation (Figure 11 B+D).

3.1.4 No significant differences in absolute numbers and frequency of CD45$^+$CD11b$^+$ cells in CNS or spleen

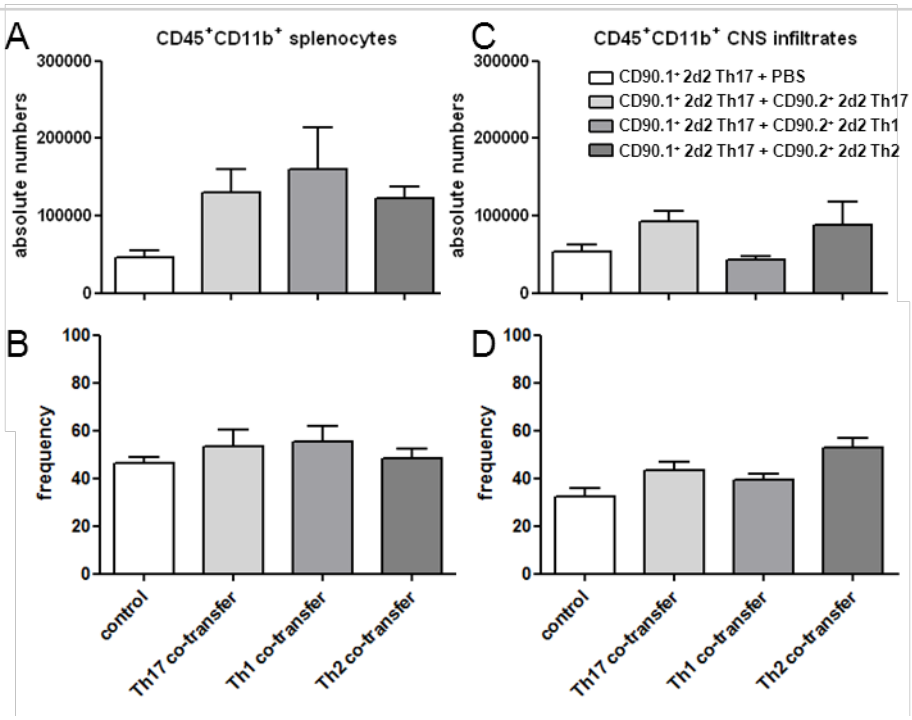

Figure 12: No significant differences in absolute numbers and frequency of CD45$^+$ CD11b$^+$ cells in CNS or spleen

CD45$^+$ CD11b$^+$ cells were isolated from the spleen and CNS of recipients at the peak of the disease and analyzed by flow cytometry. Absolute numbers of CD45$^+$ CD11b$^+$ (A) and frequency of CD45$^+$ CD11b$^+$ (B) populations extracted from the spleen. Absolute numbers of CD45$^+$ CD11b$^+$ (C) and frequency of CD45$^+$ CD11b $^+$ (D) populations extracted from the CNS. Pooled data from three independent experiments. Control n = 5 animals, co-transfer of Th17 n = 8, Th1 n = 7, or Th2 n = 8. One-way ANOVA with Bonferroni's Multiple Comparison Test; * $p < 0.05$, ** $p < 0.01$, *** $p < 0.001$, **** $p < 0.0001$. Data shown are mean ± SEM.

To shed light on the potential mechanisms implicated in Th1- and Th2-mediated attenuation of Th17-driven EAE, we first compared the impact of the different co-transfer conditions on the presence of antigen-presenting cells ($CD45^+CD11b^+$) cells in the spleen and their infiltration of the CNS. No significant differences in absolute numbers and frequency of $CD45^+CD11b^+$ cells were found in the spleen or in the CNS of the recipients of the different co-transfers (Figure 12, A-D). Therefore, there is no indication that Th1 or Th2 co-transfer ameliorates EAE by influencing the recruitment of monocytes and macrophages to the CNS.

3.1.5 Fate and plasticity of disease- inducing CD90.1$^+$ 2d2 Th17 cells following co-transfer of Th1, Th2 or Th17 cells

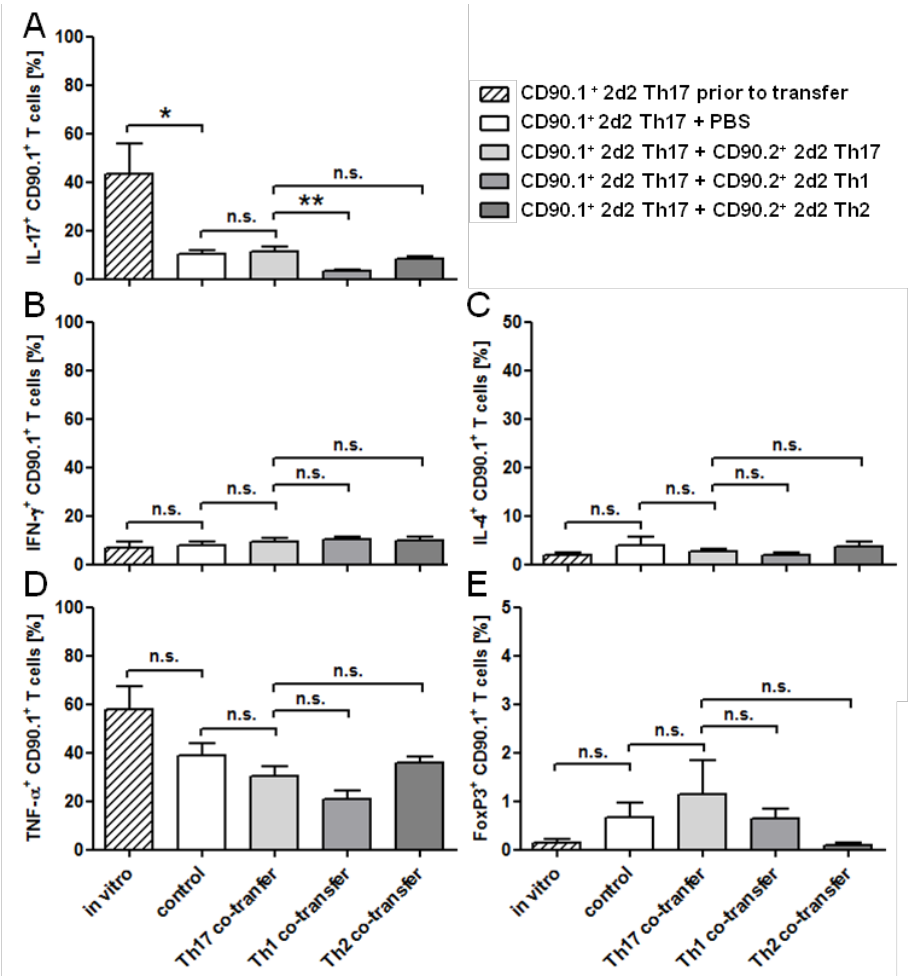

Figure 13: Fate and plasticity of disease inducing CD90.1$^+$ 2d2 Th17 cells in the spleen

$CD45^+CD4^+CD90.1^+$ cells were isolated from the spleen at the peak of the disease and their cytokine profiles analyzed by flow cytometry. Percentages of Th cells expressing IL-17 (A), IFN-γ (B), IL-4 (C), TNF-α (D) and FoxP3 (E) of the CD90.1$^+$ population. Pooled data from three independent experiments. Control n = 5 animals, co-transfer of Th17 n = 8, Th1 n = 7, or Th2 n = 8. One-way ANOVA with Dunnett's Multiple Comparison Test or unpaired t test (prior Th17 transfer vs. Th17 transfer); * $p < 0.05$, ** $p < 0.01$, *** $p < 0.001$, **** $p < 0.0001$. Data shown are mean ± SEM.

To study the impact of the distinct co-transferred populations on the phenotype of the disease-inducing Th17 cells, we further characterized the cytokine profile of the $CD45^+CD4^+CD90.1^+$ cells isolated from the spleen and the CNS of recipients at the peak of the disease. As compared to IL-17-producing cells *in vitro* (before transfer), the frequency of IL-17-producing cells *ex vivo* after transfer was significantly lower in the spleen, but not in the CNS (Figure 13 A, Figure 14 A). This suggests that $IL17^+$ Th cells preferentially entered the CNS. Co-transfer of 2d2 Th1 cells significantly reduced numbers of IL-17 expressing cells among the disease-inducing T cells in the spleen as compared to control or co-transfer of Th17 cells. However, no impact of the co-transferred Th17 and Th2 cells on the first CD90.1 population was observed in the spleen (Figure 13 A-E).

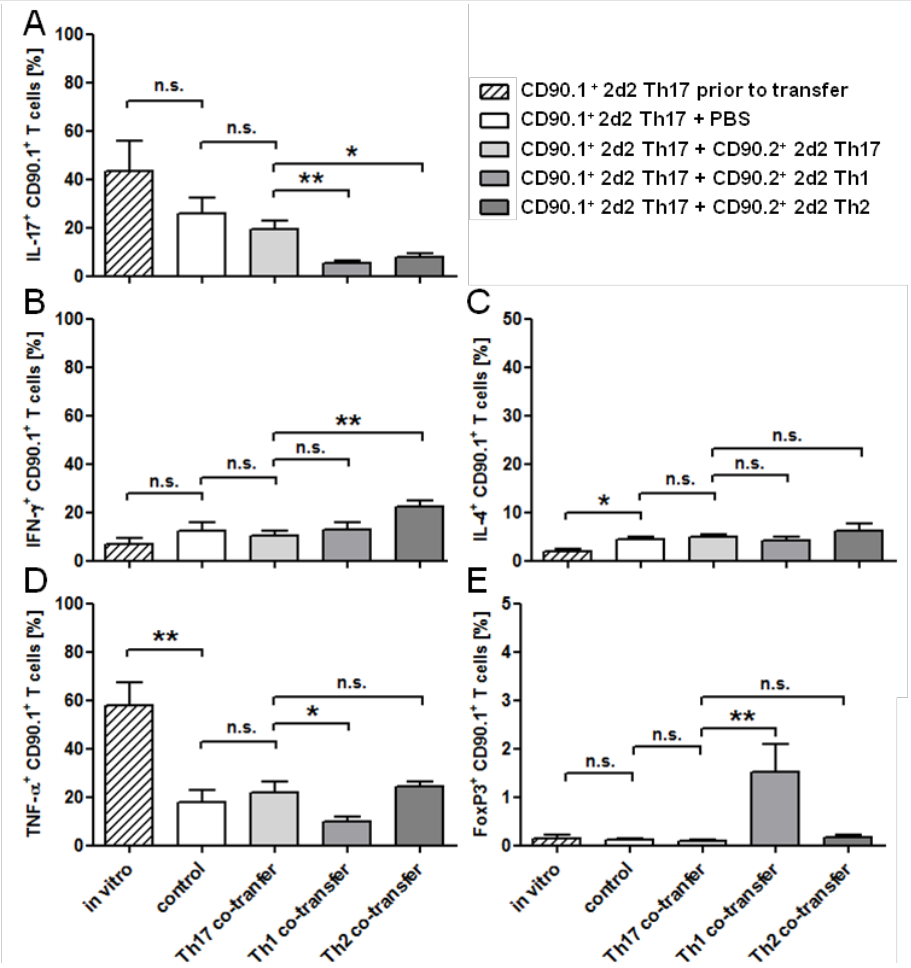

Figure 14: Fate and plasticity of disease-inducing $CD90.1^+$ 2d2 Th17 cells in the CNS

$CD45^+CD4^+CD90.1^+$ cells were isolated from the CNS at the peak of the disease and their cytokine profiles analyzed by flow cytometry. Percentages of Th cells expressing IL-17 (A), IFN-γ (B), IL-4 (C), TNF-α (D) and FoxP3 (E) of the $CD90.1^+$ population. Pooled data from three independent experiments. Control n = 5 animals, co-transfer of Th17 n = 8, Th1 n = 7, or Th2 n = 8. One-way ANOVA with Dunnett's Multiple Comparison Test or unpaired t test (prior Th17 transfer vs. Th17 transfer); * $p < 0.05$, ** $p < 0.01$, *** $p < 0.001$, **** $p < 0.0001$. Data shown are mean ± SEM.

In the CNS, co-transfer of 2d2 Th1 cells significantly reduced the frequency of IL-17- and TNF-α-producers among the disease-inducing 2d2 Th17 population (Figure 14 A+D). Furthermore, expression of the transcription factor FoxP3, which is associated with a regulatory phenotype, was significantly induced in the initial $CD90.1^+$ population upon co-transfer of Th1 cells (Figure 14 E). Those FoxP3-expressing 2d2 T cells did not produce IL-17, IFN-γ, IL-4 or TNF-α (Figure 15, panel 2). In contrast, co-transfer of Th2 cells did not induce FoxP3-expressing T cells, but modified Th17 cells so that there were more IFN-γ producers and less IL-17 producers (Figure 14 A+B). There was no significant change in cytokine expression of the $CD90.1^+$ population following co-transfer of 2d2 Th17 cells as compared to control (Figure 14 A-E). Taken together, our data demonstrate that Th1 and Th2 cells can modulate the disease-inducing 2d2 Th17 cells, skewing its cytokine profile mainly in the CNS, while co-transfer of Th17 cells did not cause any significant change. Our data demonstrate that changes in the phenotype of the disease-inducing Th17 cells underlie the improved clinical phenotype (Figure 9). We identified that the modulation of the disease-inducing 2d2 cells was largely restricted to the CNS compartment (Figure 13 vs. Figure 14).

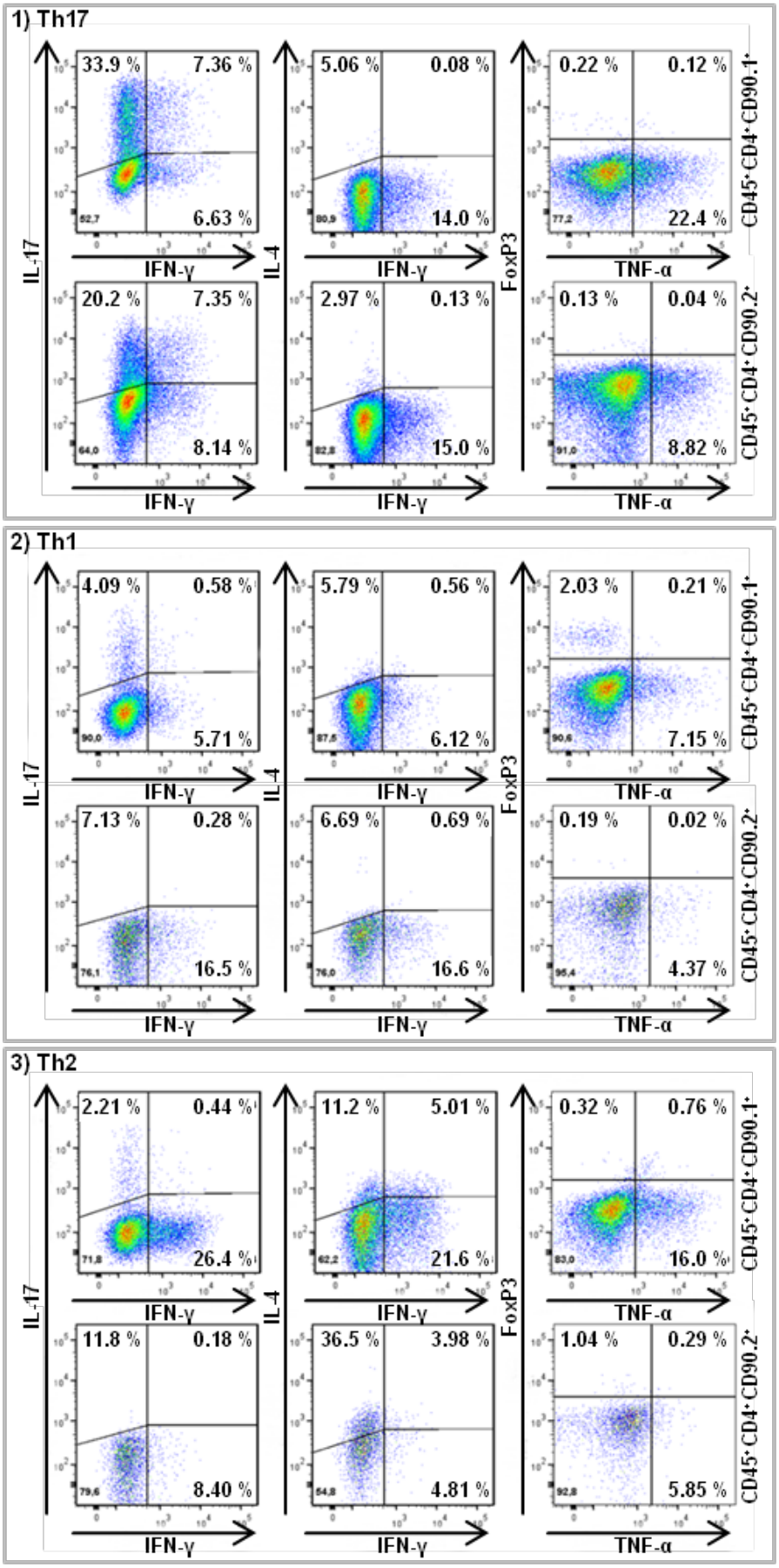

Figure 15: Representative FACS data on T cell populations in the CNS

To study the effect on the disease inducing Th17 cells by co-transfer of distinct T helper cell subsets, $CD45^+CD4^+CD90.1^+$ cells were rescued from the CNS at the peak of the disease and checked for their cytokine profiles by flow cytometry. Co-transfer of 2d2 Th1 cells silenced 2d2 Th17 cytokine expression indicated by a reduction of $IL\text{-}17^+$ and $TNF\text{-}\alpha^+$ cells of the $CD90.1^+$ population (panel 2, first row). Moreover the expression of the transcription factor FoxP3 was induced exclusively upon co-transfer of Th1 cells in $CD90.1^+$ cells. Co-transfer of Th2 cells drove $CD90.1^+$ Th17 cells to an ex-Th17 phenotype characterized by an enhanced frequency of $IFN\text{-}\gamma^+$ cells and less IL-17 producers (panel 3, first row). There was no change in cytokine expression of the $CD90.1^+$ population following the co-transfer of 2d2 Th17 cells (panel 1, first row). The $CD90.2^+$ co-transferred populations kept their subtype specific cytokine profile (panel 1-3. second row).

3.1.6 Fate and plasticity of co-transferred CD90.2$^+$ 2d2 T helper cells

To gain insight into the phenotypic stability of the co-transferred Th cell populations during disease progression, co-transferred CD45$^+$CD4$^+$CD90.2$^+$ cell populations were re-isolated from the spleen and CNS at the peak of the disease and cytokine expression profiles were measured by flow cytometry.

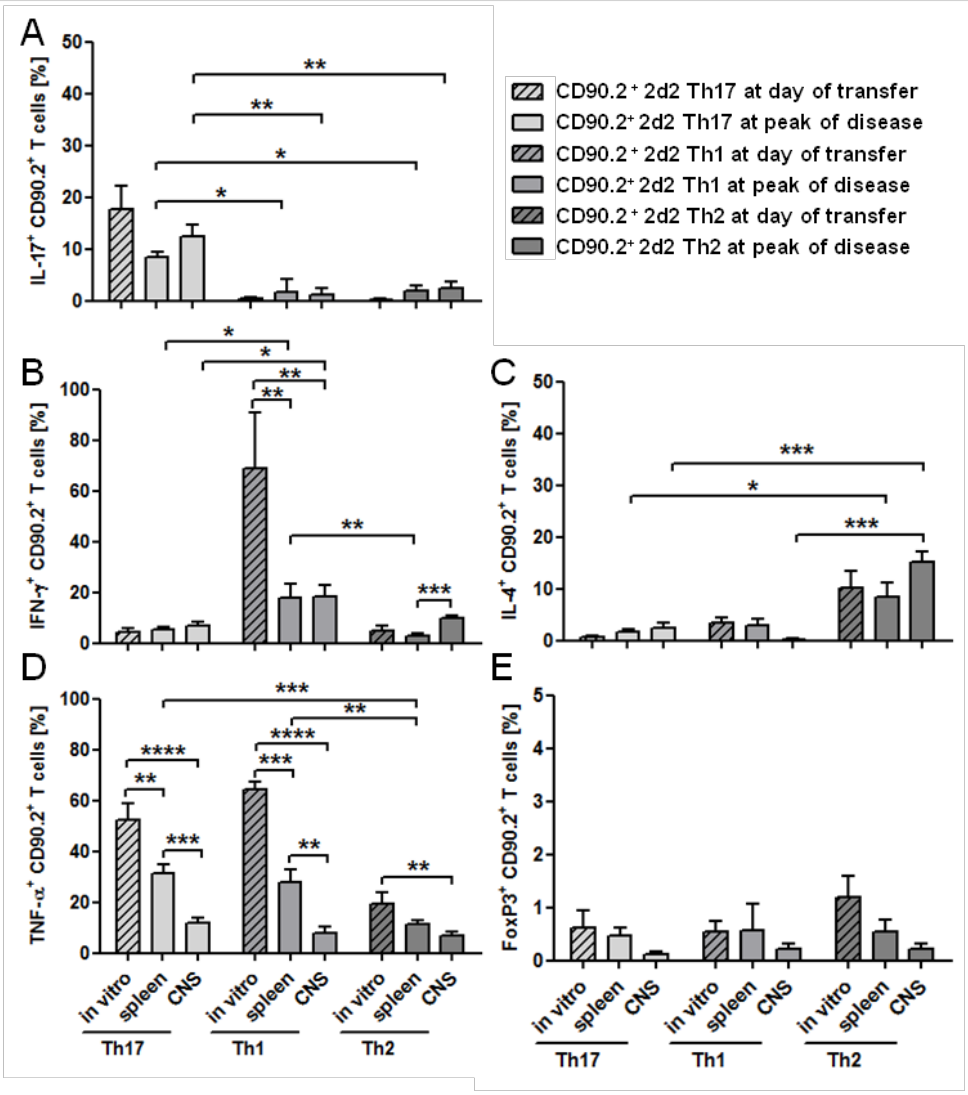

Figure 16: Fate and plasticity of co-transferred CD90.2$^+$ 2d2 T helper cells

CD45$^+$CD4$^+$CD90.2$^+$ cells were isolated from the spleen and the CNS at the peak of the disease and their cytokine profiles analyzed by flow cytometry. Percentages of Th cells expressing IL-17 (A), IFN-γ (B), IL-4 (C), TNF-α (D), and FoxP3 (E) of the CD90.2$^+$ population. Pooled data from three independent experiments. Control n = 5 animals, co-transfer of Th17 n = 8, Th1 n = 7, or Th2 n = 8. One-way ANOVA with Dunnett's Multiple Comparison Test or unpaired t test (prior Th transfer vs. Th co-transfer); * $p < 0.05$, ** $p < 0.01$, *** $p < 0.001$, **** $p < 0.0001$. Data shown are mean ± SEM.

All co-transferred T cell populations kept their Th cell subtype-specific cytokine profiles, i.e. the frequency of IL-17-producing cells was significantly higher in co-transferred Th17 populations and the frequency of IFN-γ^+ cells was superior in co-transferred Th1 populations, while most IL-4-producing cells were detected in co-transferred Th2 populations in spleen and CNS (Figure 16 A-C). Nevertheless, the frequency of TNF-α^+ *ex vivo* cells was reduced as compared to the *in vitro* cultures in all three subsets (Figure 16 D). Additionally, a significant increase in the frequency of IFN-γ^+ cells of the Th2 subsets in the CNS was observed compared to the spleen (Figure 16 B). Foxp3 was expressed in very low amounts and its expression did not change significantly in all three subsets during disease progression (Figure 16 E).

3.1.7 Different impact of neurons on the effector function of the distinct T cell subsets

Lastly, we wanted to know whether target cells are capable of shifting encephalitogenic Th17, since an induction of regulatory T cells by neurons was reported previously (Liu et al., 2006). The direct effect of a crosstalk between Th cell subsets and the neuronal compartment was investigated by performing co-cultures of *in vitro* differentiated Th cell subsets with primary neurons (2.2.12). Following exposure to neuronal cultures, Th17 populations showed significantly more IL-17$^+$ cells, indicating a shift towards a more pro-inflammatory phenotype (Figure 17, panel 1). In contrast, a significant upregulation of the regulatory cytokine IL-10 was detected in Th1 cells after co-culture (Figure 17, panel 2). The cytokine profile of Th2 cells did not change significantly (Figure 17, panel 3).

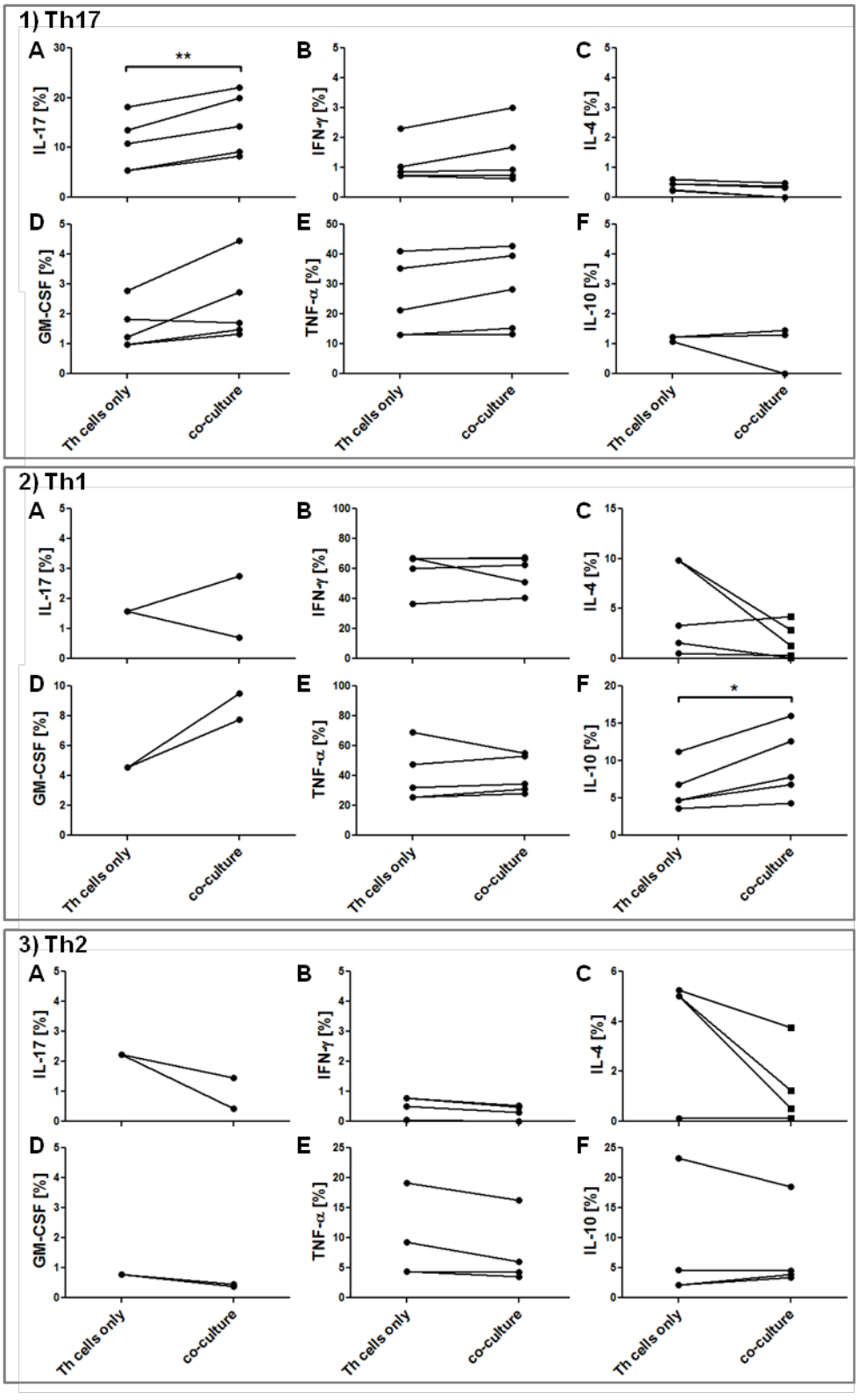

Figure 17: Different impact of neurons on the effector function of the distinct T cell subsets

Co-cultures of DIV4 primary neurons and *in vitro* primed Th cells for 24 hr with a ratio of 1:1. Subsequently, the cytokine profile of the Th cells was analyzed by flow cytometry. Expression of major cytokines (A-F) before and after co-culture with neurons of Th17 (1), Th1 (2) and Th2 (3) cells. Pooled data from two to five independent experiments. Paired t test, two-tailed; * $p < 0.05$, ** $p < 0.01$, *** $p < 0.001$, **** $p < 0.0001$.

3.2 sICAM-5 as a neuronal regulator of neuroinflammation

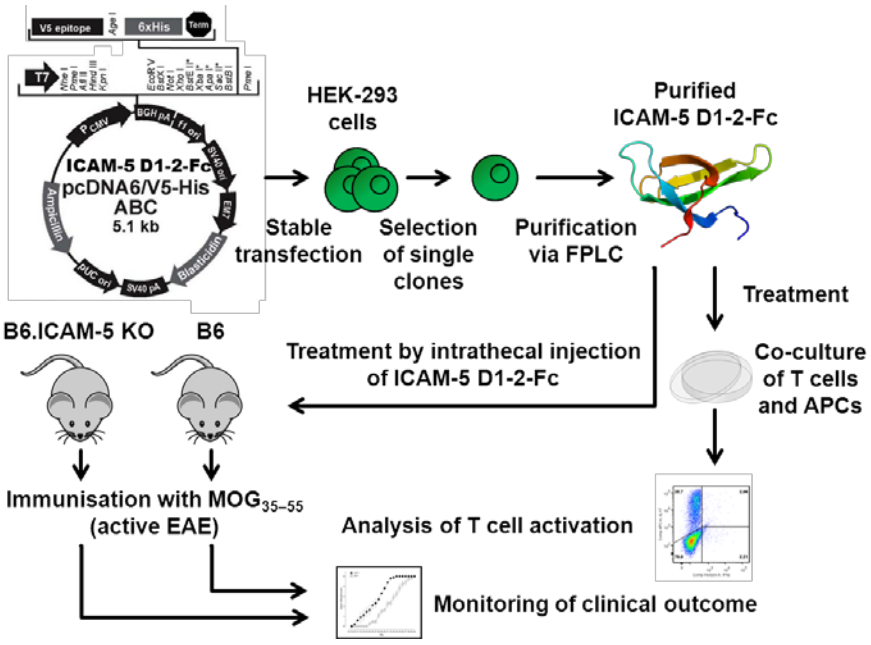

Figure 18: Experimental design project II

To define the role of ICAM-5 during neuroinflammation three experimental setups were designed. First EAE was induced in ICAM-5 KO mice to validate the consequence of the absence of soluble and membrane-bound ICAM-5 in disease progression. Additionally, to focus on the impact of soluble form of the protein, ICAM-5 D1-2-Fc was stably transfected in HEK-293 cells and purified via FPLC. Subsequently, T cell co-cultures with APCs and EAE mice were treated with ICAM-5 D1-2-Fc to investigate its potential to inhibit T cell restimulation and attenuate disease progression, respectively.

3.2.1 Generation and purification of ICAM-5 D1-2-Fc via Fast Protein Liquid Chromatography (FPLC)

To define the immunosuppressive potential of sICAM5 we used a fusionprotein consisting of the NH_2-terminal first and second domain (D1-2) of ICAM-5 combined with an Fc-tail from human IgG, called ICAM-5 D1-2-Fc. The first domain of ICAM-5 is essential for LFA-1 binding, stabilized by the second domain (Recacha et al., 2014; Tian et al., 2000). The Fc-tail serves as an anchor during the purification of the fusionprotein from the supernatant of cells via Fc-affine protein-G columns. This makes ICAM-5 D1-2-Fc an appropriate tool for mimicking sICAM-5 and treatment applications *in vitro* and *in vivo*.

The recombinant sequence of ICAM-5 D1-2-Fc was kindly provided by the Gahmberg laboratory, University of Helsinki, Finland. The sequence was cloned from the original pEF-Fc vector into the pcDNA6/V5-His B vector (data not shown) to make it suitable for

recombinant expression of the fusionprotein in human embryonic kidney (HEK)-293 cells. Subsequently, HEK-293 cells were transfected with the vector and selected according to successful insertion of the vector sequence into the genome. Those stable transfected clones were tested for ICAM-5 D1-2-Fc expression by Western blot of the cell supernatant (Figure 19 A). The clone B2 showed reasonable expression of the fusionprotein and was used henceforth for ICAM-5 D1-2-Fc production. Although the transient transfected HEK-293 cells secreted higher amounts of the fusionprotein, with the stable expression by the clone B2 we avoided repetitive demanding transfections and generated expanded productive HEK-293 cultures more frugally.

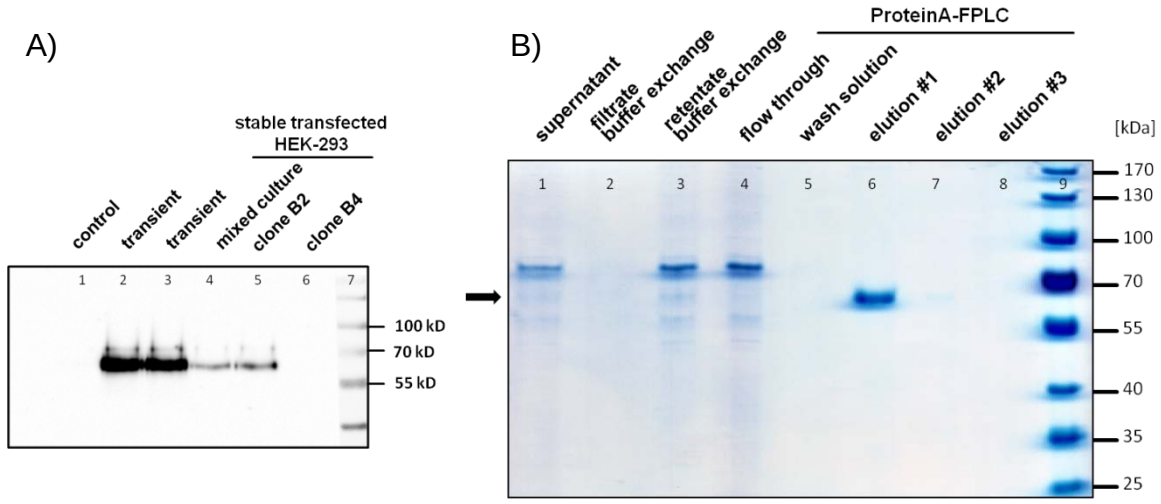

Figure 19: Generation and purification of ICAM-5 D1-2-Fc via Fast Protein Liquid Chromatography (FPLC) (A) HEK-293 cells were stably transfected with the pcDNA6 vector including the ICAM-5 D1-2-Fc sequence. Supernatants of single cell cultures were analyzed for ICAM-5 D1-2-Fc expression via Western Blot using Peroxidase-conjugated α-human-IgG-antibodies. Western-blot of supernatants obtained from single cell cultures from stably transfected HEK-293 cells (5+6) in comparison with the supernatants of a mixed culture of stable transfected cells (4) and of transient transfected cells (2+3). (7) Marker, (1) supernatant of cells transient transfected with pcDNA6 without an insert as negative control. (B) ICAM-5 D1-2-Fc was purified from the supernatant of stable transfected HEK-293 B2 clones via ProteinA-FPLC. Purity was validated on SDS-PAGE via Coomassie Blue staining. Coomassie staining of the (1) supernatant from HEK-293 B2 clone culture, (2) filtrate of buffer exchange, (3) retentate of the buffer exchange, (4) ProteinA-FPLC column flow through, (5) ProteinA-FPLC column wash solution, (6) ProteinA-FPLC column elution #1, (7) ProteinA-FPLC column elution #2, (8) ProteinA-FPLC column elution #3, (9) marker. Arrow marks 65 kDa position showing the enrichment of ICAM-5 D1-2-Fc. Experiments were performed in cooperation with the Koch-Brandt laboratory, Biochemistry Institute, University Mainz, Germany.

The purification of ICAM-5 D1-2-Fc from the supernatant of HEK-293 B2-cultures was performed using Fast Protein Liquid Chromatography (FPLC) in cooperation with the Koch-Brandt laboratory, Biochemistry Institute, University Mainz, Germany. We utilized the Fc-tail

of the fusionprotein, which has a high affinity towards Protein G, an immunoglobulin-binding protein expressed in Streptococcal bacteria. By using Protein G loaded columns we were able to produce highly pure ICAM-5 D1-2-Fc solutions without protein contaminations during FPLC runs (Figure 19 B).

3.2.2 ICAM-5 D1-2-Fc inhibits the activation and proliferation of T cells in the presence of APCs

To test the biological functionality of our purified fusionprotein we performed co-cultures of naïve 2d2 T cells and APCs in the presence of $MOG_{35–55}$. Under control conditions antigen-presentation via APCs activated MOG_{35-55}-specific T cells detected by the upregulation of the surface activation marker CD25 (Figure 20 A), an increase of the average cell size (Figure 20 A, FSC) and high proliferation rates (Figure 20 B+C). In our hands, treatment with ICAM-5 D1-2-Fc led to a dose-dependent decrease of CD25 expressing cells from 80.8 % to 61 %, the frequency of T cells increased in cell size dropped from 14.5 % to 3.7 % and the proliferations rate was limited compared to control conditions (Figure 20 A-C). The inhibitory effect did not occur when T cells were stimulated antigen-independently with α-CD3 and α-CD28 (Figure 20 A). Therefore ICAM-5 D1-2-Fc presumably blocks the immunological synapse between T cells and APCs. Treatment of T cell-APC co-cultures with human IgG applied at equal concentrations as a control peptide, which shares structural properties (Fc tail) with the fusionprotein, did not show an effect on the measured parameters (Figure 20 A). Thus, ICAM-5 D1-2-Fc inhibited dose dependent T cell activation and proliferation induced by APCs. The published data on the immune-regulatory properties of sICAM-5 and the functionality of the purified fusionprotein was hereby confirmed (Tian et al., 2008) in our MOG-dependent co-culture model. We therefore concluded that sICAM-5 has the potential to regulate T cell restimulation during ongoing neuroinflammation also *in vivo*.

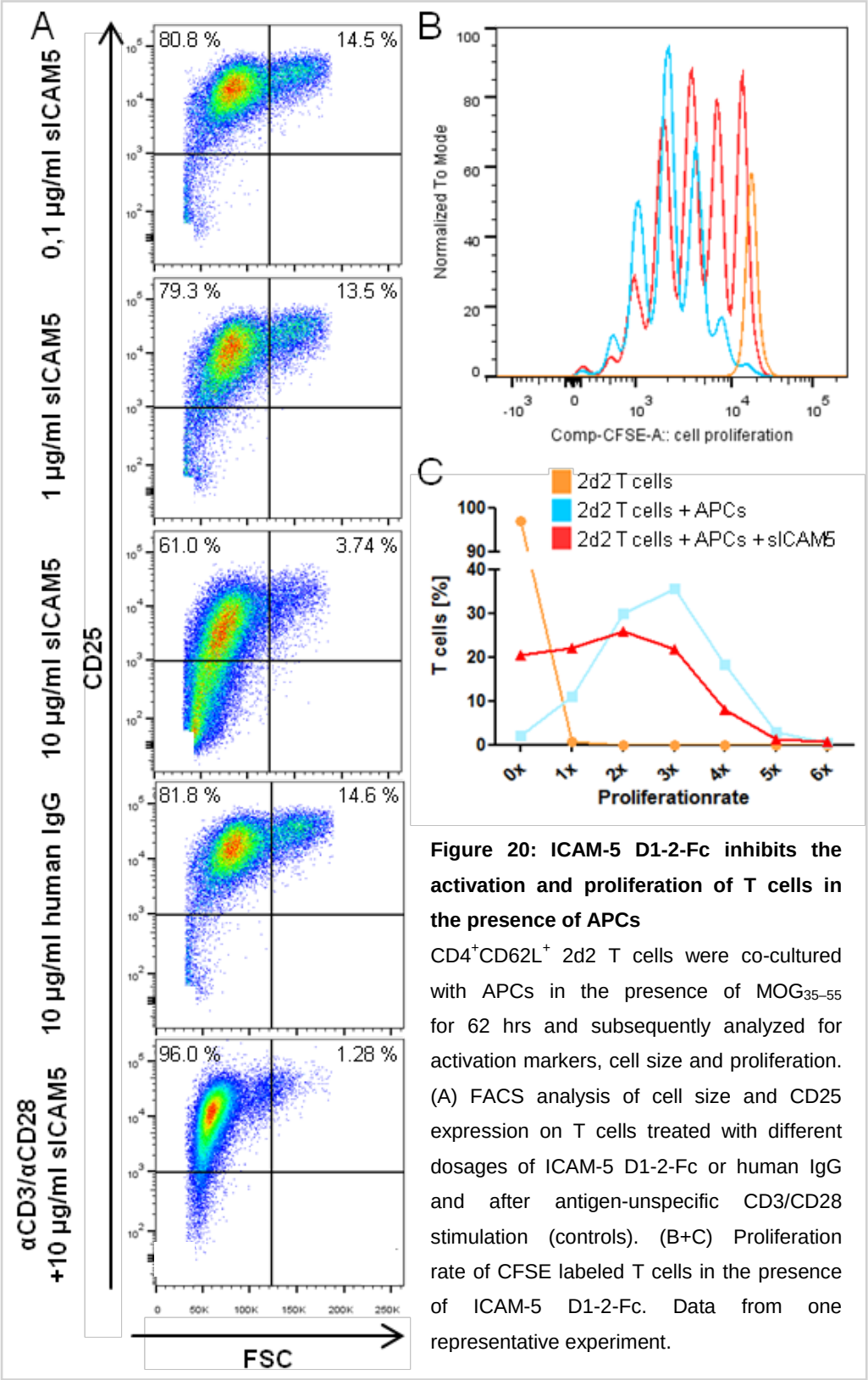

Figure 20: ICAM-5 D1-2-Fc inhibits the activation and proliferation of T cells in the presence of APCs

$CD4^+CD62L^+$ 2d2 T cells were co-cultured with APCs in the presence of $MOG_{35–55}$ for 62 hrs and subsequently analyzed for activation markers, cell size and proliferation. (A) FACS analysis of cell size and CD25 expression on T cells treated with different dosages of ICAM-5 D1-2-Fc or human IgG and after antigen-unspecific CD3/CD28 stimulation (controls). (B+C) Proliferation rate of CFSE labeled T cells in the presence of ICAM-5 D1-2-Fc. Data from one representative experiment.

3.2.3 Absence of ICAM-5 worsens disease progression in active EAE mice

Despite its potential to regulate T cell restimulation as well as function as an adhesion molecule for lymphocytes *in vitro*, the relevance of ICAM-5 in neuroinflammation has not been investigated *in vivo*. In the context of neuroinflammation, membrane bound ICAM-5 could be considered as pro-inflammatory serving as an adhesion protein for autoreactive T cells. In contrast, the shedded soluble form, sICAM-5, shows regulatory features of immune responses by inhibiting APC-driven T cell restimulation. Thus, absence of total ICAM-5 could hypothetically be a benefit in terms of a disturbed attachment of autoreactive T cells to neurons but also a disadvantage due to a loss of a neuronal defense mechanism. To elucidate the ambivalent role of ICAM-5 *in vivo*, we induced EAE in B6 mice deficient for ICAM-5 and in littermates.

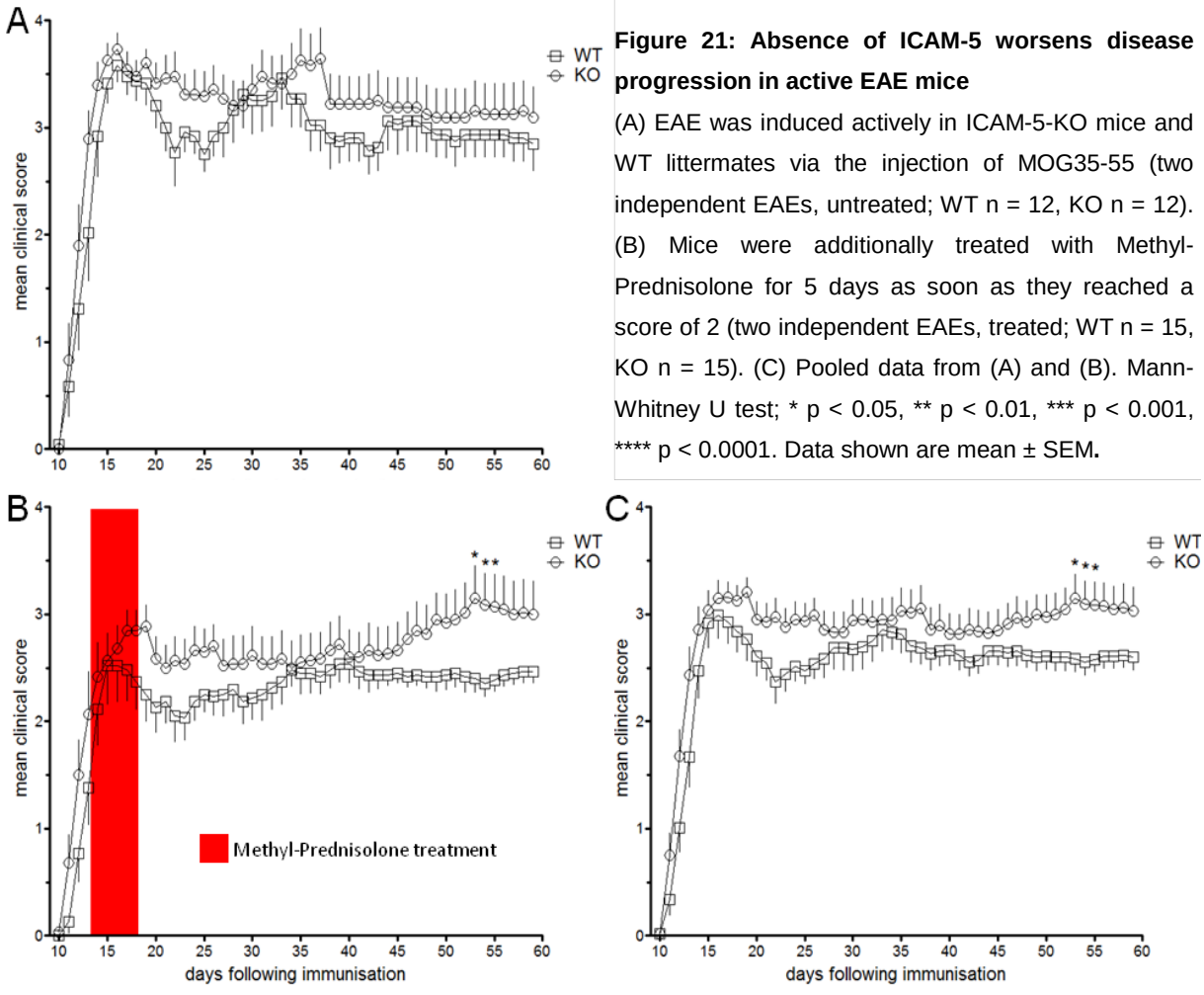

Figure 21: Absence of ICAM-5 worsens disease progression in active EAE mice
(A) EAE was induced actively in ICAM-5-KO mice and WT littermates via the injection of MOG35-55 (two independent EAEs, untreated; WT n = 12, KO n = 12). (B) Mice were additionally treated with Methyl-Prednisolone for 5 days as soon as they reached a score of 2 (two independent EAEs, treated; WT n = 15, KO n = 15). (C) Pooled data from (A) and (B). Mann-Whitney U test; * $p < 0.05$, ** $p < 0.01$, *** $p < 0.001$, **** $p < 0.0001$. Data shown are mean ± SEM.

Surprisingly, the clinical outcome of ICAM-5 mice did not differ compared to wild-type (WT) mice (Figure 21 A). There were no differences in disease severity neither at disease

onset nor in the chronic phase. The absence of ICAM-5 does not alter the measured clinical deficits significantly and therefore ICAM-5 is not essential as a neuronal adhesion or regulatory molecule in the development and perpetuation of neuroinflammation. However, a tendency towards less pronounced phases of recovery is noticeable in the ICAM-5 KO group. A possible effect of the loss of a physiological regulatory mechanism might be superimposed by the harsh induction of neuroinflammation in active EAE. Thus, we treated in follow up experiments EAE mice with anti-inflammatory steroids for 5 days as soon as they reached a score of 2 (2.2.14.3). As a result the average maximum score in the first peak dropped from 3.5 to 2.5 followed by a slow and chronic progressive deterioration of clinical disability (Figure 21 B). This model allowed us to investigate the progressive phase without being superimposed by initially occurring non-remitting disability of the first peak. Indeed, significant differences in clinical score were observed between the two groups in the chronic phase under those conditions. The absence of ICAM-5 led to higher disability in the progressive phase in EAE.

3.2.4 sICAM-5 attenuates disease progression in active EAE mice

The results from our T cell-APC co-cultures and the EAE with ICAM-5 KO mice shifted our focus towards the regulatory function of sICAM-5 during neuroinflammation. While the potential of ICAM-5 D1-2 Fc to inhibit restimulation of T cell via APCs is established, the significance of sICAM-5 in EAE is not clarified.

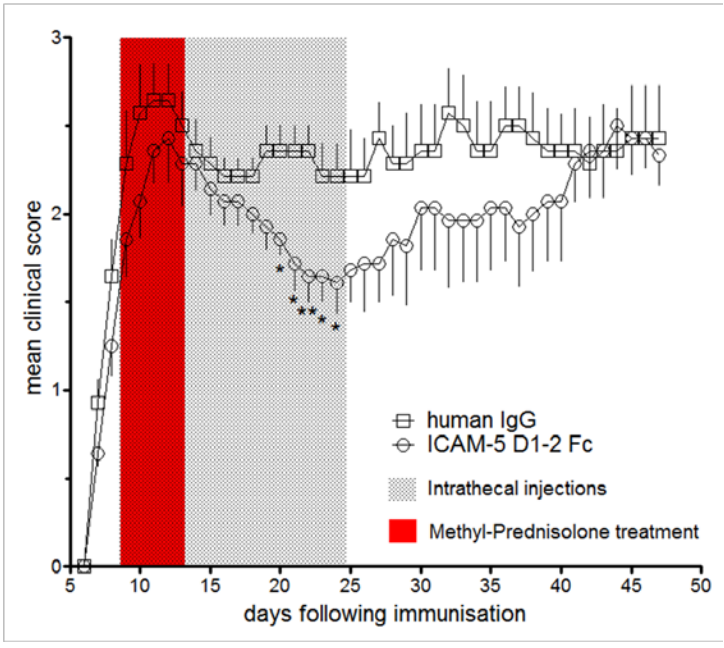

Figure 22: sICAM-5 attenuates disease progression in active EAE mice
EAE was induced actively in B6 mice via the injection of MOG_{35-55} and mice were treated with Methyl-Prednisolone for 5 days as soon as the mice reached a clinical score of 2. Additionally 0.2 µg ICAM-5 D1-2 Fc or human IgG was applied via intrathecal injection by lumbar puncture seven times on every second day beginning on the day of a clinical score of 2 (WT n = 7, KO n = 7). Mann-Whitney U test; * $p < 0.05$, ** $p < 0.01$, *** $p < 0.001$, **** $p < 0.0001$. Data shown are mean ± SEM.

We showed that the absence of ICAM-5 led to higher disability in the progressive phase in EAE, which might be due to the loss of sICAM-5 as a local neuronal regulator of inflammation. To examine the impact of sICAM-5 in ongoing neuroinflammation we applied ICAM-5 D1-2 Fc locally via intrathecal injection by lumbar puncture during EAE. The protein was injected seven times on every second day beginning on the day of a clinical score of 2. Human IgG served as a control peptide. We used our active EAE model with consecutive corticosteroids pulses for better resolution of the chronic phase of the disease. The group of mice receiving ICAM-5 D1-2 Fc displayed a more pronounced recovery after the first peak as a result of the treatment. On day 22 the group of mice treated with human IgG showed a mean clinical score of 2.36 ± 0.35, while the intrathecal injections of ICAM-5 D1-2 Fc led to a significant different score of 1.64 ± 0.35. The effect started to diminish after stopping the treatment and the mean clinical scores of the treatment and control group converged 15 days after the last injection (Figure 22).

3.3 Preventing neurodegeneration in neuroinflammation by ion channel blocking

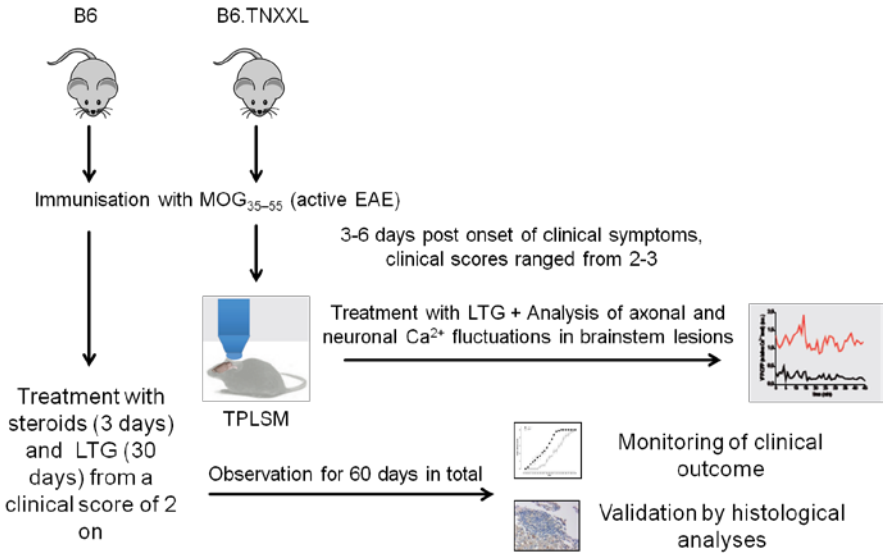

Figure 23: Experimental design project III

To elucidate the potential of ion-channel blockage to prevent neurodegeneration in neuroinflammation we applied the sodium and voltage dependent calcium channel blocker Lamotrigine (LTG) in two different EAE setups. First EAE was induced in B6.TN-XXL mice and TPLSM was performed in the brainstem of EAE affected mice in the peak of the disease. We analyzed the site-specific potential of LTG to reduce free intracellular [Ca^{2+}] in EAE lesions by imaging fluorescence-based semi-quantitative and slow [Ca^{2+}] dynamics. In parallel we immunized B6 mice and treated them beginning on the day of a clinical score of 2 (hind leg weakness) with steroids (anti-inflammatory) for 3 days and with LTG in different doses for 30 days. This model was used to investigate the effect of LTG in the progressive phase of the disease and to test its potential to prevent neuronal/axonal damage with the aim to reduce non-remitting disability.

3.3.1 Ascending cytosolic free [Ca^{2+}] precedes morphologic damage signs of neuronal processes.

We investigated the intracellular free [Ca^{2+}] dynamics in neurons and their processes in EAE of transgenic mice with a the genetically encoded Ca^{2+} indicator (GECI), TN-XXL (Thestrup et al., 2014), expressed under the neuronal promoter thy1. We correlated the ratiometrically evaluated free [Ca^{2+}] with morphologic changes in the course of time and identified neurons and neuronal processes that developed signs of neuronal injury, i.e. dendritic/axonal swelling, during the imaging period morphologic (Figure 24 a).

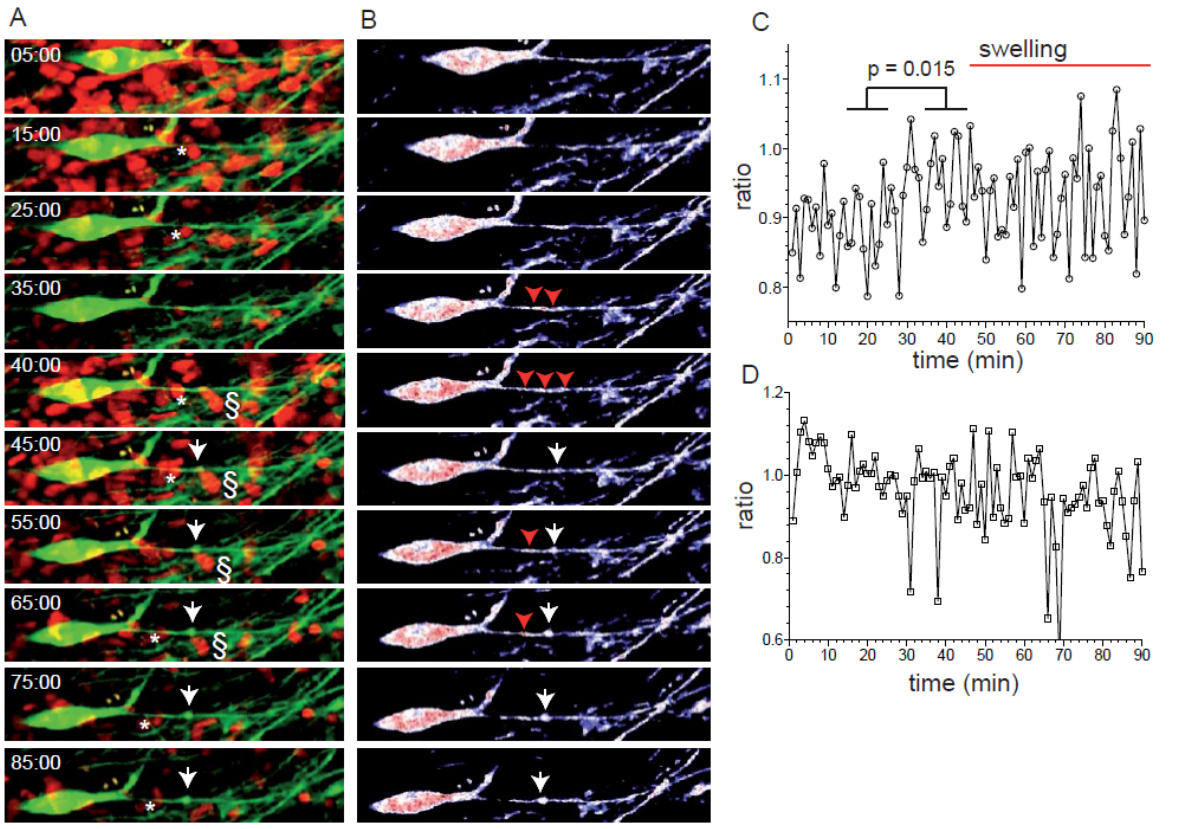

Figure 24: Intracellular free [Ca^{2+}] dynamics in neurons and their processes in EAE

(A) TPLSM imaging of neuronal processes (green) in EAE revealed developed signs of neuronal injury in the form of axonal swelling (arrow) upon interaction with T cells (red). (B) Ratiometric analysis of [Ca^{2+}] dynamics in these processes showed areas of [Ca^{2+}] increase proximal or at the site of later axonal swelling. Both local increases of [Ca^{2+}] were associated with immune cell interactions with the neuronal process (A, ☆, §). (C) Affected axons displayed a significant peak of intracellular [Ca^{2+}] in the period before axonal swelling, whereas control axons with intact axon morphology showed a decrease of [Ca^{2+}] (D).

Using ratiometric analysis of the [Ca^{2+}] dynamics in these processes of YFP and CFP fluorescence intensities revealed that there were areas of [Ca^{2+}] increase at the site of later axonal swelling as well as proximal (nearer to the soma) to this (Figure 24 b). Both of these

local increases of [Ca^{2+}] were associated with immune cell interactions with the neuronal process. In order to quantify site-specific [Ca^{2+}] modifications in single axons, e.g. as a response to interactions between neurons, neuronal processes and immune cells, we calculated the mean intensity of the YFP/CFP-ratio divided by the volume of a single axon of interest over time. To improve the signal to noise ratio of the data, which was due to movement and shift artifacts, we divided the individual area by the changes in the whole imaging area. By that we identified a clear pattern of [Ca^{2+}] modulation with a marked and significant increase in the period before axonal swelling (Figure 24 C). In the same imaging region a control axon with intact axon morphology during the whole imaging period showed rather a decrease of [Ca^{2+}] which followed a decay curve (Figure 24 D). Thus, increase of free intraneuronal [Ca^{2+}] precedes morphologic signs of neuroaxonal damage which are often resulting in irreversible loss of neurons and their connections.

3.3.2 LTG has no influence on FRET-ratiometrically identified, intraaxonal free [Ca^{2+}] in GECI-expressing axons in EAE.

LTG has been described to act on different ion channels (Xie and Hagan, 1998), in particular its main mode of action has been suggested to be the inhibition of glutamate release by blockade of voltage-gated sodium channels (VGSC, Nav1.2, Nav1.5, Nav1.8). However, also voltage-dependent Ca^{2+} channels have been described to be a target of this drug (Stefani et al., 1996). Therefore, the mechanism responsible for the clinical efficacy of this widely used broad-spectrum anti-epileptic drug is not known. Most notably, most of these mechanistic LTG reports measure blocking activity in neuronal preparations by patch-clamp technique in neurons and not in their processes. We therefore analyzed the site-specific potential of LTG to reduce free intracellular [Ca^{2+}] in EAE lesions by imaging fluorescence-based semi-quantitative and slow [Ca^{2+}] dynamics (Figure 23). Based on the hypothesis that LTG might interfere with VGSC we investigated this drug for its Ca^{2+} lowering effect in EAE lesions. We analyzed the kinetics and the effect of LTG on neurons and myelinated axons.

When we focused on the myelinated fiber tracts, we identified interaction of immune cells with the axons and focal increase of [Ca^{2+}] (Figure 25 A). When we applied a “low-dose” of LTG, which we derived from previous reports on *in vitro* preparations, which described a IC50 dose of 20 µM LTG, we found, however, no effect on intraaxonal [Ca^{2+}]. In fact, axonal pathology was ongoing in the presence of LTG (Figure 25 A, arrow). As the superfusion of

LTG in an *in vivo* preparation probably reduces local LTG concentration due to active and passive dilution processes, we hypothesized that the applied dose might be insufficient. Therefore, we increased the dose to 100 µM in the superfusion solution, which is a dose that is also frequently used as saturating concentration for LTG effects of *in vitro* studies (Calabresi et al., 1999).

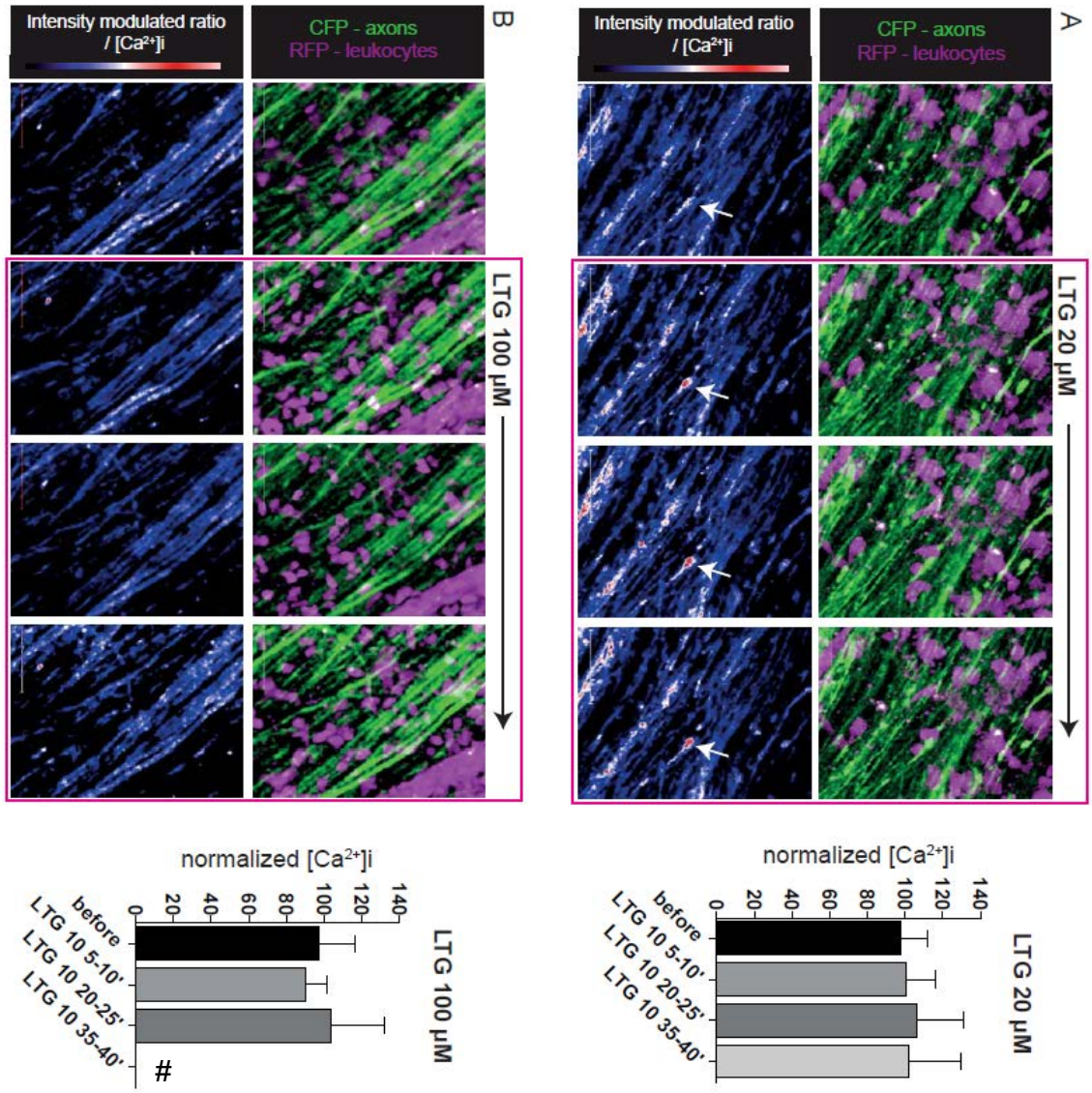

Figure 25: No effect of LTG on axonal calcium concentrations in EAE detectable

(A) TPLSM of myelinated fiber tracts showed intense interactions of immune cells with the axons and focal increase of [Ca^{2+}]. The application of 20 µM LTG did not influence intraaxonal [Ca^{2+}]. Axonal damaging in form of swelling and [Ca^{2+}] increase continued in the presence of LTG (arrow). (B) The application of 100 µM LTG did not led to a decrease of [Ca^{2+}] in axons either. The high concentration of LTG induced even a rapid deterioration of the vital signs of the animal with consecutive death (thus no data available of LTG for time points 35'-40', marked with #). One-way ANOVA with Tukey's Multiple Comparison Test; * $p < 0.05$, ** $p < 0.01$, *** $p < 0.001$, **** $p < 0.0001$. Data shown are mean ± SEM. Representative data from four independent experiments.

When analyzing intraneuronal free [Ca^{2+}], we did not see a decrease with 100 µM LTG in axons (Figure 25 B). However, this dose regimen induced a rapid deterioration of the vital signs of the animal with consecutive death pointing out that LTG is not suitable for long time treatment in high dosages.

3.3.3 LTG reduces intraneuronal free [Ca^{2+}] in brainstem neurons, which are attacked by immune cells.

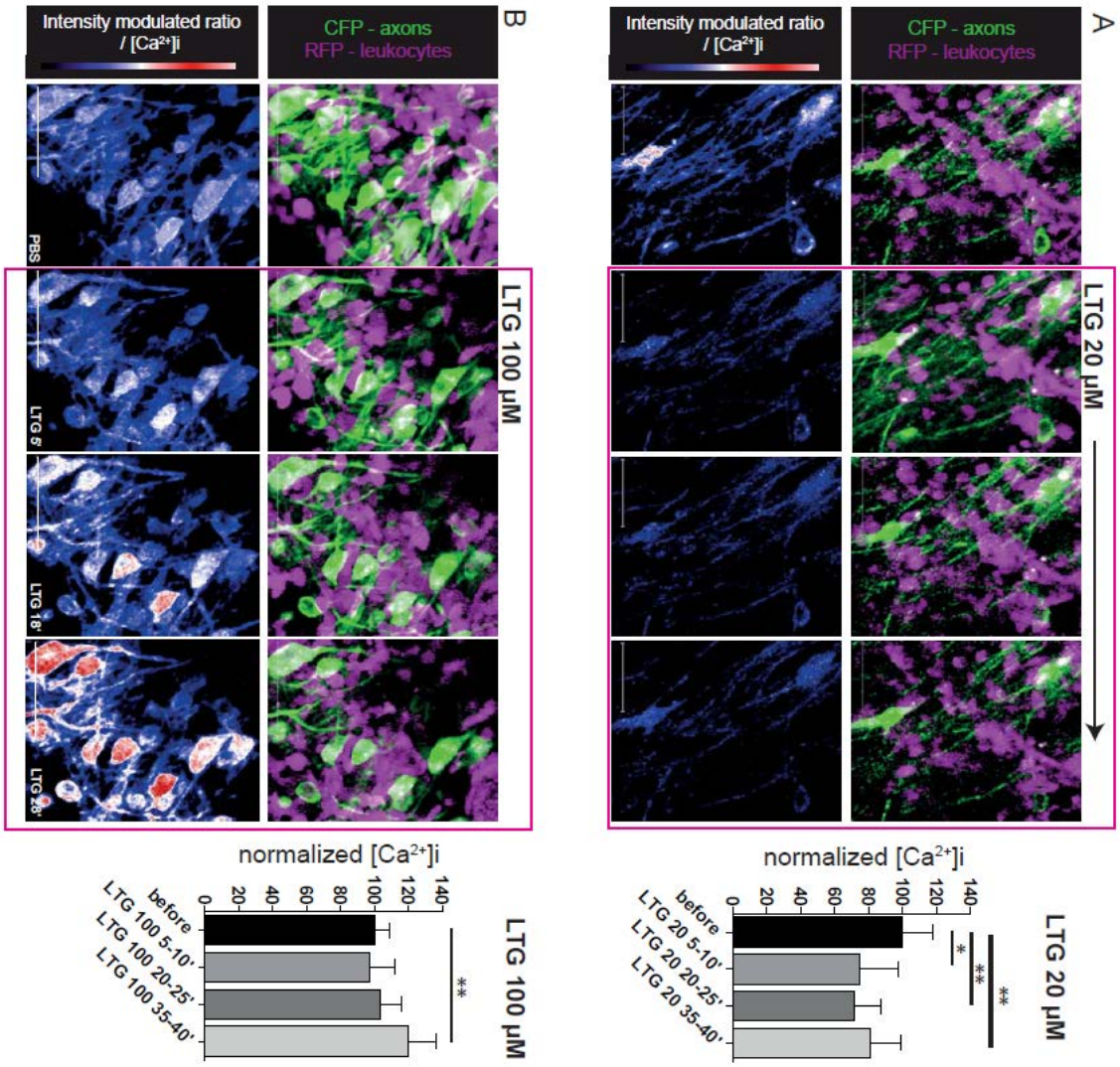

Figure 26: Low dose of LTG reduces neuronal calcium concentrations in EAE

(A) TPLSM of neuronal cell bodies showed intense interactions of immune cells with neurons and focal increase of [Ca^{2+}]. The application of 20 µM led to a rapid and sustained decrease of intraaxonal [Ca^{2+}]. This holds true for neurons severely attacked by leukocytes. (B) The application of 100 µM LTG showed a delayed strong increase of [Ca^{2+}] in neuronal somatas, accompanied with the occurrence of the death of the animal. One-way ANOVA with Tukey's Multiple Comparison Test; * $p < 0.05$, ** $p < 0.01$, *** $p < 0.001$, **** $p < 0.0001$. Data shown are mean ± SEM. Representative data from four independent experiments.

Next, we evaluated the neuronal nuclear areas which were involved in EAE lesion formation. Here, we saw strong interaction of immune cells with neuronal somata, which was associated with high intraneuronal free [Ca^{2+}]. Analogously to the experiments with focus on myelinated axons, we superfused the brainstem of the living anaesthetized mice with 20 µM LTG.

Here, we saw a rapid and sustained downregulation of intraaxonal [Ca^{2+}] as defined by semiquantitative [Ca^{2+}] measurements (Figure 26 A). Even severely attacked neurons exhibited a reduction in intraneuronal [Ca^{2+}]. Quantification of the whole neuronal area over several experiments confirmed a reduction of [Ca^{2+}] in neuronal nuclear area. We also evaluated here the effect of a 100 µM dose, which showed inverse results, i.e. delayed but strong increase of neuronal soma [Ca^{2+}] (Figure 26 B). This correlated with the imminent death of the animal. Based on these findings, we concluded that low-dose LTG (< 20 µM) is reducing intraneuronal but not intraaxonal [Ca^{2+}] as defined by our *in vivo* EAE TPLSM paradigm.

3.3.4 LTG has no influence on T cell proliferation or cytokine production.

We could previously show that $CD4^+$ T cells were strongly and directly involved in neuronal damage formation by contact dependent mechanisms. To investigate a potential effect of LTG on T cells, we performed *in vitro* experiments where we tested the effect of different doses of LTG on T cell proliferation and cytokine production. Myelin specific Th17 cells were labeled with CFSE and the dilution upon antigenic stimulation was evaluated after antigen specific restimulation by the cognate peptide in the presence of spleen derived antigen presenting cells (2.2.10).

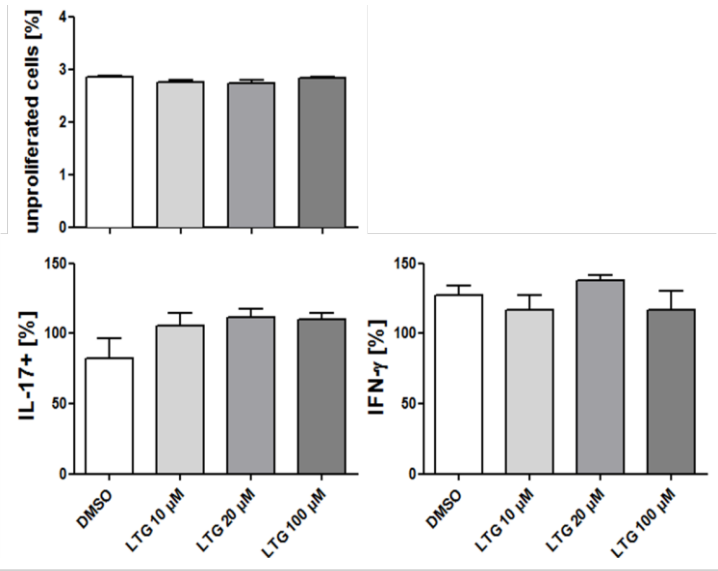

Figure 27: LTG treatment of T cells
2d2 Th17 cells were co-cultured with APCs in the presence of $MOG_{35–55}$ and different concentrations of LTG. No significant impairment of T cell proliferation or cytokine production compared to the DMSO control was measured. One-way ANOVA with Dunnett's Multiple Comparison Test; * p < 0.05, ** p < 0.01, *** p < 0.001, **** p < 0.0001. Data shown are mean ± SEM.

We did not find a significant difference in the proliferative response of $CD4^+$ Th17 cells when treated with 10, 20 or 100 µM LTG. Similarly, we did not find an influence on the number of cytokine producers in Th17 cell cultures. These findings support that there is no major anti-inflammatory effect of LTG on T cells, which are the vital cell subset responsible for EAE lesion formation. This supports that the [Ca^{2+}] lowering effect of low-dose LTG is a distinct effect on neuronal somata, which are attacked by immune cells.

3.3.5 In vivo application of low-dose LTG protects from clinical disability in EAE

To evaluate the role of our observation of a [Ca^{2+}] lowering effect of low-dose LTG as defined by TPLSM of neurons in EAE lesions, we performed a treatment study in animals suffering from EAE. Here we chose a design of LTG as add-on treatment to an anti-inflammatory treatment with corticosteroids (2.2.14.3).

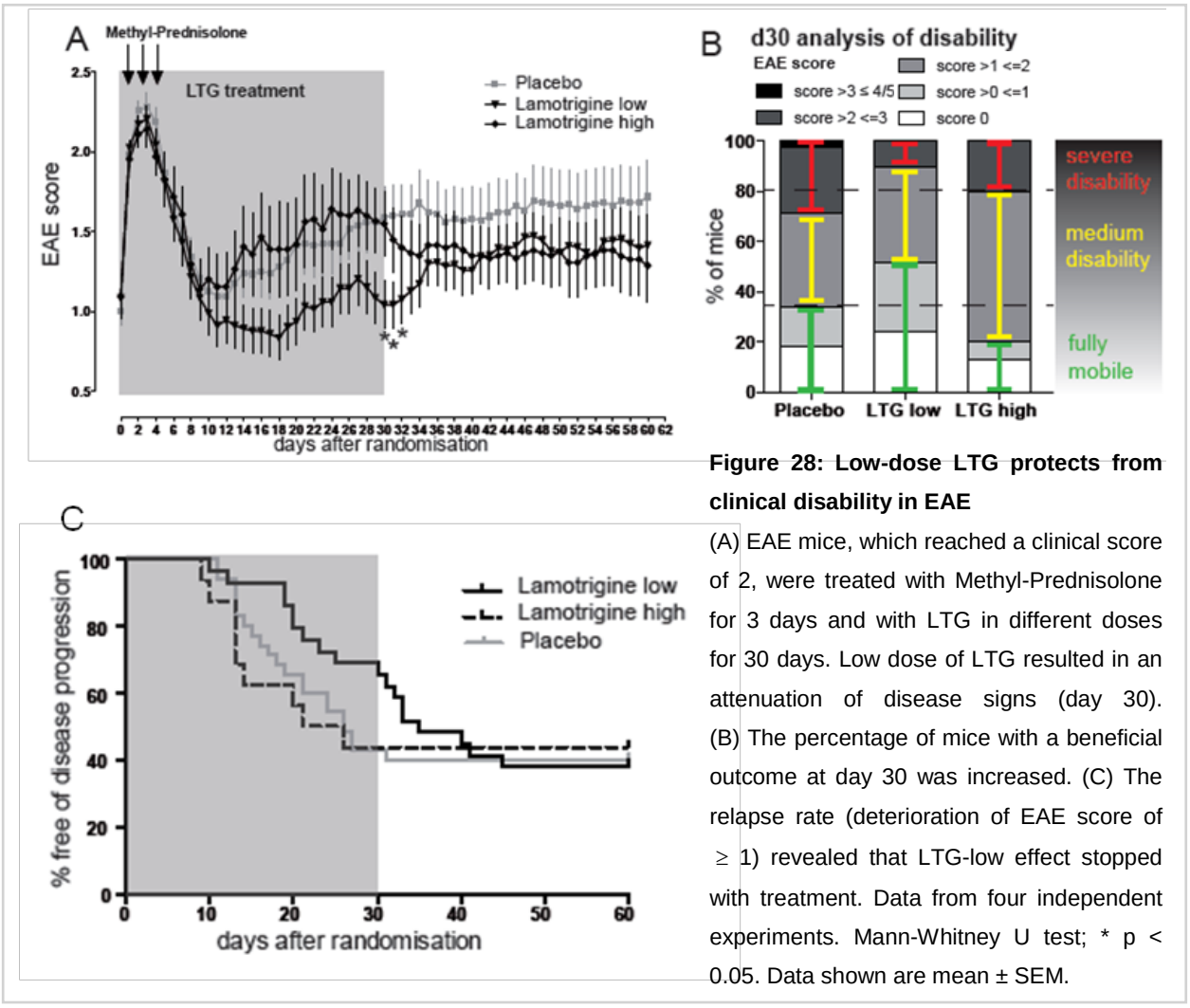

Figure 28: Low-dose LTG protects from clinical disability in EAE

(A) EAE mice, which reached a clinical score of 2, were treated with Methyl-Prednisolone for 3 days and with LTG in different doses for 30 days. Low dose of LTG resulted in an attenuation of disease signs (day 30). (B) The percentage of mice with a beneficial outcome at day 30 was increased. (C) The relapse rate (deterioration of EAE score of ≥ 1) revealed that LTG-low effect stopped with treatment. Data from four independent experiments. Mann-Whitney U test; * $p < 0.05$. Data shown are mean ± SEM.

Using steroid pulses on three consecutive days, we induced a rapid remission of symptoms which was followed by a slow and chronic progressive deterioration of clinical disability. This model is ideal to investigate the progressive phase of the disease and to test the reversal of neuronal/axonal damage with the aim to reduce non-remitting disability.

Based on our TPLSM findings, we hypothesized that a low LTG dose ranges would be preferable. A previous study of LTG in rat EAE evaluated the doses of 20 mg/kg/day and 30 mg/kg/day, which resulted in serum drug concentrations of 8 - 20 µg/ml (Bechtold et al., 2006). We found here that the low dose of LTG resulted in a robust attenuation of disease signs when treatment was started in the peak of the disease in addition to anti-inflammatory treatment with a corticosteroid pulse (Figure 28 A). The effect of treatment was not only measureable by significantly decreased mean clinical score (results from 4 pooled experiments) at the end of treatment (day 30) but also in numbers of percentage of mice with a beneficial outcome at day 30 (>50 % vs. <40 %, Figure 28 B). Looking at the disease progression (deterioration of an EAE score of ≥ 1) revealed that the effect of LTG-low was lost after stopping the drug (Figure 28 C).

4. Discussion

4.1 Impact and fate of distinct T cell subsets in the course of autoimmune neuroinflammation

While Th1 and Th17 lymphocytes are associated with MS relapses and Th2 and Treg cells with MS quiescence, it is not yet understood why relapses are followed by remission periods in RRMS and in EAE. When the BBB is permissive in neuroinflammation, most likely secondary to infiltrating encephalitogenic lymphocytes, additional T cell populations - among them regulatory cells - can enter the CNS, providing a possible explanation for this clinical amelioration. However, subsequently infiltrating lymphocyte populations may also consist of pro-inflammatory T cells. In order to unravel the impact of different lymphocyte waves entering the CNS, we designed a co-transfer system making use of T cell deficient $Rag2^{-/-}$ background to allow interaction of defined Th cell subsets. Both pro-inflammatory (Th1 and Th17) as well as anti-inflammatory T cells (Th2), were co-transferred as early as 7 days after the initiating encephalitogenic T cells to allow an influence on the disease course in this fulminant disease model with rapid exacerbation of clinical symptoms. Here, we found a reduction in disease severity by Th2 cells as expected, yet an unexpected disease-ameliorating impact of pro-inflammatory encephalitogenic Th1 cells. Most surprisingly, both Th1 and Th2 cells promote anti-inflammatory properties of Th17 cells, with Th1 cells even inducing upregulation of FoxP3 in CNS-infiltrating Th17 cells.

As reported previously, the induction of EAE by adoptive transfer of highly activated and differentiated 2d2 Th17 cells into $Rag2^{-/-}$ mice led to a severe relentless progressive disease (Langrish et al., 2005; Siffrin et al., 2010b). Here, we demonstrate that subsequent co-transfer of a second population of activated $CD4^{+}$ 2d2 Th cells associates with a significant shift of Th17 effector cells towards a less pro-inflammatory subset and thereby ameliorate disease severity and infiltration of the CNS in a subset-specific manner. Moreover, the second Th cell population seems to exert its influence specifically in the CNS compartment, not only influencing infiltration but also cytokine expression of the disease-inducing population.

The co-transfer of a second population of MOG_{35-55}-reactive Th17 cells on day 7 post-transfer of the disease-initiating T cells did not significantly influence the course of the disease, suggesting that the maximal severity of the disease was already reached, and that a second wave Th17 cells display no immunoregulatory or neuroprotective function in the active and chronic phase of the disease. In support of the absence of clinical impact, the co-transfer of a

second Th17 population did not influence the total number of CNS-invading T cells or the profile of cytokine expression in the spleen or the CNS. The significant reduction of IL-17 producers in the spleen, but not in the CNS, in comparison to the pre-transfer expression *in vitro* most likely reflects the tendency of MOG_{35-55}-reactive $IL17^+$ T cells to transmigrate to the CNS. The higher frequencies of IL-17^+ cells observed in the CNS could also result from the local microenvironment, since Th17 cells showed significantly increased numbers of cells producing their characteristic cytokine IL-17 following co-culture with neurons *in vitro*. Taken together, our data indicate that Th17 cells are efficient effectors to induce and to perpetuate neuroinflammation, showing high encephalitogenic capacity and resistance to immunoregulation by the neuronal compartment (Tanabe et al., 2014; Chavarria et al., 2013; Liu et al., 2006).

In contrast, the co-transfer of MOG_{35-55}-reactive Th1 cells attenuated the severity of ongoing EAE, suggesting anti-inflammatory properties of Th1 cells during active and chronic Th17-driven neuroinflammation. The transfer of Th1 cells was associated with a significant reduction in the total number of CNS-infiltrating cells, which was not observed in the spleen, suggesting that Th1 cells can specifically reduce the encephalitogenicity of disease-inducing Th17 cells, either by reducing their capacity to transmigrate to the CNS or by rendering the CNS environment less hospitable for Th17 cells. Possibly through secretion of IFN-γ, co-transfer of Th1 significantly reduced the frequency of IL-17^+ cells in the disease-inducing Th17 population in the spleen, which would indeed decrease their capacity to destabilize the BBB and gain access to the CNS (Kebir et al., 2007; Huppert et al., 2010).

In accordance with a beneficial impact on disease severity, the co-transfer of Th1 cells further modified the profile of the disease-inducing population in the brain, resulting in significantly lower frequencies of IL-17^+ and TNF-α^+ cells but significantly higher numbers of $FoxP3^+$ cells, suggesting a shift towards a less inflammatory phenotype. The co-transferred Th1 population exhibited a high proportion of IFN-γ producers during the disease progression serving as a potential source of the cytokine to influence the inflammatory microenvironment of the CNS. IFN-γ KO mice are susceptible to EAE and treatment with IFN-γ-neutralizing antibodies worsens EAE, stressing a potentially beneficial role of IFN-γ in the control of inflammation (Billiau et al., 1988; Ferber et al., 1996). However, this is controversial since human studies have produced opposite results (Panitch and Bever, 1993). Additionally, Heremans and colleagues have shown that, in EAE, spontaneous relapses are facilitated by

administration of neutralizing IFN-γ antibodies, while the administration of exogenous IFN-γ during the remission phase provides some protection against subsequent relapses (Berghmans et al., 2011; Heremans et al., 1996). In line with our results, this suggests that the site and time point of action of IFN-γ^+ Th1 cells might define their role during inflammation. Hence, Th1 cells are capable of inducing the disease, but co-transferred in an already Th17-induced EAE model, they ameliorate the disease; probably by affecting the first wave of inflammation. For instance, it was shown that Th1 orchestrate the numbers and function of Th17 cells lowering the susceptibility of mice to develop EAE (Berghmans et al., 2011).

Furthermore, IFN-γ was found to induce Foxp3 expression and subsequent conversion of $CD4^+$ $CD25^-$ T cells to $CD4^+$ Treg cells in mouse and human systems (Wang et al., 2006). In this study IFN-γ treatment of T cells led to an induction of regulatory properties as evidenced by the suppression of EAE via adoptive transfer. Here, we showed consistently that a second transfer of Th1 cells decreases the capacity of Th17 cells to invade the CNS compartment and promotes down-regulation of pro-inflammatory cytokines and induces FoxP3 expression. Conversion of Th17 cells into regulatory T cells was recently described in several disease models, especially during the resolution of inflammation, which highlights in line with our observations its incidence as a phenomenon of ongoing inflammation (Gagliani et al., 2015). Although FoxP3 is a key transcription factor for $CD4^+CD25^+$ T regulatory cells (Treg), its expression is neither sufficient nor obligatory for immune suppressive functions (Fontenot et al., 2003; Huber et al., 2011; Kohm et al., 2002). Nevertheless, the developmental pathways for the generation of pathogenic Th17 and regulatory T cell are reciprocal and depending on a TGF-β driven balance of RORγt and Foxp3 (Bettelli et al., 2006; Zhou et al., 2008). Thus, the induction of Foxp3 and the reduction of the expression of inflammatory cytokines might not be a prove for the formation of functional Treg cells but a sign for silencing Th17 function upon transfer of Th1 cells during ongoing inflammation resulting in a significant attenuation of EAE severity. The induction of FoxP3 in the disease-inducing population was exclusively observed in the CNS, and could be secondary to the capacity of IFN-γ to induce TGF-β secretion by neurons (Chavarria et al., 2013). Neurons are a potential source for TGF-β and are involved in the generation of regulatory T cells from IFN-γ and TNF-α producing T cells during EAE in a cell-to-cell dependent and antigen independent way through the TGF-β1–TGF-βR and TCR signaling pathway (Liu et al., 2006). This might explain why the conversion occurred in the CNS, but not in the spleen.

The induction of IL-10 production by Th1 cells in the CNS environment, as suggested by our *in vitro* data following co-culture with neurons, is another potential factor in the process of Th1 induced control of inflammation. The *in vitro* results suggest a crosstalk of Th1 cells and neurons resulting in a CNS-specific response with the potential to regulate inflammation. For instance, it was shown that TGF-β signaling drives IL-10 production in effector Th1 cells and reduces T cell trafficking in EAE (Huss et al., 2011). Furthermore, Th17 cells express interleukin-10 receptor and IL-10 signaling can suppress their effector function efficiently (Huber et al., 2011), suggesting another mechanism underlying the observed shift in the profile of the disease-inducing population. Moreover, after spinal cord injury the adoptive transfer of Th1 cells promoted axonal remodeling and functional recovery in an IL-10 dependent way, indicating an neuroprotective effect of an IL-10 increase in the microenvironment of the inflammation site (Ishii et al., 2012). Thus, we demonstrate that a second transfer of IFN-γ-producing Th1 cells decreases the capacity of Th17 cells to invade the CNS compartment and promote a shift towards a less inflammatory phenotype, probably accompanied by IL-10 secretion as a response to neurons, resulting in a significant attenuation of EAE severity.

As expected, co-transfer of Th2 cells led to a less severe disease course as compared to the co-transfer of Th17 cells. The decline in disease severity was similar to the effect of the co-transfer of Th1 cells, but a delay in disease onset was additionally observed, suggesting that a potentially regulatory effect of the Th2 cells occurred earlier in the induction phase of the disease. Interestingly, an impact of the co-transferred subset on the phenotype of the disease-inducing Th17 population was observed again, with significantly decreased numbers of $IL17^+$ cells and increased frequency of IFN-γ-producing cells in the CNS compartment, while the proportions of TNF-α^+ and $FoxP3^+$ cells remained unchanged. This form of plasticity of CNS-infiltrating Th17 cell towards a more Th1-like cytokine-profile has been described before as a typical feature of Th17-mediated EAE leading to ex-Th17 cells (Gagliani et al., 2015; Hirota et al., 2011). Despite its common cytokine profile exTh17 cells cannot be considered as Th1 cells and their role is still under debate (Hoppmann et al., 2015; Kurschus et al., 2010). While Th17 cells are essential for the development of EAE, the expression of IL-17 as its exclusiv characteristic cytokine among the T cell subsets is dispensable, since IL-17 KO mice develop EAE normally (Haak et al., 2009; Langrish et al., 2005). Nevertheless the reduction of IL-17 as a pro-inflammatory cytokine is beneficial during neruoinflammtion

(Waisman et al., 2015). Thus, the conversion of Th17 cells to ex-Th17 cell is a possible mechanism to explain the observed attenuation of EAE by the co-tranfer of Th2 cells.

Co-culturing with neurons did not change the cytokine profile of Th2 cells, giving no hints of a crosstalk between the two cell types. Nevertheless, the major cytokine IL-4 of Th2 cells might positively influence the microenvironment of the CNS, as it was recently published that $CD4^+$ T cells protect injured CNS neurons via IL-4 (Walsh et al., 2015). Thus, plasticity of Th17 cells towards an ex-Th17 phenotype seems to be facilitated by the co-transfer of Th2 cells leading to a possible mitigation of the disease inducing population and an attenuation of EAE severity, which might be supported by neuroprotective effects via local IL-4 secretion during ongoing inflammation.

Effector Th cells dominate the immunopathology in MS and EAE by orchestrating repetitive infiltrations of immune cells into the CNS (Nylander and Hafler, 2012). In this process, Th cells exhibit lineage instability, plasticity and transdifferentiation presumably resulting in a change of their function during inflammation (Gagliani et al., 2015; Hirota et al., 2011). We demonstrated attenuation of a Th17-driven EAE by a second wave of MOG_{35-55}-reactive cells during ongoing inflammation with the co-transfer of Th1 or Th2 but not Th17. Th1 and Th2 reduced clinical symptoms, presumably by competing with Th17 cells, by promoting plasticity of the disease-inducing population in the CNS, and by changing the CNS microenvironment via secreting anti-inflammatory cytokines in response to contact with the neuronal compartment. Shedding light on the immunological effects of distinct Th cell subsets during disease progression might primary help to define the main drivers of the chronic phase of the disease. But it also provides approaches for immunotherapy by transfer, blocking or activation of the right T cell subset at the right time; without incurring the harmful side-effects that accompany current systemic chronic immunosuppressive therapies (Roncarolo and Battaglia, 2007).

4.2 sICAM-5 as a neuronal regulator of neuroinflammation

T cell-mediated induction of axonal and neuronal damage during neuroinflammation is presumably a contact dependent mechanism (Reuter et al., 2015; Siffrin et al., 2010b). Intercellular contact formation and signal transduction is depending on surface proteins, such as adhesion molecules. The Repulsive Guidance Molecule-a (RGMa) was recently described as one T cell surface protein with significance in T cell-neuronal interaction during

neuroinflammation (Tanabe and Yamashita, 2014). RGMa, in particular expressed in encephalitogenic Th17 cells, binds to neuronal neogenin and leads to neuronal cell death by inducing the PI3K/AKT signaling pathway. Neutralizing antibodies to RGMa attenuates severity of Th17 cell-mediated EAE by reducing neurodegeneration without altering the immune response. This indicates that RGMa is involved in T cell-induced neurodegeneration in EAE, especially in the signal transduction between T cells and neurons during contact formation. However, RGMa is not essential in T cell-neuronal contact formation, since blocking of RGMa does not limit adherent activity of T cells towards neurons. We sought to identify adhesion proteins, which are crucial for initial contact formation preceding signal-transduction. In 2010 we demonstrated that the absence of LFA-1 on T cells reduces T cell-mediated neuronal cell death *in vitro*, while the Gahmberg Laboratory described ICAM-5 as the neuronal counterpart important in contact formation with T cells (Siffrin et al., 2010b; Tian et al., 2000). Here, we investigated the significance of membrane bound ICAM-5 in the context of neuroinflammation by inducing EAE in ICAM-5 KO mice and WT littermates. The disease induction and severity of the first peak was comparable in both groups suggesting that ICAM-5 is not essential for T cell-mediated neuroinflammation by serving as a neuronal adhesion protein for autoreactive T cells. Considering the clinical symptoms it appears that spinal damage can be induced by T cells even in the case of genetic deletion of ICAM-5. This is consistent with the fact that ICAM-5 is predominantly expressed in the brain but not in the spinal cord in WT mice (Oka et al., 1990). Thus, we conclude that T cell-mediated neuroinflammation *in vivo* is dependent on other neuronal adhesion molecules serving as a ligand to lymphocytic LFA-1 but not membrane bound ICAM-5.

Interestingly, ICAM-5 KO mice show even a more severe disease progression in the chronic phase of active EAE compared to WT littermates. This led to the hypothesis that the soluble form of ICAM-5, shedded from the neuronal membrane, has regulatory features during ongoing neuroinflammation by inhibiting APC-driven T cell restimulation. The potential of sICAM-5 to block T cell activation by APCs could has been demonstrated *in vitro* and confirmed by us during MOG-dependent stimulations of T cells via APCs (Tian et al., 2008). We therefore produced and purified the fusionprotein ICAM-5 D1-2 Fc, which consists of the functional binding site of sICAM-5 and tested its effect in EAE via intrathecal injection by lumbar puncture. The local application of ICAM-5 D1-2 Fc attenuated the clinical score of the recipients compared to the control group treated with human IgG; and the effect disappeared

after stopping the treatment. This supports the hypothesis that sICAM-5 exhibits immune-regulatory function. Besides its potential to inhibit T cell restimulation, another mechanism of action could be the binding of sICAM-5 on LFA-1 of autoreactive T cell to block this adhesion molecule as a ligand for contact formation with neurons. In both cases sICAM5 serves as a neuronal defense mechanism to limit locally T cell-mediated neuroinflammation. Such a protective effect would probably led to less active T cells and less T cell-mediated neuronal and axonal damage resulting in a decrease of non-remitting disability after the first peak as seen in our two observed EAE models. The ambivalent role of ICAM5 in its soluble and membrane-bound form could be further defined *in vitro* by performing co-cultures of T cells with ICAM5-KO and WT neurons and/or in the presence with ICAM5 D1-2 Fc by quantification of the resulting neuronal damage under each condition. Taken together, sICAM5 has potential for therapeutic application in modulating T cell (re)activation as well as proliferation and hypothetically T cell-neuron interactions.

4.3 Preventing neurodegeneration in neuroinflammation by ion channel blocking

The availability of new treatments for Multiple Sclerosis has accumulated in recent years. However, it has become clear that risk-benefit analysis is urgently needed, as highly effective anti-inflammatory drugs have been shown to entail significant side effects which have to be counterbalanced especially in those patients with a relatively benign disease progression. Therefore, the notion of this project was to design a treatment regimen which allows the combination of safe, mildly to moderately effective anti-inflammatory treatment with neuroprotective agents in the early stages of disease. This might be a reasonable way to address the needs of the majority of MS patients, who require safe treatment for approximately 30-50 years if a positive diagnosis is made in early adulthood.

Interestingly, the “high-dose” LTG regime (corresponding to lower level range of epilepsy treatment) did not show the improvement which we saw with the lower dose, which might be either consequence of detrimental effect of high-range Na^+ channel blockade or differential blockade of VGCC vs. Na^+ channels. Therefore, we think this might explain the non-effectiveness concerning clinical markers of the drug in a recently performed clinical trial, which used higher dose ranges of LTG compared to what we used (Kapoor et al., 2010). Interestingly, in this trial there were potential beneficial effects as defined by the secondary outcome parameter of reduced CSF neurofilament levels as sign of reduced

neurodegeneration (Gnanapavan et al., 2013). Therefore the results of our study indicate that testing very low doses might be efficient for neuroprotection in T cell mediated-neuroinflammation - and would be most likely well tolerated by MS patients.

4.4 Summary & Outlook

The mechanisms behind T cell-mediated neuroinflammtion mirrors the complexity of the pathophysiology of MS as a multiphasic and chronic disease affecting the two most multifaceted systems of the human body, the immune and nervous system. While it is beyond dispute that autoimmune T cells are one of the key players in MS, the specific role of different T cells throughout the diesease progression is not revealed. This question got even more essential, since recent immunological findings imposed us to consider T cell repertoires as very plastic and adaptable towards changing microenvironments. Thus, it is crucial to combine informations about the cytokine, transcription factor and surface molecule profile as well as the site and time point of action of a T cell subset to predict its role in a specific context.

This is the main meassage of the first part of this thesis, which demonstrated that different Th cell subsets can alter the disease progression during ongoing neuroinflammation. Being co-transferred just before the onset of clinical symptoms Th1 and Th2 cells changed the microenvironment of Th17-induced neuroinflammation resulting in a promotion of Th17 cell instability or even plasticity. This highlights the capacity of T cells to influence each other, to act pro- or anti-inflammatory depending on the site and time point, and to adapt on new circumstances. It remains to be a core challenge to identify new markers to define the encephalitogenity of T cell subsets and to focus on T cells beyond the classical subtypes, which display a mixture of the unsual subtype specific charactristics. The data of the performed co-transfer experiments could be complemented by measuring more EAE relevant cytokines, e.g. GM-CSF or IL-10, adhesion molecules like LFA-1 or MCAM via FACS or screenings methods investigating the transcriptom (NGS), (surface-)proteome and lipidome (both mass spectrometry). Furthermore, additional T cell populations like T_{reg} cells or differently *in vitro* primed Th1, Th2 and Th17 cells could be co-transferred combined with other time points of injection and analysis to get a better temporal resolution of the processes.

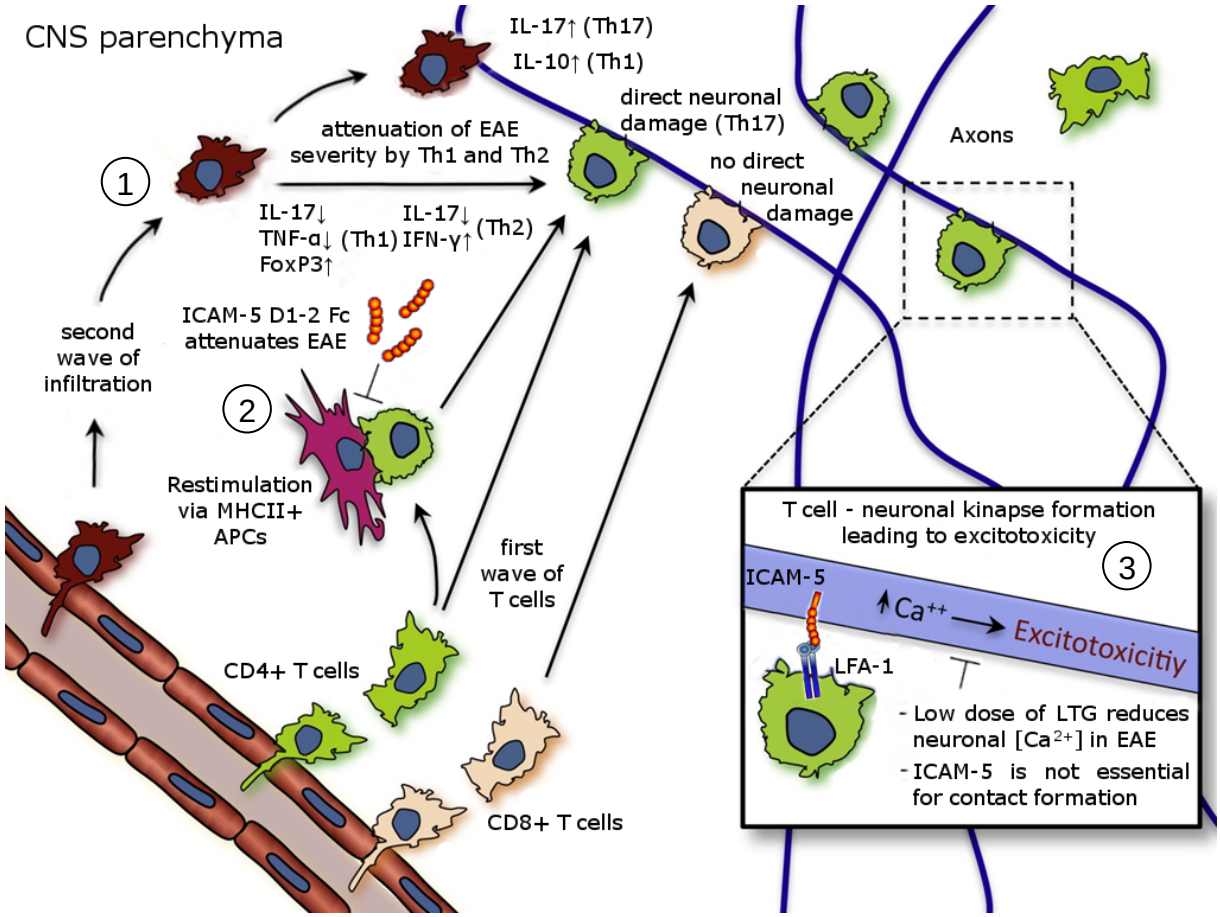

Figure 29: Mechanisms behind T cell-mediated neuroinflammation II (adapted from Egen and Ouyang, 2010) Succeeding T cells have the capacity to modulate ongoing CNS inflammation, response to neuronal contact and impact on the disease inducing population in a subtype specific way (1). CNS hosted APCs trigger the migration of T cells into and their survival within the CNS via antigen presentation and reactivation. Here sICAM5, shedded from the membrane of neurons, might serve locally as a regulator of ongoing inflammation (2). Axonal and neuronal Ca^{2+}-fluctuation as an early sign for T cell-contact induced damage can be targeted with selective blocking of ion-channels by low concentrations of LTG. Membrane bound ICAM-5 does not appear to be essential for T cell-mediated neuroinflammation (3).

The second part handels with the recent insight in MS research, that a crosstalk between the two completely different cell types, T cells and neurons, occurs in the immune privileged CNS. Direct interactions between T cells and axons leading to detrimental neuronal Ca^{2+}-fluctuations have been observed *in vivo* with $CD4^+$ but not $CD8^+$ T cells. Since this process is contact dependent the search for the involved adhesion molecules on both sides is not only important to find a new marker for encephalitogenity but also to identify a target for therapeutic approaches, which have less side effects the more specific the kinapse-formation is. Due to the detailed work of the Gahmberg laboratory, ICAM-5 seemed to be a candidate on the neuronal side, but in our experiments it turned out not to be essential in the full

development of EAE. It even appears that shedded ICAM-5 inhibits the (re)activation of T cells via APCs and could be understood as an endogenous neuronal defense mechanism. The mechanism has not be pinned down with the data gained from our studies. Nevertheless, ICAM-5 is one of the most interesting candiates involved in T cell-neuronal crosstalk. The potential of sICAM-5 to disturb T cell attachment on neurons through the blocking of LFA-1 could be further tested in co-cultures of T cells and neurons combined with TPLSM for neuronal damage quantification. Its function in inhibiting T cell restimulation should be confirmed by repeting the treatment study with ICAM-5 D1-2 Fc also with different regimes and *ex vivo* investigations on the cellular level. On the long run ICAM-5 D1-2 Fc might have the therapeutical potential to inhibit T cell restimulation with less harsh systemic side effects like LFA-1 blocking by antibodies already tested in MS.

Finally, a primarly consequence of T cell invasion of the CNS and contact formation with neurons is an increase of Ca^{2+}-concentrations in neurons and axons as an early sign for celluar damage. In the third part we elucidated, whether selective neuronal ion-channel blocking via LTG prevents calcium influx, axonal fragmentation and neurodegeneration. We found that low LTG concentrations were effective in reducing neuronal, but not axonal free [Ca^{2+}]. Therefore, our data demonstrate, that ion-channels are involved in the process of T cell induced dysfunctions in the neuronal compartement and that it can be prevented or reversed by therapeutic treatment depending on the site of T cell attack. Although LTG gives already hints on the involvement of sodium and calcium channels, selective blocking of ion-channels by other chemicals (MK-801 and Memantine for NMDAr; NBQX for AMPAr; Nifedipine for VGCC, Phenytoine for Na^{+} channels) in the same experimental settings would be a possibility to rule out the significance of each channel class. Insights could help to understand the basic mechanisms of T cell-induced neuronal damage and might help to find approches for neuroprotective therapies in MS.

Taken together this thesis gives new insights into autoimmune-neurodegenerative mechanisms. It bridges from the CNS invasion of different T cell subsets, across neuronal-T cell interactions, towards the prevention of the consequences of the detrimental cascade of T cell mediated neuroinflammation.

5. Bibliography

Basso, A.S., Frenkel, D., Quintana, F.J., Costa-Pinto, F.A., Petrovic-Stojkovic, S., Puckett, L., Monsonego, A., Bar-Shir, A., Engel, Y., Gozin, M., et al. (2008). Reversal of axonal loss and disability in a mouse model of progressive multiple sclerosis. J. Clin. Invest. *118*, 1532–1543.

Bechtold, D. a., Miller, S.J., Dawson, A.C., Sun, Y., Kapoor, R., Berry, D., and Smith, K.J. (2006). Axonal protection achieved in a model of multiple sclerosis using lamotrigine. J. Neurol. *253*, 1542–1551.

Berghmans, N., Nuyts, A., Uyttenhove, C., Van Snick, J., Opdenakker, G., and Heremans, H. (2011). Interferon-γ orchestrates the number and function of Th17 cells in experimental autoimmune encephalomyelitis. J. Interferon Cytokine Res. *31*, 575–587.

Bettelli, E., Korn, T., and Kuchroo, V.K. (2007). Th17: the third member of the effector T cell trilogy. Curr. Opin. Immunol. *19*, 652–657.

Billiau, a, Heremans, H., Vandekerckhove, F., Dijkmans, R., Sobis, H., Meulepas, E., and Carton, H. (1988). Enhancement of experimental allergic encephalomyelitis in mice by antibodies against IFN-gamma. J. Immunol. *140*, 1506–1510.

Bjartmar, C., Kidd, G., Mörk, S., Rudick, R., and Trapp, B.D. (2000). Neurological disability correlates with spinal cord axonal loss and reduced N-acetyl aspartate in chronic multiple sclerosis patients. Ann. Neurol. *48*, 893–901.

Calabresi, P., Centonze, D., Marfia, G. a, Pisani, a, and Bernardi, G. (1999). An in vitro electrophysiological study on the effects of phenytoin, lamotrigine and gabapentin on striatal neurons. Br. J. Pharmacol. *126*, 689–696.

Chard, D.T., Griffin, C.M., Parker, G.J.M., Kapoor, R., Thompson, A.J., and Miller, D.H. (2002). Brain atrophy in clinically early relapsing-remitting multiple sclerosis. Brain *125*, 327–337.

Compston, A., and Coles, A. (2008). Multiple sclerosis. Lancet *372*, 1502–1517.

Cua, D.J., Sherlock, J., Chen, Y., Murphy, C. a, Joyce, B., Seymour, B., Lucian, L., To, W., Kwan, S., Churakova, T., et al. (2003). Interleukin-23 rather than interleukin-12 is the critical cytokine for autoimmune inflammation of the brain. Nature *421*, 744–748.

DeCoster, M.A. (1995). Calcium dynamics in the central nervous system. Adv. Neuroimmunol. *5*, 233–239.

Egen, J.G., and Ouyang, W. (2010). Even neurons are excited by Th17 cells. Immunity *33*, 298–300.

Ellwardt, E., and Zipp, F. (2014). Molecular mechanisms linking neuroinflammation and neurodegeneration in MS. Exp. Neurol. *262*, 8–17.

Ferber, I.A., Brocke, S., Taylor-Edwards, C., Ridgway, W., Dinisco, C., Steinman, L., Dalton, D., and Fathman, C.G. (1996). Mice with a disrupted IFN-gamma gene are susceptible to the induction of experimental autoimmune encephalomyelitis (EAE). J. Immunol. *156*, 5–7.

Fontenot, J.D., Gavin, M.A., and Rudensky, A.Y. (2003). Foxp3 programs the development and function of CD4+CD25+ regulatory T cells. Nat. Immunol. *4*, 330–336.

Gagliani, N., Vesely, M.C.A., Iseppon, A., Brockmann, L., Xu, H., Palm, N.W., de Zoete, M.R., Licona-Limón, P., Paiva, R.S., Ching, T., et al. (2015). Th17 cells transdifferentiate into regulatory T cells during resolution of inflammation. Nature 1–5.

Giuliani, F., Goodyer, C.G., Antel, J.P., and Yong, V.W. (2003). Vulnerability of human neurons to T cell-mediated cytotoxicity. J. Immunol. *171*, 368–379.

Gnanapavan, S., Grant, D., Morant, S., Furby, J., Hayton, T., Teunissen, C.E., Leoni, V., Marta, M., Brenner, R., Palace, J., et al. (2013). Biomarker Report from the Phase II Lamotrigine Trial in Secondary Progressive MS - Neurofilament as a Surrogate of Disease Progression. PLoS One *8*, e70019.

Goverman, J. (2009). Autoimmune T cell responses in the central nervous system. Nat. Rev. Immunol. *9*, 393–407.

Grifka-Walk, H.M., Lalor, S.J., and Segal, B.M. (2013). Highly polarized Th17 cells induce EAE via a T-bet independent mechanism. Eur. J. Immunol. *43*, 2824–2831.

Haak, S., Croxford, A.L., Kreymborg, K., Heppner, F.L., Pouly, S., Becher, B., and Waisman, A. (2009). IL-17A and IL-17F do not contribute vitally to autoimmune neuro-inflammation in mice. J. Clin. Invest. *119*, 61.

Hayton, T., Furby, J., Smith, K.J., Altmann, D.R., Brenner, R., Chataway, J., Hunter, K., Tozer, D.J., Miller, D.H., and Kapoor, R. (2012). Longitudinal changes in magnetisation transfer ratio in secondary progressive multiple sclerosis: Data from a randomised placebo controlled trial of lamotrigine. J. Neurol. *259*, 505–514.

Heremans, H., Dillen, C., Groenen, M., Martens, E., and Billiau, A. (1996). Chronic relapsing experimental autoimmune encephalomyelitis (CREAE) in mice: Enhancement by monoclonal antibodies against interferon-?? Eur. J. Immunol. *26*, 2393–2398.

Herz, J., Zipp, F., and Siffrin, V. (2010). Neurodegeneration in autoimmune CNS inflammation. Exp. Neurol. *225*, 9–17.

Hirota, K., Duarte, J.H., Veldhoen, M., Hornsby, E., Li, Y., Cua, D.J., Ahlfors, H., Wilhelm, C., Tolaini, M., Menzel, U., et al. (2011). Fate mapping of IL-17-producing T cells in inflammatory responses. Nat. Immunol. *12*, 255–263.

Hoppmann, N., Graetz, C., Paterka, M., Poisa-Beiro, L., Larochelle, C., Hasan, M., Lill, C.M., Zipp, F., and Siffrin, V. (2015). New candidates for CD4 T cell pathogenicity in experimental neuroinflammation and multiple sclerosis. Brain.

Huber, S., Gagliani, N., Esplugues, E., O'Connor, W., Huber, F.J., Chaudhry, A., Kamanaka, M., Kobayashi, Y., Booth, C.J., Rudensky, A.Y., et al. (2011). Th17 Cells Express Interleukin-10 Receptor and Are Controlled by Foxp3- and Foxp3+ Regulatory CD4+ T Cells in an Interleukin-10-Dependent Manner. Immunity *34*, 554–565.

Huseby, E.S., Liggitt, D., Brabb, T., Schnabel, B., Ohlén, C., and Goverman, J. (2001). A pathogenic role for myelin-specific CD8(+) T cells in a model for multiple sclerosis. J. Exp. Med. *194*, 669–676.

Ishii, H., Jin, X., Ueno, M., Tanabe, S., Kubo, T., Serada, S., Naka, T., and Yamashita, T. (2012). Adoptive transfer of Th1-conditioned lymphocytes promotes axonal remodeling and functional recovery after spinal cord injury. Cell Death Dis. *3*, e363.

Jäger, A., Dardalhon, V., Sobel, R.A., Bettelli, E., and Kuchroo, V.K. (2009). Th1, Th17, and Th9 effector cells induce experimental autoimmune encephalomyelitis with different pathological phenotypes. J. Immunol. *183*, 7169–7177.

Kanwar, J.R., Kanwar, R.K., and Krissansen, G.W. (2004). Simultaneous neuroprotection and blockade of inflammation reverses autoimmune encephalomyelitis. Brain *127*, 1313–1331.

Kapoor, R., Furby, J., Hayton, T., Smith, K.J., Altmann, D.R., Brenner, R., Chataway, J., Hughes, R.A., and Miller, D.H. (2010). Lamotrigine for neuroprotection in secondary progressive multiple sclerosis: a randomised, double-blind, placebo-controlled, parallel-group trial. Lancet Neurol. *9*, 681–688.

Kawakami, N., Nägerl, U.V., Odoardi, F., Bonhoeffer, T., Wekerle, H., and Flügel, A. (2005). Live imaging of effector cell trafficking and autoantigen recognition within the unfolding autoimmune encephalomyelitis lesion. J. Exp. Med. *201*, 1805–1814.

Kebir, H., Kreymborg, K., Ifergan, I., Dodelet-Devillers, A., Cayrol, R., Bernard, M., Giuliani, F., Arbour, N., Becher, B., and Prat, A. (2007). Human TH17 lymphocytes promote blood-brain barrier disruption and central nervous system inflammation. Nat. Med. *13*, 1173–1175.

Kohm, a. P., Carpentier, P. a., Anger, H. a., and Miller, S.D. (2002). Cutting Edge: CD4+CD25+ Regulatory T Cells Suppress Antigen-Specific Autoreactive Immune Responses and Central Nervous System Inflammation During Active Experimental Autoimmune Encephalomyelitis. J. Immunol. *169*, 4712–4716.

Kurschus, F.C., Croxford, A.L., P. Heinen, A., Wörtge, S., Ielo, D., and Waisman, A. (2010). Genetic proof for the transient nature of the Th17 phenotype. Eur. J. Immunol. *40*, 3336–3346.

Langrish, C.L., Chen, Y., Blumenschein, W.M., Mattson, J., Basham, B., Sedgwick, J.D., McClanahan, T., Kastelein, R. a, and Cua, D.J. (2005). IL-23 drives a pathogenic T cell population that induces autoimmune inflammation. J. Exp. Med. *201*, 233–240.

Larochelle, C., Alvarez, J.I., and Prat, A. (2011). How do immune cells overcome the blood-brain barrier in multiple sclerosis? FEBS Lett. *585*, 3770–3780.

Leuenberger, T., Paterka, M., Reuter, E., Herz, J., Niesner, R.A., Radbruch, H., Bopp, T., Zipp, F., and Siffrin, V. (2013). The role of CD8+ T cells and their local interaction with CD4+ T cells in myelin oligodendrocyte glycoprotein35-55-induced experimental autoimmune encephalomyelitis. J. Immunol. *191*, 4960–4968.

Liblau, R.S., Gonzalez-Dunia, D., Wiendl, H., and Zipp, F. (2013). Neurons as targets for T cells in the nervous system. Trends Neurosci. *36*, 315–324.

Liu, Y., Teige, I., Birnir, B., and Issazadeh-Navikas, S. (2006). Neuron-mediated generation of regulatory T cells from encephalitogenic T cells suppresses EAE. Nat. Med. *12*, 518–525.

Lo, A.C., Saab, C.Y., Black, J. a, and Waxman, S.G. (2003). Phenytoin protects spinal cord axons and preserves axonal conduction and neurological function in a model of neuroinflammation in vivo. J. Neurophysiol. *90*, 3566–3571.

Lonskaya, I., Partridge, J., Lalchandani, R.R., Chung, A., Lee, T., Vicini, S., Hoe, H.S., Lim, S.T., and Conant, K. (2013). Soluble ICAM-5, a Product of Activity Dependent Proteolysis, Increases mEPSC Frequency and Dendritic Expression of GluA1. PLoS One *8*, 1–12.

Lu, R., and Schmidtko, A. (2013). Direct Intrathecal Drug Delivery in Mice for Detecting In Vivo Effects of cGMP on Pain Processing. In Methods in Molecular Biology (Clifton, N.J.), pp. 215–221.

Mank, M., Santos, A.F., Direnberger, S., Mrsic-Flogel, T.D., Hofer, S.B., Stein, V., Hendel, T., Reiff, D.F., Levelt, C., Borst, A., et al. (2008). A genetically encoded calcium indicator for chronic in vivo two-photon imaging. Nat. Methods *5*, 805–811.

Martinez-Sanchez, M.E., Mendoza, L., Villarreal, C., and Alvarez-Buylla, E.R. (2015). A Minimal Regulatory Network of Extrinsic and Intrinsic Factors Recovers Observed Patterns of CD4+ T Cell Differentiation and Plasticity. PLOS Comput. Biol. *11*, e1004324.

Merrill, J.E., Kono, D.H., Clayton, J., Ando, D.G., Hinton, D.R., and Hofman, F.M. (1992). Inflammatory leukocytes and cytokines in the peptide-induced disease of experimental allergic encephalomyelitis in SJL and B10.PL mice. Proc. Natl. Acad. Sci. U. S. A. *89*, 574–578.

Mizuno, T., Yoshihara, Y., Kagamiyama, H., Ohsawa, K., Imai, Y., Kohsaka, S., and Mori, K. (1999). Neuronal adhesion molecule telencephalin induces rapid cell spreading of microglia. Brain Res. *849*, 58–66.

Muir, K.W., and Lees, K.R. (1995). Clinical experience with excitatory amino acid antagonist drugs. Stroke. *26*, 503–513.

Najafian, N., Chitnis, T., Salama, A.D., Zhu, B., Benou, C., Yuan, X., Clarkson, M.R., Sayegh, M.H., and Khoury, S.J. (2003). Regulatory functions of CD8+CD28- T cells in an autoimmune disease model. J. Clin. Invest. *112*, 1037–1048.

Niedringhaus, M., Chen, X., Dzakpasu, R., and Conant, K. (2012). MMPs and soluble ICAM-5 increase neuronal excitability within in vitro networks of hippocampal neurons. PLoS One *7*, 1–9.

Nikić, I., Merkler, D., Sorbara, C., Brinkoetter, M., Kreutzfeldt, M., Bareyre, F.M., Brück, W., Bishop, D., Misgeld, T., and Kerschensteiner, M. (2011). A reversible form of axon damage in experimental autoimmune encephalomyelitis and multiple sclerosis. Nat. Med. *17*, 495–499.

Ning, L., Tian, L., Smirnov, S., Vihinen, H., Llano, O., Vick, K., Davis, R.L., Rivera, C., and Gahmberg, C.G. (2012). Interactions between Intercellular Adhesion Molecule-5 (ICAM-5) and 1 integrins regulate neuronal synapse formation. J. Cell Sci.

Nylander, A., and Hafler, D.A. (2012). Multiple sclerosis. J Clin Invest *122*, 1180–1188.

O'Connor, R. a., Cambrook, H., Huettner, K., and Anderton, S.M. (2013). T-bet is essential for Th1-mediated, but not Th17-mediated, CNS autoimmune disease. Eur. J. Immunol. *43*, 2818–2823.

O'Connor, R.A., Prendergast, C.T., Sabatos, C.A., Lau, C.W.Z., Leech, M.D., Wraith, D.C., and Anderton, S.M. (2008). Cutting edge: Th1 cells facilitate the entry of Th17 cells to the central nervous system during experimental autoimmune encephalomyelitis. J. Immunol. *181*, 3750–3754.

Odoardi, F., Kawakami, N., Klinkert, W.E.F., Wekerle, H., and Flügel, A. (2007). Blood-borne soluble protein antigen intensifies T cell activation in autoimmune CNS lesions and exacerbates clinical disease. Proc. Natl. Acad. Sci. U. S. A. *104*, 18625–18630.

Oka, S., Mori, K., and Watanabe, Y. (1990). Mammalian telencephalic neurons express a segment-specific membrane glycoprotein, telencephalin. Neuroscience *35*, 93–103.

Ortega, S.B., Kashi, V.P., Tyler, A.F., Cunnusamy, K., Mendoza, J.P., and Karandikar, N.J. (2013). The disease-ameliorating function of autoregulatory CD8 T cells is mediated by targeting of encephalitogenic CD4 T cells in experimental autoimmune encephalomyelitis. J. Immunol. *191*, 117–126.

Panitch, H.S., and Bever, C.T. (1993). Clinical trials of interferons in multiple sclerosis. What have we learned? J. Neuroimmunol. *46*, 155–164.

Pitt, D., Werner, P., and Raine, C.S. (2000). Glutamate excitotoxicity in a model of multiple sclerosis. Nat. Med. *6*, 67–70.

Recacha, R., Jiménez, D., Tian, L., Barredo, R., Gahmberg, C.G., and Casasnovas, J.M. (2014). Crystal structures of an ICAM-5 ectodomain fragment show electrostatic-based homophilic adhesions. Acta Crystallogr. Sect. D Biol. Crystallogr. *70*, 1934–1943.

Reuter, E., Gollan, R., Grohmann, N., Paterka, M., Salmon, H., Birkenstock, J., Richers, S., Leuenberger, T., Brandt, a. U., Kuhlmann, T., et al. (2015). Cross-Recognition of a Myelin Peptide by CD8+ T Cells in the CNS Is Not Sufficient to Promote Neuronal Damage. J. Neurosci. *35*, 4837–4850.

Roncarolo, M., and Battaglia, M. (2007). Regulatory T-cell immunotherapy for tolerance to self antigens and alloantigens in humans. Nat. Rev. Immunol. *7*, 585–598.

Rothhammer, V., Heink, S., Petermann, F., Srivastava, R., Claussen, M.C., Hemmer, B., and Korn, T. (2011). Th17 lymphocytes traffic to the central nervous system independently of 4 integrin expression during EAE. J. Exp. Med. *208*, 2465–2476.

Sawcer, S., Hellenthal, G., Pirinen, M., Spencer, C.C. a., Patsopoulos, N. a., Moutsianas, L., Dilthey, A., Su, Z., Freeman, C., Hunt, S.E., et al. (2011). Genetic risk and a primary role for cell-mediated immune mechanisms in multiple sclerosis. Nature *476*, 214–219.

Schulze-Topphoff, U., Prat, A., Prozorovski, T., Siffrin, V., Paterka, M., Herz, J., Bendix, I., Ifergan, I., Schadock, I., Mori, M.A., et al. (2009). Activation of kinin receptor B1 limits encephalitogenic T lymphocyte recruitment to the central nervous system. Nat. Med. *15*, 788–793.

Siffrin, V., Brandt, A., and Herz, J. (2007). New insights into adaptive immunity in chronic neuroinflammation. Adv. Immunol. *96*, 1–40.

Siffrin, V., Brandt, A.U., Radbruch, H., Herz, J., Boldakowa, N., Leuenberger, T., Werr, J., Hahner, A., Schulze-Topphoff, U., Nitsch, R., et al. (2009). Differential immune cell dynamics in the CNS cause CD4+ T cell compartmentalization. Brain *132*, 1247–1258.

Siffrin, V., Vogt, J., Radbruch, H., Nitsch, R., and Zipp, F. (2010a). Multiple sclerosis - candidate mechanisms underlying CNS atrophy. Trends Neurosci. *33*, 202–210.

Siffrin, V., Radbruch, H., Glumm, R., Niesner, R., Paterka, M., Herz, J., Leuenberger, T., Lehmann, S.M., Luenstedt, S., Rinnenthal, J.L., et al. (2010b). In vivo imaging of partially reversible th17 cell-induced neuronal dysfunction in the course of encephalomyelitis. Immunity *33*, 424–436.

Siffrin, V., Paterka, M., Hoppmann, N., Werr, J., Voss, J., Gollan, R., Birkenstock, J., Bopp, T., Esplugues, E., Flavell, R.A., et al. (2015a). Gatekeeper role of central nervous system CD11c + in neuroinflammation. EMBO J - Revison.

Siffrin, V., Birkenstock, J., Luchtman, D.W., Gollan, R., Baumgart, J., Niesner, R. a., Griesbeck, O., and Zipp, F. (2015b). FRET based ratiometric Ca2+ imaging to investigate immune-mediated neuronal and axonal damage processes in experimental autoimmune encephalomyelitis. J. Neurosci. Methods *249*, 8–15.

Stefani, A., Spadoni, F., Siniscalchi, A., and Bernardi, G. (1996). Lamotrigine inhibits Ca2+ currents in cortical neurons: Functional implications. Eur. J. Pharmacol. *307*, 113–116.

Sühs, K.-W., Fairless, R., Williams, S.K., Heine, K., Cavalié, A., and Diem, R. (2014). N-methyl-D-aspartate receptor blockade is neuroprotective in experimental autoimmune optic neuritis. J. Neuropathol. Exp. Neurol. *73*, 507–518.

Sun, D., Whitaker, J.N., Huang, Z., Liu, D., Coleclough, C., Wekerle, H., and Raine, C.S. (2001). Myelin antigen-specific CD8+ T cells are encephalitogenic and produce severe disease in C57BL/6 mice. J. Immunol. *166*, 7579–7587.

Tanabe, S., and Yamashita, T. (2014). Repulsive Guidance Molecule-a Is Involved in Th17-Cell-Induced Neurodegeneration in Autoimmune Encephalomyelitis. Cell Rep. *9*, 1459–1470.

Thestrup, T., Litzlbauer, J., Bartholomäus, I., Mues, M., Russo, L., Dana, H., Kovalchuk, Y., Liang, Y., Kalamakis, G., Laukat, Y., et al. (2014). Optimized ratiometric calcium sensors for functional in vivo imaging of neurons and T lymphocytes. Nat. Methods *11*, 175–182.

Tian, L., Yoshihara, Y., Mizuno, T., Mori, K., and Gahmberg, C.G. (1997). The neuronal glycoprotein telencephalin is a cellular ligand for the CD11a/CD18 leukocyte integrin. J. Immunol. *158*, 928–936.

Tian, L., Kilgannon, P., Yoshihara, Y., Mori, K., Gallatin, W.M., Carpén, O., and Gahmberg, C.G. (2000). Binding of T lymphocytes to hippocampal neurons through ICAM-5 (telencephalin) and characterization of its interaction with the leukocyte integrin CD11a/CD18. Eur. J. Immunol. *30*, 810–818.

Tian, L., Stefanidakis, M., Ning, L., Van Lint, P., Nyman-Huttunen, H., Libert, C., Itohara, S., Mishina, M., Rauvala, H., and Gahmberg, C.G. (2007). Activation of NMDA receptors

promotes dendritic spine development through MMP-mediated ICAM-5 cleavage. J. Cell Biol. *178*, 687–700.

Tian, L., Lappalainen, J., Autero, M., Hanninen, S., Rauvala, H., and Gahmberg, C.G. (2008). Shedded neuronal ICAM-5 suppresses T-cell activation. Blood *111*, 3615–3625.

Trapp, B.D., Peterson, J., Ransohoff, R.M., Rudick, R., Mörk, S., and Bö, L. (1998). Axonal transection in the lesions of multiple sclerosis. N. Engl. J. Med. *338*, 278–285.

Turner, D. a., Haile, Y., and Giuliani, F. (2013). IL-25 prevents T cell-mediated neurotoxicity by decreasing LFA-1 expression. J. Neuroimmunol. *265*, 11–19.

Villoslada, P., Arrondo, G., Sepulcre, J., Alegre, M., and Artieda, J. (2009). Memantine induces reversible neurologic impairment in patients with MS. Neurology *72*, 1630–1633.

Vulchanova, L., Schuster, D.J., Belur, L.R., Riedl, M.S., Podetz-Pedersen, K.M., Kitto, K.F., Wilcox, G.L., McIvor, R.S., and Fairbanks, C. a (2010). Differential adeno-associated virus mediated gene transfer to sensory neurons following intrathecal delivery by direct lumbar puncture. Mol. Pain *6*, 31.

Waisman, A., Hauptmann, J., and Regen, T. (2015). The role of IL-17 in CNS diseases. Acta Neuropathol. 625–637.

Walsh, J.T., Hendrix, S., Boato, F., Smirnov, I., Zheng, J., Lukens, J.R., Gadani, S., Hechler, D., Gölz, G., Rosenberger, K., et al. (2015). MHCII-independent CD4+ T cells protect injured CNS neurons via IL-4. J. Clin. Invest. *125*, 699–714.

Wang, Z., Hong, J., Sun, W., Xu, G., Li, N., Chen, X., Liu, A., Xu, L., Sun, B., and Zhang, J.Z. (2006). Role of IFN-γ in induction of Foxp3 and conversion of CD4 +CD25- T cells to CD4+ Tregs. J. Clin. Invest. *116*, 2434–2441.

Wylezinska, M., Cifelli, A., Jezzard, P., Palace, J., Alecci, M., and Matthews, P.M. (2003). Thalamic neurodegeneration in rel apsing-remitting multiple sclerosis. Neurology *60*, 1949–1954.

Xie, X., and Hagan, R.M. (1998). Cellular and molecular actions of lamotrigine: Possible mechanisms of efficacy in bipolar disorder. In Neuropsychobiology, pp. 119–130.

Yang, H. (2012). Structure, expression, and function of ICAM-5. Comp. Funct. Genomics *2012*.

Zhou, L., Lopes, J.E., Chong, M.M.W., Ivanov, I.I., Min, R., Victora, G.D., Shen, Y., Du, J., Rubtsov, Y.P., Rudensky, A.Y., et al. (2008). TGF-beta-induced Foxp3 inhibits T(H)17 cell differentiation by antagonizing RORgammat function. Nature *453*, 236–240.

6. Appendix

6.1 Abbreviations

[Ca^{2+}]	Ca^{2+} concentration
°C	degree Celsius
µg	microgram
µl	microliters
AF	Alexa Fluor
AMPAr	α-amino-3-hydroxy-5-methyl-4-isoxazolepropionic acid receptor
APC	antigen presenting cells
BBB	blood brain barrier
BSA	bovine serum albumin
CD	cluster of differentiation
CFP	cyan fluorescent protein,
CNS	central nervous system
DAPI	4′,6-Diamidino-2-phenylindole dihydrochloride
DMSO	dimethyl sulfoxide
EAE	experimental autoimmune encephalomyelitis
EtOH	ethanol
FACS	fluorescence-activated cell sorting
FCS	fetal calf serum
FITC	Fluorescein isothiocyanate
Foxp3	forkhead box P3
FPLC	fast protein liquid chromatography
FRET	fluorescence resonance energy transfer
g	g-force
GECI	genetically encoded Ca^{2+} indicator
GFP	green fluorescence protein
gr	gram
HBSS	Hank's Buffered Salt Solution
HEK	human embryonic kidney
HEPES	4-(2-hydroxyethyl)-1-piperazineethanesulfonic acid
HLA	human leukocyte antigen
hrs	hours
hu	human
ICAM	intercellular adhesion molecule
Ig	immunoglobulin
IL	interleukin
IMDM	Iscove's Modified Dulbecco's Medium

KO	knockout
LFA-1	lymphocyte function-associated antigen 1
LTG	Lamotrigine
MACS	magnetic-activated cell sorting
MHC	major histocompatibility complex
min	minutes
MK-801	5-methyl-10,11- dihydro-5H-dibenzo[a,d]cyclohepten-5,10-imine
MMP	matrix metallopreteoase
MOG	myelin oligodendrocyte glycoprotein
MRI	magnetic resonance imaging
MRSI	magnetic resonance spectroscopic imaging
MS	multiple sclerosis
NBM	Neurobasalmedium
NBQX	2,3-Dihydroxy-6-nitro-7-sulfamoyl-benzo[f]chinoxalin-2,3-dion
NeuN	Neuronal Nuclei
NMDAr	N-Methyl-D-aspartate receptor
OVA	ovalbumin
PBS	Phosphate-buffered saline
PE	Phycoerythrin
PET	Polyethylene terephthalate
PI	propidium iodide
PP	polypropylene
PPMS	primary-progressive multiple sclerosis
RFP	red fluorescence protein
RGMa	repulsive guidance molecule-a
RORγt	retinoic acid-related orphan receptor
rpm	rounds per minute
RPMI	Roswell Park Memorial Institute medium
RRMS	relapsing-remitting multiple sclerosis
RT	room temperature
sec	seconds
sICAM	soluble intercellular adhesion molecule
SPMS	secondary-progressive multiple sclerosis
TCR	T cell receptor
TF	transcription factor
TGF	transforming growth factor
Th cells	T helper cells
TNF	tumor necrosis factor
TPLSM	Two photon laser scanning microscopy
T_{reg}	regulatory T cells

TUNEL	terminal deoxynucleotidyl transferase-mediated X-dUTP nick end labeling
VGCC	voltage gated calcium channels
WT	wild type
YFP	yellow fluorescence protein

6.2 Index of Illustrations and Tables